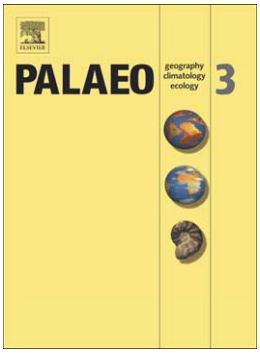

Depositional age, provenance, tectonic and palaeoclimatic settings of the late Mesoproterozoic - middle Neoproterozoic Mbuji-Mayi Supergroup, Democratic Republic of Congo

Franck Delpomdor, Ulf Linnemann, Ariel Boven, Andreas Gärtner, Aleksey Travin, Christian Blanpied, Aurélien Virgone, Hielke Jelsma, Alain Préat

PII: S0031-0182(13)00289-7
DOI: doi: 10.1016/j.palaeo.2013.06.012
Reference: PALAEO 6536

To appear in: *Palaeogeography, Palaeoclimatology, Palaeoecology*

Received date: 23 November 2012
Revised date: 3 June 2013
Accepted date: 5 June 2013

Please cite this article as: Delpomdor, Franck, Linnemann, Ulf, Boven, Ariel, Gärtner, Andreas, Travin, Aleksey, Blanpied, Christian, Virgone, Aurélien, Jelsma, Hielke, Préat, Alain, Depositional age, provenance, tectonic and palaeoclimatic settings of the late Mesoproterozoic - middle Neoproterozoic Mbuji-Mayi Supergroup, Democratic Republic of Congo, *Palaeogeography, Palaeoclimatology, Palaeoecology* (2013), doi: 10.1016/j.palaeo.2013.06.012

Depositional age, provenance, tectonic and palaeoclimatic settings of the late Mesoproterozoic - middle Neoproterozoic Mbuji-Mayi Supergroup, Democratic Republic of Congo

Franck Delpomdor[*,a], Ulf Linnemann[b], Ariel Boven[c], Andreas Gärtner[b], Aleksey Travin[d], Christian Blanpied[e], Aurélien Virgone[f], Hielke Jelsma[g] and Alain Préat[a]

[a] Biogeochemistry & Modeling of the Earth System, Université libre de Bruxelles, 1050 Brussels, Belgium, [b] Museum für Mineralogie und Geologie, Sektion Geochronologie, GeoPlasma Lab, Senckenberg Naturhistorische Sammlungen, 01109 Dresden, Germany, [c] Section of Isotope Geology, Royal Museum for Central Africa, 3080 Tervuren, Belgium, [d] United Institute of Geology, Geophysics and Mineralogy, Siberian Branch, Novosibirsk 630090, Russia, [e] Total SA, 92078 Paris, France, [f] Total SA, 92078 Paris, France, [g] De Beers Exploration, Southdale 2135, Johannesburg, South Africa

[*] Corresponding author at: avenue F.D. Roosevelt, 50 CP260/2 1050 Brussels, Belgium. Tel: +32 2 650 29 01. E-mail address: franck.delpomdor@ulb.ac.be (Franck Delpomdor)

Keywords: Mbuji-Mayi Supergroup; Ages; Chemostratigraphy; Palaeoclimate; Sankuru-Mbuji-Mayi-Lomami-Lovoy Basin

Abstract

The late Mesoproterozoic - middle Neoproterozoic period (*ca*. 1300 Ma - 800 Ma) heralded extraordinary climatic and biological changes related to the tectonic changes that resulted in the assembly (~1.0 Ga) and the break-up of Rodinia (880 Ma - 850 Ma). In the Democratic Republic of Congo, these changes are recorded in the Mbuji-Mayi Supergroup which was deposited in the SE-NW trending siliciclastic-carbonate failed-rift Sankuru-Mbuji-Mayi-Lomami-Lovoy Basin. New LA-ICP-MS U-Pb laser ablation data on detrital zircon grains retrieved from the lower arenaceous-pelitic

sequence (BI group) together with C and Sr isotopic data on carbonates from the upper dolomitic-pelitic sequence (BII group) and an $^{40}Ar/^{39}Ar$ age determination on a dolerite gives a new depositional time frame between 1174 ± 22 Ma and *ca*. 800 Ma for the Mbuji-Mayi Supergroup. The upper age limit is based on the assumption that the transition between the BIIb and BIIc subgroup recorded the Bitter Springs anomaly. In terms of tectonic and palaeoclimatic settings, the BII group was deposited in the eastern passive margin of the Congo Craton during warm periods interlaced with temporarily dry and wet seasons, suggesting greenhouse conditions during the fragmentation of Rodinia.

1. Introduction

Since the demise of the Rodinia Supercontinent (McMenamin and McMenamin, 1990) to the assembly of the eastern Gondwana (eastern Africa, Arabian-Nubian Shield, Seychelles, India, Madagascar, Sri Lanka, East Antratica and Australia) in the ~750 Ma to ~530 Ma interval (Fitzsimons, 2000; Meert, 2003), it has long been argued that the extraordinary biogeochemical and climatic fluctuations are deeply intertwined with global tectonics (Kaufman et al., 1993, 1997; Halverson et al., 2007). The low-latitude distribution of continents in the late Neoproterozoic (Kirschvink, 1992; Hoffman et al., 1998; Hoffman and Schrag, 2002; Li et al., 2008) would have favoured a cool climate due to the nature of continental chemical weathering, atmospheric and oceanic circulation, and the magnitude of planetary albedo (Halverson et al., 2010). These effects led to several icehouse climate periods throughout the Neoproterozoic times. These dramatic climatic changes, global-carbon cycling and atmospheric oxygen budget (Knoll et al., 1986; Derry et al., 1992; Knoll, 1992; Des Marais, 1994; Strauss, 1997; Hoffman et al., 1998; Canfield, 1999) were recorded in the well-pronounced fluctuations of C, Sr and S isotopic compositions observed in the woldwide mid- (Cryogenian, i.e. 850 Ma - 635 Ma) to late (Ediacaran, i.e. 635 Ma - 541 Ma)

Neoproterozoic series (Kaufman and Knoll, 1995; Asmeron et al., 2001; Halverson et al., 2005, 2007; Kaufman et al., 2006; Tewari and Sial, 2007).

In contrast to the late Neoproterozoic, the late Mesoproterozoic - early Neoproterozoic successions (*ca*. 1300 Ma - 850 Ma) are less well isotopically constrained. This interval exhibits moderately $\delta^{13}C$ variations between -2‰ and +4‰ (Fairchild et al., 1990; Knoll et al., 1995; Podkovyrov et al., 1998; Kah et al., 1999; Bartley et al., 2001), with pronounced negative shifts of up 5‰ in average. The second large negative $\delta^{13}C$ anomaly (Bitter Springs stage) is recorded at *ca*. 800 Ma and appears to be unrelated to glaciation, but, in fact, to be related to eustatic changes (Halverson et al., 2005). The most common explanation of such negative excursions, is that they result of organic matter burial with oxidation and input of massive volumes of ^{13}C-depleted carbon from reduced reservoirs, such as sedimentary methane clathrates, labile organic matter, or dissolved organic carbon (Rothman, et al., 2003). In contrast, the $\delta^{13}C$ rise reflects increased biomass, e.g. along continental margins during periods of rifting, and/or proportional burial of ^{13}C-depleted organic matter, potentially attributable to one of several tectonic forcing mechanisms (Knoll, 1992; Hoffman, 1999; Bartley et al., 2001).

Secular change in Sr isotopic composition is a useful indicator of global-scale changes of seawater related to tectonics and climatic regimes thoughout the Neoproterozoic times. The late Mesoproterozoic seawater rose from early Mesoproterozoic lows (~0.7040) to values as high as 0.7060-0.7065 at 1300 Ma, evolving to 0.7051-0.7055 at the Mesoproterozoic-Neoproterozoic boundary (1000 Ma; Gorokhov et al., 1995; Bartley et al., 2001), and 0.7060 for the early Neoproterozoic (Veizer et al., 1983; Asmeron et al., 1991; Melezhik et al., 2001; Halverson et al., 2005, 2007). $^{87}Sr/^{86}Sr$ ratios have risen from 0.7070 to 0.7063 with the onset

of the *ca*. 800 Ma Bitter Springs anomaly, to >0.7085 for the late Neoproterozoic (Burke et al., 1982; Jacobsen and Kaufman, 1999; Shieds, 1999; Brasier et al., 2000; Halverson et al., 2007) and ~0.7093 (Montanez et al., 1996) for the Late Cambrian.

In this paper, we present new age constraints for the late Mesoproterozoic - middle Neoproterozoic Mbuji-Mayi Supergroup (Democratic Republic of Congo) through various methods such as LA-ICP-MS U-Pb geochronology on detrital zircon grains, C-O-Sr chemostratigraphy and $^{40}Ar/^{39}Ar$ dating. Here, we attempt to better constrain the provenance of the Mbuji-Mayi sediments and to establish correlations with other late Meso- and middle Neoproterozoic units in Central Africa, and to constrain the minimum age of the Mbuji-Mayi Supergroup.

2. Paleogeography

The span of geologic time that streches from the late Mesoproterozoic through the early-middle Neoproterozoic (1300 Ma - 800 Ma) heralded extraordinary climatic and biological changes related to the tectonic changes that resulted in the assembly and the break-up of Rodinia. Although the timing of the Rodinia assembly will continue to be debated for some time (Piper, 1976; Bond et al., 1984; McMenamin and McMenamin, 1990; Dalziel, 1991; Hoffman, 1991; Kalstrom et al., 1999), as the exact configuration of various elements surrounding Rodinia is still not clear (Dalziel, 1997; Piper, 2000; Sears and Price, 2000). The greatest certainty is that Laurentia occupied the center of a major landmass, with in periphery a multitude of blocks, which were not yet coherently positionned on the margin of East Gondwana from ~1.0 Ga until all its constituents became assembled in late Neoproterozoic and early Cambrian time (Meert, 2003).

The first Rodinia models placed the southwestern Laurentia margin adjacent to East Antartica (SWEAT hypothesis; Dalziel, 1991, 1997; Hoffman, 1991; Moores, 1991; Weil et al., 1998). While a second model placed the southwestern Laurentia adjacent to Australia (AUSWUS, Karlstrom et al., 1999; Burret and Berry, 2000). However, these SWEAT and AUSWUS models were replaced based on new palaeomagnetic data of Western Australia, by a configuration proposing the AUSMEX (Australia-Mexico) connection (Wingate et al., 2002).

The paleocontinental configuration of the Congo Craton in the assembly of Rodinia is therefore still debated. Dalziel (1997) placed the Congo Craton, associated with the Kalahari Cratons, in the western margin of Laurentia. According to palaeomagnetic results, Pisarevsky et al. (2003) suggested that the Congo Craton was independent from Rodinia in the late Mesoproterozoic, and only joined along its south-eastern margin with facing Laurentia at *ca*. 1000 Ma (Hoffman, 1991; Li et al., 2008). During this time-span, the Congo Craton was marked by the Kibaran (1.4-1.0 Ga) and Irumide (*ca*. 1.02 Ga) orogenic events (De Waele, 2005; De Waele and Fitzsimons, 2007 Johnson et al., 2005; Begg et al., 2009; Fernandez-Alonso et al., 2012), which result of the accretion of Congo-Tanzania-Bangweulu-Kalahari cratons (Pinna et al., 1996).

In the eastern margin of the Congo Craton, the early Neoproterozoic Era is characterized by the *ca*. 880-850 Ma continental break-up of Rodinia (Porada and Berhorst, 2000), which probably started at the newly eastern passive margin formed during the opening of the Mozambique ocean (Li et al., 2008). It gradually spread westwards into the area of the Zambezi rift-basin, and thereafter northwestwards into the area of the Katanga rift-basin (Porada and Berhorst, 2000), and finally in the Sankuru-Mbuji-Mayi-Lomami-Lovoy (SMLL)

rift-basin with deposition of the Mbuji-Mayi Supergroup. In the eastern part of Katanga rift-basin, a differential movement of Congo-Tanzania cratons caused the opening of Kundelungu Rift (aulacogen), accompanied at *ca.* 765 Ma by felsic intrusions (Kafue rhyolites: 879 Ma; Nchanga Granite: 877 Ma; Lusaka Granite: 865 Ma; Armstrong et al., 2005) and the development of an extensional basin trending northeastwards along pre-existing Kibaran structures. This rifting propagation is not recorded in the SMLL Basin indicating that sedimentation related to the collision of Congo and Kalahari cratons along the Mwembeshi Shear Zone ceased with subsequent development of strike-slip systems. This induced clockwise rotation of the Lufilian Belt (Unrug, 1983) which can be correlated with a first phase of deformation in the Lufilian Belt ('Kolwezian phase'), between 790 Ma and 750 Ma, and with the collisional deformation in the Zambezi Belt at 820 Ma (Hanson et al., 1988).

The Pan-African tectonic episode was related to a *ca*. 560-550 Ma collision between the western margin of the Congo Craton and the São Francisco Craton, and between the Kasai-(Angola)-Kalahari cratons and Congo-Tanzania cratons along a southeast-northwest trending suture linking up the southern Mozambique Belt with the Araçuai-West Congo Belt (Porada and Berhorst, 2000; Pedrosa-Soares et al. 2001, 2007, 2011; Alkmim et al. 2006, 2007). The Pan-African orogen ended with the polyphase assembly of Gondwana during the East Africa, Brasiliano, Kuungan and Damaran orogenic events that extended to at least the end of the Cambrian (~490 Ma; Meert, 2003; Gray et al., 2008; Begg et al., 2009; **Fig. 1**).

3. Geological setting

The SMLL Basin (**Fig. 2**) is an intracratonic failed-rift basin (Kadima et al., 2011) located between 6°S and 8°S latitude and 23°E and 26°E longitude, in the Kasai-Oriental Province

(Democratic Republic of Congo). The 'System of Bushimay', herein renamed Mbuji-Mayi Supergroup, established by Raucq (1957) who mapped the geology of the Mbuji-Mayi area (geological map of 1/200,000, Raucq, 1958). Since 1977, petrographic and geochronological data for stratigraphic correlations in Central Africa have been acquired (Cahen et al., 1984; Bertrand-Sarfati, 1972). The stratigraphy may be summarized, following Raucq (1970), as follows:

3.1. Basement rocks

In the western part of the SMLL Basin, the basement consists of migmatitic gneisses with granitic to tonalitic compositions. Weakly deformed and undeformed granites (e.g. Malafudi granites) are present in the SE part of the Mbuji-Mayi area, and considered as the product of migmatisation related to the Neoarchean Moyo deformation event (2680 Ma; Delhal, 1991). Rb-Sr ages of the Malafudi granites gave an age of 2590 (Delhal, 1991). Hf-isotope analyses indicated that this magmatic event was related to reworking of 2.8-3.0 Ga crust (Batumike et al., 2009). In northwestern Zambia, Key et al. (2001) reported zircon U-Pb SHRIMP crystallisation ages of 2561 ± 10 Ma and 2538 ± 10 Ma in granitic gneisses.

In the southern part of the SMLL Basin, the Mbuji-Mayi Supergroup rests on Kibaran Belt lithologies including from base to top (i) the Kiaora (K1) or Mitwaba Group (~4300 m; Cahen, 1954; Van de Steen, 1959; Cahen et al., 1984; Kokonyangi et al., 2001a); (ii) the Kataba Conglomerate (~3900-5500 m); (iii) the Nzilo Group (K2, ~400-600 m; Mortelmans, 1951; Cahen, 1954; Kokonyangi et al., 2001a); (iv) the Hakansson Group (K3, ~1700 m; Cahen, 1954; Van de Steen, 1959; Cahen et al., 1984); and (v) the Lubudi Group (K4, ~1000-1300 m). The Kibaran sedimentary successions are poorly constrained in age. However, the

Kiaora Group is shown to be older than 1.38 Ga, as indicated by cross-cutting relationships with intrusive 1.38-1.4 Ga orthogneisses (Kokonyangi et al., 2004, 2005). Youngest detrital zircons show U-Pb ages of 1329 ± 32 Ma in the Kataba Conglomerate and of 1360 ± 27 Ma in pink quartzites of the Nzilo Group (Kokonyangi et al., 2006), providing a lower limit to the age of deposition. An upper limit to the age of deposition of the Mbuji-Mayi Supergroup is provided by a multi-mineral K-Ar age of 1152 ± 15 Ma (Delhal et al., 1989, recalculated to 1118 ± 15 Ma using the decay constants from Steiger and Jäger, 1977) on biotite, pyroxene and amphibole from E-W trending syenodiorite dykes which outcrop in the eastern part of the Lulua Complex.

3.2. Mbuji-Mayi Supergroup (**Fig. 2**, **Table 1**)

In this paper, we focused our work in the western part of the SMLL Basin. In this area, the lower siliciclastic series of the Mbuji-Mayi Supergroup (BI group) is ~500 m thick, and consists of five subgroups: BIb, BIc, BId, BIE (only visible in the Kafuku region) and BIe. The BIa subgroup is missing in the Sankuru-Mbuji-Mayi area, but has been observed near Makululu and Kiankodi villages in the southern part of the SMLL Basin. Detailed descriptions of this subgroup have been given by Cahen and Mortelmans (1947) and Cahen and Lepersonne (1967). It consists, from base to top, of ~1500 m-thick of red quartzites and shales with an interbedded pink chert horizon.

The BIb subgroup comprises basal conglomerates (17 m) including fragments of crystalline basement passing lateraly to the north at grey calcareous shales (4 m). The overlying subgroups display (i) red shales and argillaceous psammites (~180 m) interbedded of thin sandstone layers (BIc subgroup); (ii) red sandstones and psammites (~250 m), sometimes

dolomitic, (BId); (iii) brownish to pinkish shales and psammites (31.5 m), overlying red shales and grey calcareous dolostones (28 m; BIE); and (iv) grey/pink sandstones (21.5 m) overlying shaly dolomites (26.5 m) with cherts and galena (BIe). The galena from the Tshisomboia river has been studied by Polinard (1929) who considered the mineralization as epigenetic and related to faults. However, three samples of galena from the Lubi and Senga-Senga valleys yielded conventional $^{207}Pb/^{206}Pb$ ages of 910 Ma, 1040 Ma and 1065 Ma (Cahen, 1954; Holmes and Cahen, 1955; Raucq, 1957). Ages of 1040 and 1065 Ma have been attributed syngenetic growth of galena.

The overlying carbonate series of the Mbuji-Mayi Supergroup (BII group) is ~1000 m-thick and consists of five subgroups: BIIa, BIIb, BIIc, BIId and BIIe. The BII group consists from base to top, of (i) grey dolomites (105 m) with columnar stromatolites (BIIa subgroup); (ii) argillaceous and calcareous dolomites often conglomeratic (BIIb subgroup; 125 m); (iii) stromatolitic dolomites with intercalations of shales (BIIc subgroup; 291.5 m); (iv) shales passing to grey cherty dolomites at the top (BIId subgroup, 400 m); and (v) brecciated and zoned limestones with stromatolites (BIIe subgroup; ~100 m).

3.3. Dolerites

Basic igneous rocks have been described from three localities: (i) basaltic lavas overlie the BII group at the confluence of the Mbuji-Mayi and Sankuru rivers (Cahen et al., 1984); (ii) dolerite sills were emplaced within the succession close to the contact between the BI and BII groups in the Lomami area; and (iii) within the BI group along Kiankodi and Lovoy rivers, where they consist of sills of dolerite with large extensions of amygdaloidal lavas (Cahen and Mortelmans, 1947). The rocks consist of ±40 m-thick brownish- to blue-coloured massive to

amygdaloidal basaltic lavas (Raucq, 1957). In the Sankuru-Mbuji-Mayi type area, five nearly concordant K-Ar whole-rock ages (Cahen et al., 1974) on amygdaloidal basalts overlying the Mbuji-Mayi Supergroup range from 870 ± 20 Ma to 953 ± 20 Ma. Of these, three results on two samples were concordant: 916 ± 20 Ma, 942 ± 20 Ma, and 953 ± 20 Ma with an estimated age of 948 ± 20 Ma. Note that the authors indicated that the analyses were carried out on altered samples and that no geochemical controls were used in the selection of samples.

3.4. Kabenga and Kabele Conglomerate

Along the Kiankodi and Lovoy rivers, Cahen and Mortelmans (1947) reported a polymictic conglomerate with more than 50% of clasts material derived from the Mbuji-Mayi carbonates. The conglomerates unconformably overlie the Kibaran Belt and Mbuji-Mayi Supergroup lithologies. The authors correlated this conglomerate with the 'Grand Conglomérat Formation' of the Katanga Supergroup. The Kabele and Kabenga Conglomerate is younger than the Mbuji-Mayi Supergroup and older than the Karoo periglacial tillites of the Lukuga Group, which rest unconformably on the conglomerate.

4. Material and methods

4.1. Samples

The sites of the studied drillholes are shown in **Fig. 3**. Five of the drillsites are situated within the Sankuru-Mbuji-Mayi area between the Lubi and Luembe rivers, the sixth one is situated within the Lomami area. The five first cores are stored in the Geological Department from the Royal Museum for Central Africa (RMCA), the sixth one at the 'Société Minière de

Bakwanga' (MIBA) in Mbuji-Mayi. A detailed petrological description of this drillcore is provided by Raucq (1970), which allowed recognition of corresponding stratigraphic units. Delpomdor et al. (*in* revision) updated these descriptions using a newer nomenclature. The overall studied sequence covers a thickness range of ~525 m. In addition, five samples from five different outcrop localities sampled by Raucq were retrieved from the Royal Museum for Central Africa (RMCA). In this study, we have conserved, for each sample, the RMCA serial number, i.e. RG for 'Registre Géologique' followed by the sample number, and we have attributed a new serial number for each collected sample from cores, i.e. ULB for 'Université libre de Bruxelles' followed by the sample number.

The studied sequence comprises dolostones and limestones crossing the contact between the BI and BII groups (**Fig. 3**). In this paper, we use the lithological descriptions of Raucq (1957, 1970) for the siliciclastic series (BI group) intersected in the S70 Tshinyama (RG57624-57826 of the RMCA serial number) and Kafuku 15 (RG41330-41384 of the RMCA serial number) drillcores. For the carbonate series (BIe subgroup and BII group) intersected in the Bena Kalenda (samples RG31146 to RG31413 of the RMCA serial number), B13 Kanshi (samples RG32201 to RG32464 of the RMCA serial number), and Bena Tshovu (samples RG31534 to RG31646 of the RMCA serial number) drillcores, we had to update the descriptions using a new nomenclature to control the degree of diagenetic alteration. A total of 755 samples of carbonates were collected from split core (10 cm in diameter) at sampling intervals of ± 0.3 m, and investigated for petrography, sedimentology and sequence stratigraphy (Delpomdor and Préat, 2012). Thirty-three additional handspecimen samples intersecting the BIIa (RG31042, RG31070 and RG31072 of the RMCA serial number), BIId (RG31531 to RG31533 of the RMCA serial number) and BIIe (Forminière samples: RG31674 to RG31685, and Lubilash samples: RG31888 to RG31926 of the RMCA serial

number) subgroups were studied from the collection of the RMCA. A brief description of these samples was provided by Raucq (1957, 1970). Amongst these, 246 samples have been selected for chemostratigraphy and geochemistry. Each sample, in thin section, has been etched with Alizarine red S and potassium ferricyanide for recognition of carbonate minerals.

The Lomami dolerite was intersected in drillcore drilled by de Beers Exploration in 2007. This drill site (193/174/X066) is, contrary to the other drillsites located within the eastern part of the SMLL Basin in the Lomami area near the confluence of the Lufubu and Lomami rivers, to the ESE of Kabinda (coordinates 6°28'S - 25°11'E, **Fig. 2**). The dolerite represents the lower part of the drillhole core and was sampled in 2010 at the MIBA warehouse in Mbuji-Mayi. The drillcore shows moderate recovery and dolerite was intersected at the depth of between 13 m and 29 m. The selected specimen reveals that the dolerite is very fresh, although veinlets cross-cut the sample in various directions.

4.2. LA-ICP-MS U-Pb geochronology on detrital zircon grains

Samples were collected from siliciclastic rocks belonging to the BI group, particularly from the S70 Tshinyama and the Kaf.15 drillholes. The stratigraphic position of the four coarse-grained sandstone samples is shown in **Fig. 3**, and U-Pb-Th data and U/Th ratios of detrital zircon grains are presented in **Table 2**. In the Kaf. 15 drillhole, two sandstone samples (RG41375 and RG41382 of the RMCA serial number) were selected, respectively, at -116.25 m and -157.00 m depth, with the former assigned to the BId_2 formation, and consisting of a fine- to medium-grained pinkish/greyish sandstone, slightly micaceous and quartzitic, and the latter assigned to the BId_2 formation. The S70 Tshinyama samples (RG57673 and RG57809 of the RMCA serial number) were taken from BIc-d_4 and BIc-d_1 formations, respectively.

Sample RG57673 was collected at -119.50 m, and is a purple/green and whitish fine-grained shaly/sandy psammite. Sample RG57809 (-317.00 m to -314.00 m) is a massive grey/pinkish quartzitic, slightly dolomitic sandstone.

Investigated detrital zircon grains (355 grains in total) are sub- to well-rounded and have a magmatic origin. Most zircons are brownish coloured or transparent. Ultra-high pressure and temperature zircon grains have not been identified following their morphology. Zircon concentrates were processed from 0.596 to 1.670 kg sample material at Department of Isotope Geochemistry at the Free University of Amsterdam (Netherlands) using standard separation methods. Final selection of zircon grains for U-Pb dating was achieved by handpicking under a binocular microscope. Zircon grains, ranging from 60 µm to 120 µm in size and displaying all morphological types, were selected, mounted in resins blocks and polished to half their thickness. They were analyzed for U, Th and Pb isotopes using LA-ICP-MS techniques at the Museum für Mineralogie und Geologie (GeoPlasma Lab, Senckenberg Naturhistorische Sammlungen Dresden, Germany) with a Thermo-scientific Element 2 XR sector field ICP-MS coupled to New Wave UP-193 Excimer Laser System. A teardrop-shaped, low volume laser cell constructed by Ben Jähne (Dresden) and Axel Gerdes (Institute of Geosciences, Johann Wolfgang Goethe-University Frankfurt, Frankfurt am Main, Germany) was used to enable sequential sampling of heterogeneous grains during time resolved data acquisition.

Each analysis consisted of approximately 15 s background acquisition followed by 30 s data acquisition, using a laser spot-size of 25 µm and 35 µm, respectively. A common-Pb correction based on interference- and background-corrected ^{204}Pb signal and a Pb model composition (Stacey and Kramers, 1975) was carried out where necessary. Raw data were corrected for background signal, common Pb, laser induced elemental fractionation,

instrumental mass discrimination, and time-dependent elemental fractionation of Pb/Th and Pb/U with an Excel® spreadsheet program developed by Axel Gerdes. Reported uncertainties were propagated by quadratic addition of the external reproducibility obtained from standard zircon Gj-1 (±0.6% and 0.5-1% for the $^{207}Pb/^{206}Pb$ and $^{206}Pb/^{238}U$, respectively) during individual analytical sessions and within-run precision of each analysis. Concordia diagrams (2σ error ellipses) and Concordia ages (95% confidence level) were produced using Isoplot/Ex 2.49 (Ludwig, 2001), with frequency and relative probability plots using AgeDisplay (Sircombe, 2004).

$^{207}Pb/^{206}Pb$ ages were taken for interpretation of all zircons >1.0 Ga, and $^{206}Pb/^{238}U$ ages for younger grains. Th/U ratios are obtained from LA-ICP-MS measurements of investigated zircon grains. U and Pb contents and Th/U ratios were calculated relative to Gj-1 zircon standard and are accurate to approximately 10%.

4.3. Major and trace elements

The carbonates were analyzed for major, trace and REE concentrations from 174 samples (**Table 3**) by ICP-MS using a Perkin Elmer SCIEX ELAN at Activation Laboratories Ltd. (Canada). Two methods of preparations were used, aqua regia and total digestion. Aqua regia consists of a 0.5 g digested sample at 90°C in a microprocessor controlling digestion block for 2 hours. The solution is diluted and analyzed by ICP/MS using a Perkin Elmer SCIEX ELAN ICP/MS. The 'ultratrace 3 analyses' (Actalabs, Canada) using the total digestion consisted of a combination of our 1H procedure (INAA and multi-acid digestion ICP) associated with ICP/MS on same solution used for ICP/OES. Some elements reported by ICP/MS were duplicated by INAA and indicated the degree of dissolution as certain elements resided in

very resistant phases like zircon, monazite, titanite, xenotime, chromite, barite, etc. which can't be totally dissolved with acids. ICP/MS used for this package is a Perkin Elmer-SCIEX ELAN 6000. Total digestion used for ICP portion (0.25 g aliquot of sample) was achieved with HF and then with $HClO_4$ –HNO_3 at 260°C to fuming and was diluted with aqua regia. Additional elements were determined by ICP/MS on the previous multi-acid digested solutions. The samples were diluted and analyzed on a Perkin Elmer Sciex ELAN ICP/MS.

4.4. Chemostratigraphy

A total of 246 samples from the BIe to BIIe subgroups were selected for whole rock carbon and oxygen isotopic analyses (**Table 3**). Carbonate powders were reacted with 100% phosphoric acid (density >1.9; Wachter and Hayes, 1985) at 75°C using a Kiel III online carbonate preparation line connected to a ThermoFinnigan 252 mass spectrometer at the University of Erlangen-Nürnberg (Germany). All values are reported in per mil relative to V-PDB by assigning a $\delta^{13}C$ value of +1.95‰ and a $\delta^{18}O$ value of -2.20‰ to NBS19. Reproducibility was checked by replicate analysis of laboratory standards and is better than ± 0.06 ‰. Oxygen isotopic compositions of dolomite were corrected using the fractionation factors given by Rosenbaum and Sheppard (1986).

Thirty-three organic-rich carbonate and shale samples from the BIe to BIIe subgroups have been selected for carbon isotope and total organic matter analyses (**Table 3**). Bulk organic carbon analyses were performed from powdered-rock acidified in a 25% HCl solution at 35°C using a standard LECO carbon analyzer (CS-244) to determine total organic carbon (TOC) and sulfur content percentages. For stable isotope analysis, the sample was weighed into tin capsules for continuous flow combustion and isotopic analysis using a Carlo Erba EA1110

elemental analyser coupled to a mass spectrometer (ThermoFinnigan delta plus XP) in Parme University (Italy). Measured isotopic compositions were calibrated with inter-laboratory standards: sucrose IAEA-CH-6, oil NBS-22 and graphite USGS-24. Organic carbon isotope values are reported in the $\delta^{13}C$ notation normalized to the international PDB standard (V-PDB, Vienna Peedee Belemnite). The overall precision of carbon isotope analyses is within 0.2 ‰ (1σ).

A total of 42 samples from the BIe to BIIe subgroups were selected for Sr-analyses (whole-rock; **Table 3**) on the basis of petrographic screening. Recrystallized phases were avoided and the degree of chemical alteration was determined on Sr/Ca, Mn/Sr and Rb/Sr ratios. Powdered samples were leached with 0.5 M acetic acid and centrifuged to separate soluble fraction from insoluble fraction. Strontium was eluted from solutions by ion exchange chromatography using a Sr-Spec resin. Sr isotopes were measured on a VG54 multicollector mass spectrometer at Université libre de Bruxelles (Belgium). $^{87}Sr/^{86}Sr$ values were normalized to $^{86}Sr/^{88}Sr = 0.1194$.

4.5. $^{40}Ar/^{39}Ar$ dating (**Table 4**)

$^{40}Ar/^{39}Ar$ analyses were performed on two different noble gas mass spectrometers both operated in the static mode, a MicroMass 5400 mass spectrometer and a newly installed high-sensitivity GV instruments ARGUS multi-collector magnetic sector mass spectrometer at the Ar-Ar laboratory of the Institute of Geology and Mineralogy from the Siberian Branch of the Russian Academy of Sciences in Novosibirsk (Russia).

The selected crystals from the -500 to + 250 μm sieve fraction were washed with de-ionised water and acetone, and individually wrapped in aluminium foil and filled in two separate vacuum sealed quartz glass vials together with interspersed aliquots of the irradiation standards MCA-11 muscovite, Bern-4m muscovite and LP-6 biotite and packets of K and Ca salts to monitor interfering isotopes. The samples were irradiated separately in two consecutive batches at the VVR-K research reactor of the Polytechnic Institute at Tomsk (Siberia, Russia) for 48 hours and with the use of the VEK-11 carrier. The J-value was determined with a precision about to 0.5% and its error is included in the internal 1σ analytical uncertainty.

Mass discrimination was monitored by regular analysis of the Ar isotopic composition of a standard air volume released from a pipette system. Typical ^{40}Ar line blank values for 1200°C steps did not exceed 10^{-10} mlSTP and the blank composition remained atmospheric excluding any fractionation problem. The following correction factors for interfering reactions were used: (i) for the first irradiation batch $(^{39}Ar/^{37}Ar)_{Ca}$ = 0.000679 ± 0.000007, $(^{36}Ar/^{37}Ar)_{Ca}$ = 0.000270 ± 0.000004, $(^{40}Ar/^{39}Ar)_{K}$ = 0.00088 ± 0.00069; and (ii) for a second irradiation batch $(^{39}Ar/^{37}Ar)_{Ca}$ = 0.000679 ± 0.000007, $(^{36}Ar/^{37}Ar)_{Ca}$ = 0.000270 ± 0.000004, $(^{40}Ar/^{39}Ar)_{K}$ = 0.00088 ± 0.00069. Intensities of the radioactive isotopes ^{39}Ar and ^{37}Ar were corrected for decay and reactor interferences. All uncertainties on the results are stated at the 1σ level, except for the errors on the concluding mean average age computed for each sample, which allow comparison (at 2σ level) with data from other methods.

5. Results

5.1. LA-ICP-MS U-Pb geochronology on detrital zircon grains

A total of 84 detrital zircon grains were analyzed in sample RG57809 (BIc-d_1 formation in the S70 Tshinyama drillhole), of which only 6 grains are 91 to 106% concordant (**Fig. 4-A**). The youngest concordant grain is 2658 ± 8 Ma in age. The oldest zircon yielded an age of 2973 ± 11 Ma.

A total of 56 detrital zircon grains were analyzed in sample RG57673 (BIc-d_4 formation in S70 Tshinyama drillhole), of which 29 grains were concordant (i.e. in the range of 92-104%, **Fig. 4-A**). The youngest concordant grain is 1223 ± 13 Ma old. The oldest zircon yielded an age of 2870 ± 6 Ma. The majority (89%) of the zircons are Proterozoic in age (**Fig. 4-A**), and the probability plot shows maxima at ~1225 Ma, ~1300 Ma, ~1400 Ma, ~1525 Ma, ~1660 Ma, ~1775 Ma and ~1857 Ma (**Fig. 4-B**). Eleven percent of the zircons gave Archean ages between 2745 ± 7 Ma and 2870 ± 6 Ma (**Fig. 4-B**).

A total of 115 detrital zircon grains were analyzed in sample RG41382 (BId_2 formation in the Kaf. 15 drillhole), of which 87 grains were concordant (**Fig. 5-A**). The youngest concordant grain is 1174 ± 22 Ma in age. The oldest zircon yielded an age of 2741 ± 13 Ma. The majority (95.4%) of the zircons are Proterozoic in age, and the probability plot displays two large peaks at ~1100-1600 Ma and ~1700-1900 Ma, with maxima at ~1325 Ma and ~1850 Ma (**Fig. 5-B**). Five Archean grains (4.6% in abundance) gave ages between 2691 ± 8 Ma and 2741 ± 13 Ma (**Fig. 5-B**).

A total of 77 detrital zircon grains were analyzed in sample RG41375 (BId_2 formation in the Kaf. 15 drillhole), of which 43 grains were concordant in the range of 91-106% (**Fig. 5-A**). The youngest concordant grain is 1176 ± 17 Ma in age. The oldest zircon yielded an age of

2706 ± 12 Ma. The majority (95.3%) of the zircons are Proterozoic in age, and the probability plot shows four large peak intervals with maxima at 1225 Ma, 1425 Ma, 1750 Ma and 1875 Ma. One grain is Archean in age at 2706 ± 12 Ma (**Fig. 5-B**).

5.2. Major and trace elements (**Table 3**)

The BIe subgroup shows mean Sr/Ca ratios of 8.3 x 10^{-4} (*n = 9*) and 5.5 x 10^{-4} (*n = 9*), respectively, for the S70 Tshinyama and Kaf. 15 drillholes. The higher Sr/Ca ratio (3.0 x 10^{-3}) is measured in ULB11 sample. The mean Mn concentrations in the two drillholes are 1410.9 ppm and 445.2 ppm. In the BIIa carbonate subgroup, the mean Sr/Ca ratio is 5.6 x 10^{-4} and Mn concentrations vary between 697 and 1830 ppm (*n = 2*). The BIIb subgroup displays mean Sr/Ca ratios between 3.7 x 10^{-4} (*n = 15*) and 1.8 x 10^{-3} (*n = 20*) in the B-13 Kanshi and Bena Kalenda drillholes, successively. The lower part of the Bena Kalenda drillhole shows higher Sr/Ca ratios two to eight times more that its upper part. Their mean Mn concentrations are 66.7 ppm (*n = 15*) and 44.2 ppm (*n = 20*) respectively. In the BIIc subgroup, carbonates exhibit mean Sr/Ca ratios of 3.0 x 10^{-3} (*n = 51*), and higher values are found near and inside the shaly dolostones and shales. The BIId subgroup exhibits low Sr/Ca ratios (mean Sr/Ca = 3.9 x 10^{-3}; *n = 16*) and very low Mn concentrations (mean Mn = 54.3 ppm). In the BIIe subgroup, Sr/Ca ratios are high (mean Sr/Ca = 1.4 x 10^{-3}; *n = 8*) with mean Mn concentrations of 497.3 ppm.

Sr concentrations in the carbonates of the Mbuji-Mayi Supergroup range from 10.6 to 942.0 ppm (*n = 130*) except in samples of the BIIb and BIIe subgroups and several samples from the BIe subgroup. Higher Sr concentrations are measured in the BIIb (mean Sr = 286.7 ppm:

n = 16) and BIIe (mean Sr = 220.0 ppm: *n = 7*) subgroups of the Bena Kalenda drillcore and BIIe handspecimens, respectively.

The BIe subgroup displays high Fe concentrations (*n = 18* ; mean Fe = 1.0% in the S70 Tshinyama drillhole; mean Fe = 1.4% in the Kaf.15 drillhole). In the BIIa carbonate subgroup, Fe concentrations are 0.33 and 0.71% (*n = 2*). The BIIb subgroup shows lower Fe concentrations than the BIe and BIIa subgroups, ranging between 0.10 and 0.28% (*n = 20*). In the Kanshi B-13 drillhole, BIIb carbonates Fe concentrations range between 0.10 and 0.39% (*n = 20*) with maximum contents in silicified and clay-rich dolostones. The BIIc subgroup exhibits low Fe concentrations (0.13-0.91%; *n = 29*) in stromatolitic dolostones and high values (1.6-9.8%; *n = 22*) in shaly dolostones. In the BIId subgroup, mean Fe concentration is low (0.3%; *n = 16*). Finally, the BIIe subgroup displays two Fe patterns: (i) low Fe concentrations between 0.3 and 0.9% in the Lubilash samples; and (ii) high Fe concentrations between 0.4 and 1.4% in the Forminière samples. Mn concentrations of the BIIb and BIId subgroups are very low (13-161 ppm), as compared with high Mn contents (200-2410 ppm) of the BIe, BIIa, BIIc and BIIe subgroups.

5.3. C, O and Sr chemostratigraphy

5.3.1. Inorganic $\delta^{13}C_{carb}$

$\delta^{13}C_{carb}$ isotopic compositions of carbonates of the Mbuji-Mayi Supergroup were analyzed from nine sections **(Fig. 6)**. The first 25 m of Mbuji-Mayi carbonates, in particular the shaly dolostones of the BIe subgroup intersected by the S70 Tshinyama drillhole show a strong decrease of $\delta^{13}C_{carb}$ values, from base to top, from +1.8‰ to -5.7‰ (*n = 9*). The smallest

$\delta^{13}C_{carb}$ value is -7.5‰. Other 50 m-thick shaly dolostones in the Kaf.15 drillhole present also a $\delta^{13}C_{carb}$ decrease from base to top in the BIe subgroup, with a narrow range of values between +0.0‰ and -5.0‰ (*n = 10*). The minimum $\delta^{13}C_{carb}$ value is -5.3‰. The grey laminated dolostones of the BIIa subgroup display $\delta^{13}C_{carb}$ values from -2.4‰ to -1.6‰ (*n = 2*). $\delta^{13}C_{carb}$ values (*n = 22*) of the BIIb subgroup are established from Bena Kalenda cores. Shaly limestones display a negative $\delta^{13}C_{carb}$ values (-2.9 ‰ to +0.0‰) followed by positive $\delta^{13}C_{carb}$ values between +0.0‰ and +3.2‰ in overlying shaly dolostones. In the B-13 Kanshi drillhole, dolostones of the BIIb subgroup show increasing $\delta^{13}C_{carb}$ values from -1.77‰ and +3.0‰ (*n = 22*). Stromatolitic dolostones interbedded with thin shale layers of the BIIc subgroup present decreasing $\delta^{13}C_{carb}$ values in a narrow range between +2.2‰ to -1.0‰ (*n = 20*) in the first 20 m, and an increase of $\delta^{13}C_{carb}$ values occurs in the overlying 90 m stromatolitic dolostones. These dolostones are interbedded with thin shaly layers characterized by increasing $\delta^{13}C_{carb}$ values, from 1.5‰ to +4.6‰ (*n = 45*). The dolostones at top of the drillhole show a positive $\delta^{13}C_{carb}$ excursion with values between +2.2‰ and +4.9‰ (*n = 82*). Isotopic data of the BIId subgroup from Bena Tshovu cores show a positive $\delta^{13}C_{carb}$ excursion (+0.2‰ and +2.3‰; *n = 17*). Two shaly dolostones with cherts gave negative $\delta^{13}C_{carb}$ values of -0.3‰. The BIIe subgroup shows negative $\delta^{13}C_{carb}$ values between -7.1‰ and -2.3 (*n = 5*). The latter displays similar negative $\delta^{13}C_{carb}$ values in the limestones, with a narrow range between -2.1‰ and -1.6‰ (*n = 4*).

5.3.2. Organic $\delta^{13}C_{org}$

$\delta^{13}C_{org}$ composite profiles of the Mbuji-Mayi Supergroup are given in **Fig. 6**. The BIe subgroup dolostones of the upper part of the S70 Tshinyama drillhole record negative $\delta^{13}C_{org}$ values (*n = 2*) of -27.8‰ and -27.4‰. In the Kaf. 15 drillhole, grey BIe subgroup shaly

dolostones gave negative $\delta^{13}C_{org}$ values (*n = 2*) of -27.7‰ and -28.1‰. $\delta^{13}C_{org}$ isotopic compositions of shaly dolostones of the BIIb subgroup obtained in the Bena Kalenda and B-13 Kanshi cores display negative $\delta^{13}C_{org}$ values (*n = 2*) of -25.1‰ and -24.7‰. From base to top of the BIIb subgroup in the Kanshi B-13 drillhole, $\delta^{13}C_{org}$ values range between -30.2‰ and -26.1‰ (*n = 3*). No $\delta^{13}C_{org}$ isotopic compositions were measured in the first 20 m of the BIIc subgroup, composed of stromatolitic dolostones interbedded with thin shale layers. The following 90 m of dolostones, often stromatolitic, interbedded with thin shale layers record negative $\delta^{13}C_{org}$ values between -30.0‰ and -22.8‰ (*n = 8*). The smallest $\delta^{13}C_{org}$ values are in the shales with a narrow range of -23.0‰ to -22.8‰. The overlying dolostones show a negative $\delta^{13}C_{org}$ excursion between -27.5‰ and -22.8‰ (*n = 17*). Only one $\delta^{13}C_{org}$ value has been obtained in BIId dolostones with of -24.2‰. The BIIe subgroup have negative $\delta^{13}C_{carb}$ values of -32.0‰ and -30.9‰ (*n = 3*).

5.3.3. Inorganic $\delta^{18}O_{carb}$

$\delta^{18}O_{carb}$ composite profiles of the Mbuji-Mayi Supergroup were established from nine sections, the same defined previously for carbon isotopes (**Fig. 6**). BIe dolostones of the S70 Tshinyama drillhole show a strong decrease of the $\delta^{18}O_{carb}$ values, from base to top, from -2.7‰ to -1.1‰ (*n = 9*). In the Kaf.15 drillhole, the BIe subgroup displays $\delta^{18}O_{carb}$ values between -6.5‰ and -1.6‰ (*n =10*). The overlying grey laminated dolostones of the BIIa subgroup gave $\delta^{18}O_{carb}$ values from -7.4‰ to -1.7‰ (*n = 2*). $\delta^{18}O_{carb}$ values (*n = 22*) of the BIIb subgroup carbonates were obtained in the Bena Kalenda drillhole. The first 43 m of shaly limestones of lower part of the drillhole record a negative $\delta^{18}O_{carb}$ excursion (-4.5 ‰ to +0.8‰), followed by positive values between +1.6‰ and +3.9‰ in the 7 m of shaly dolostones, and finally by a negative $\delta^{18}O_{carb}$ values (-2.5 ‰ to -0.8‰) in the last 17 m of

dolostones. The BIIb subgroup of the Kanshi B-13 drillhole show negative $\delta^{13}C_{carb}$ values from -5.7‰ and +0.2‰ (*n = 22*). All samples of the BIIc subgroup display a negative $\delta^{18}O_{carb}$ values from -7.1‰ to -0.5‰ (*n = 145*). Oxygen isotopic compositions of the BIId subgroup were obtained from Bena Tshovu drillcores; and record principally negative $\delta^{18}O_{carb}$ values (-15.1‰ and +0.6‰; *n = 17*). The BIIe subgroup consists of calcareous dolostones with negative $\delta^{18}O_{carb}$ compositions (*n = 9*) between -8.7‰ and -4.3‰.

5.3.4. $^{87}Sr/^{86}Sr$ (**Fig. 6**)

In the S70 Tshinyama drillhole, BIe subgroup shaly dolostones have highly variable radiogenic values ranging between 0.70729-0.72051 (*n = 6*) with Sr concentrations > 71-357 ppm and average Mn/Sr = 13.4, indicative of diagenetic alteration. Radiogenic $^{87}Sr/^{86}Sr$ values of 0.71601-0.72946 (*n = 3*) in the BIe subgroup of the Kaf.15 drillhole are associated with high Mn (average Mn/Sr = 7.60) and low-Sr (average Sr = 77.5 ppm) concentrations and record chemical alteration processes. $^{87}Sr/^{86}Sr$ ratios (*n = 16*) of BIIb subgroup shaly dolostones of the Bena Kalenda drillhole present weak radiogenic $^{87}Sr/^{86}Sr$ values, with two less radiogenic $^{87}Sr/^{86}Sr$ values of 0.70625-0.70707 with Rb/Sr > 0.01, and three more radiogenic $^{87}Sr/^{86}Sr$ values between 0.70650-0.70897 with Rb/Sr > 0.01. Least altered samples are those with Sr concentrations of 168.3 ppm and Mn/Sr ratio of 0.34 in average. BIIb dolostones in the Kanshi B-13 drillhole gave $^{87}Sr/^{86}Sr$ values between 0.70616-0.70695 (*n = 6*), with Sr-low concentrations (97-117 ppm) and Mn/Sr ratios of 0.26-0.59. The BIIc subgroup displays high $^{87}Sr/^{86}Sr$ values between 0.70623 and 0.74256 (*n = 10*) and high Mn/Sr ratios between 1.31 and 10.97, consistent with diagenetic alteration. $^{87}Sr/^{86}Sr$ ratios of the BIIb subgroup are 0.70590-0.70872 (*n = 8*) with low Sr concentrations (average Sr = 39.6 ppm) and Mn/Sr ratios varying between 0.45 and 1.74. The BIIe dolostones and limestones

have high $^{87}Sr/^{86}Sr$ values of 0.70801-0.71031 (*n = 3*) with Sr concentrations of 151-161 ppm and Mn/Sr ratios of 0.95-1.18. An additional BIIe sample set displays $^{87}Sr/^{86}Sr$ ratios ranging between 0.70509 and 0.70702 (*n = 3*) with Mn/Sr varying between 0.82 and 2.29. The samples with Mn/Sr > 1.5 and Rb/Sr > 3 are considered like least-altered samples.

5.4. $^{40}Ar/^{39}Ar$ dating on dolerite

An overview of the $^{40}Ar/^{39}Ar$ step-heating results obtained on the dolerite groundmass separates is provided in **Table 4**. Two aliquots were irradiated separately. Separate step-heating experiments and Ar isotopic analyses were performed on both mass spectrometers. Aliquot weights are given in the table.

The $^{40}Ar/^{39}Ar$ step-heating spectra obtained on two aliquots from sample ABMB10 are displayed in **Fig. 7**. The first aliquot (graph with black error boxes) was incrementally heated in 7 steps and measured on the Micromass 5400. The Ca/K spectrum is disturbed at low and high temperature steps. The age spectrum starts with a rising staircase pattern most likely reflecting a loss of radiogenic argon out of less retentive sites with proportionally higher Ca/K ratios. From step 4 onward, we start tapping isotopic signatures coming from a more K-rich phase (refer to the corresponding range in the Ca/K spectrum). Step 5 yields the highest apparent age with a value of 878.2 ± 8.8 Ma. Contiguous steps 4 and 5 with statistically indistinguishable ages and representing 36% of the total ^{39}Ar released during the experiment yield a weighted mean average age of 875 ± 12 Ma (2σ MSD). A subsequent decrease in apparent ages is displayed as a sudden drop with step 6 yielding an apparent age of 705.5 ± 7.6 Ma.

To get a better insight in the variability of the apparent ages and check the reproducibility, the experiment was repeated on a second aliquot, but this time with twice as many (namely 14) steps, likely to release smaller gas amounts, an analytical challenge which the ARGUS equipment with its higher sensitivity. The shape of the age spectrum displays a similar starting pattern with a rising staircase. Step 5 yields the highest apparent age with a value of 889.4 ± 8.7 Ma, which is within error limits the same as the apparent age on step 5 of the first aliquot. This time subsequent steps display a well defined decreasing staircase shaped spectrum dropping down until a "saddle" level comprising 3 consecutive steps which define a plateau with a weighted-mean average age of 643.7 ± 6.7 Ma (2σ MSD). This age figure is distinctively lower then the apparent age obtained for step 6 on the first aliquot and is likely to yield a better estimate for the age of a reactivation which induced a loss of radiogenic argon within this sample.

6. Interpretation

6.1. Provenance of detrital zircon grains

The data set of 165 concordant U-Pb ages of detrital zircon grains of the BI group displays that the bulk (45.6%) of zircon ages falls in the range of ~1100-1400 Ma (**Fig. 8**). These ages may be attributed to a Mesoproterozoic Kibaran Belt (KIB) orogenic event in Central Africa. The timing of deposition and provenance of the Kibaran successions are constrained by the 1.38 Ga-1.4 Ga orthogneisses in the Kiaora Group (Kokonyangi et al., 2004, 2005; Tack et al., 2010), and the detrital zircons yielded U-Pb ages of 1329 ± 32 Ma in the Kataba Conglomerate and 1360 ± 27 Ma in the pink quartzites of the Nzilo Group (Kokonyangi et al., 2006). In the Kiaora Group, four distinct generations of granitoids (Cahen et al., 1967, 1974,

1984; Gérard and Ledent, 1970; Ledent, 1979), commonly associated with gabbroic-dioritic intrusions (Van de Steen, 1953; Cahen, 1954; Lonchampt and Heinry, 1972; Kampunzu et al., 1986; Kokonyangi et al., 2004, 2005), yielded coeval ages. In term of tectonic, the Kibaran Belt presents two tectono-thermal orogenic events at 1.38 Ga (D1) and 1.1 Ga (D2) (Kokonyangi et al., 2004, 2005). The earliest D1 deformation occured in the Kiaora Group and predated deposition of the Nzilo, Hakansson and Lubudi groups. The second D2 deformation corresponded to the climax of Kibaran orogeny at 1079 ± 14 Ma (Kokonyangi et al., 2006).

A possible provenance of the zircon grains from the Karagwe-Ankole Belt ('KAB'; former NE Kibaran belt) is not excluded. In the KAB, three sedimentation periods have been reported between: (i) 1780-1375 Ma for the Eastern Domain or 'ED' Basin; (ii) 1420-1375 Ma for the first sedimentation domain; and (iii) >1375-1222 Ma for the second sedimentation period in the Western Domain or 'WD' Basin (Fernandez-Alonso et al., 2012). Thirteen U-Pb ages, between 1200 and 1225 Ma, on zircon grains of the BI group in the SMLL Basin may be correlated with a U-Pb age of 1222 ± 28 Ma on detrital zircon grains from the base of the Nya-Ngezie unit in the Kivu-Maniema area of the Democratic Republic of Congo (Villeneuve and Chorowicz, 2004), corresponding to the beginning of the third sedimentation period in the western domain of the KAB.

The second-largest zircon population (28.3%; **Fig. 8**) ranges between ~1.7 Ga and 2.1 Ga reflecting (direct or indirect) input of (i) Eburnean basement rocks of the Bangweulu Block (Andersen and Unrug, 1984), unconformably overlain by the >1.9 Ga Mporokoso Group (Brewer et al., 1979; Schandelmeier, 1980, 1983); and/or (ii) the granulitic-amphibolitic

gneisses and metasedimentary rocks of the Ubendian Belt constrained by U-Pb zircons and $^{40}Ar/^{39}Ar$ dating at *ca*. 2.0 Ga (Lenoir et al., 1994; Ring et al., 1997; Boven et al., 1999).

Analyses of 18 detrital zircons from the Mbuji-Mayi BI group yielded U-Pb ages between 1.86-1.90 Ga. They can be correlated with *ca.* 1.88-1.85 Ma volcano-plutonic events that consolidated the NE Congo (Uganda-DR. Congo), Kasai (Angola-DR. Congo) and Tanzania cratons (Schandelmeier, 1983; Kabengele et al., 1991; Lenoir et al., 1994; Kapenda et al., 1998).

The third largest zircon population (9.0%; **Fig. 8**) ranging between ~2.7 Ga and 2.9 Ga may be attributed to detrital input of crystalline rocks from the Kasai Craton. Amongst the latter, the Sandoa-Kapanga Complex gneisses yielded a whole-rock Rb-Sr errorchron at 2852 ± 46 Ma (Delhal and Liégeois, 1982), and Pb-Pb errorchrons of 3086 and 3021 ± 48 Ma (Walraven and Rumvegeri, 1993). Hf-isotope analyses indicated that this magmatic event was related to the reworking of a 2.8-3.0 Ga crust (Batumike et al., 2009). Moreover, the youngest granite within this complex yielded a Rb-Sr age of 2595 ± 92 Ma (Cahen et al., 1984).

Exotic zircon populations (18.1%; **Fig. 8**) consist of Meso- and Paleoproterozoic zircon grains ranging from ~1.4 to 1.7 Ga (17.5%) and ~2.1 to 2.7 Ga (0.6%). These ages are unknown in the Democratic Republic of Congo, due to a gap in magmatic activity. However, the ~1.4-1.7 Ga zircon grains and intruded granitoids, with crystallization ages ranging between 1664 ± 4 and 1551 ± 33 Ma, are reported along the southern margin of the Paleoproterozoic Bangweulu Block and in the Kibaran Belt of SW-Uganda. Three distinctive $^{207}Pb/^{206}Pb$ batholithe crystallization ages in granitoids have been dated in the Karagwe-

Ankole Belt ("KAB") around 1565 Ma, ~1445 Ma, and 1330-1367 Ma, namely Chitwe, Ntungamo and Rwentobo, successively (Buchwaldt et al., 2008).

The interpretation of LA-ICP-MS U-Pb analyses on zircon grains point to a west (Archean) and south-east or east provenance for the BI group in the SMLL Basin from (i) the Kasai Craton to the west; and (ii) a collage of belts to the southeast and east including the Kibaran Belt, the Ubendian-Rusizian Belt (and perhaps the Karagwe-Ankole Belt), and the Bangweulu Block.

6.2. Chemostratigraphy

6.2.1. Diagenetic alteration

High $\delta^{18}O_{carb}$ values of BIIb, BIIc and BIId carbonates are related to evaporitic diagenesis (Delpomdor and Préat, 2012) during early stages of deposition. **Fig. 9** shows $\delta^{13}C_{carb}$ and $\delta^{18}O_{carb}$ relationships in Mbuji-Mayi carbonates, and allows recognition of meteoric and burial lithification from marine excursions**.** The process yields a roughly co-variant relationship between $\delta^{13}C_{carb}$ and $\delta^{18}O_{carb}$ in which $\delta^{13}C_{carb}$ and $\delta^{18}O_{carb}$ decrease. In mixed meteoric/marine pore fluids, meteoric waters are depleted in ^{18}O relative to ocean water, causing a distinct $\delta^{18}O$ decrease with increase of meteoric waters (Knauth and Kennedy, 2009). Only a minor part of Mbuji-Mayi carbonates (BIe, BIIb and BIIe subgroups) are superimposed to the 'lithification domain', reflecting a mixing of seawater and meteoric waters. Samples plotted left of the 'lithification' trend, record a partial isotopic resetting causing carbonate $\delta^{18}O_{carb}$ driven to lower values, as a result of a higher-temperature equilibration during burial. Nevertheless, dolostones of the BIIc subgroup did not seem to be

affected by a thermal burial effect, since $\delta^{18}O_{carb}$ values are the same than those reported in the BIIc stromatolitic dolostones corresponding to the 'lithification' domain. The slightly higher $\delta^{13}C_{carb}$ values are probably related to a $^{13}C_{carb}$ sequestration into a later dolomitization phase from a calcitic precursor (Minoura, 1992). BIIc dolostones have generally high ^{13}C values resulting of an increase in net storage rates of organic carbon. The carbon isotopic composition of primary carbonate minerals can be incorporated in secondary calcite without any modification of ^{13}C concentration (Dickson and Coleman, 1980). Thus ^{13}C enrichment in BIIc evaporitic dolomites probably reflects a high level of 'heavy' carbon in the original carbonate phase.

The Sr/Ca elemental ratios and Mn concentrations provide a sensitive indication of diagenesis (Brand and Veizer, 1980; Veizer et al., 1983). **Fig. 10-A** shows a rapid drop of the Sr/Ca ratio followed by an increase of Mn abundance in all dolostones. Kah (2000) suggested that this Sr/Ca ratio fall and Mn increase are caused by carbonates mixed with meteoric, mixed waters or seawater-derived evaporitic brines. Sr/Ca ratios are less than 1.7×10^{-3} in average, well below present-day seawater ratio (8.6×10^{-3}). The low Sr/Ca ratios suggest that dolomitization was related to meteoric or freshwater Sr-depleted fluids (Pierson, 1981) or that the Sr/Ca ratios of the initial carbonates were low (Kah, 2000). Moreover, the low Sr concentrations in carbonates have been considered as an indicator of alteration by freshwater (Land and Epstein, 1970; Gross, 1964), while the high Sr concentrations are indicative of (i) precipitation in evaporitic environments, i.e. in the BIIb subgroup; (ii) detrital input; or (iii) contamination by diagenetic fluids, i.e. in the BIe and BIIe subgroups.

Fe concentrations, as Mn concentrations, reflect the redox state of the diagenetic environment (Azmy et al., 2001). Low Mn concentrations reflect weak interaction with Mn-rich diagenetic

fluids (Kah, 2000) compared with high Mn concentrations related to non-marine (reducing) dolomitizing fluids or *in situ* microbial Mn reduction of organic matter (Hendry, 1993). **Fig. 10-B** shows a non-covariant distribution between Mn and Fe concentrations in the BIIb and BIId subgroups, as compared with other subgroups. Fe and Mn concentration increase reflects redox conditions with significant Fe^{2+} amounts brought by diagenetic pore fluids or hydrothermal circulating fluids.

Mn concentration *vs.* $\delta^{18}O_{carb}$ composition reveals different patterns between meteoric, mixed-water diagenesis fluids and evaporitic brines (**Fig. 10-C**) and can therefore be used to infer the main driving diagenetic process. Dolomitization stabilisation through meteoric or mixed-water diagenesis should result in a rapid decrease in oxygen isotopic composition followed by increasing Mn as diagenesis evolves, providing reducing conditions and available source for Mn (Kah, 2000). In this paper, three trends are observed: (i) decrease of $\delta^{18}O_{carb}$ followed by Mn increase, indicative of meteoric or mixed-water diagenetic influences; (ii) increase of $\delta^{18}O_{carb}$ followed by minor Mn rising concentrations, indicative of evaporitic brines; and (iii) constant $\delta^{18}O_{carb}$ followed by Mn increase, indicative of early diagenetic alterations at the vadose/phreatic boundary (Allan and Matthews, 1982).

Mn/Sr *vs*. Rb/Sr ratios of all Mbuji-Mayi carbonates record therefore the degree of chemical alteration (Asmerom et al. 1991; Derry et al., 1992; Kaufman et al., 1993; Kuznetsov et al., 1997; Semikhatov et al., 1998; Bartley et al., 2001). In our paper, we considered that non-diagenetic carbonate rocks are characterized by Mn/Sr < 3 and Rb/Sr < 0.01 (dolostones), because most dolostones have low Sr contents, due to crystallographic exclusion of Sr, and Mn/Sr < 1 and Rb/Sr < 0.01 (limestones). Using these values, the BIIb, BIIc, except their shaly layers, and BIId subgroups are not or less altered than those of the BIe, BIIa and BIIe

subgroups (**Fig. 11**). Low Sr concentrations (between 50 and 100 ppm; **Fig. 12**) correspond to a large range of high $^{87}Sr/^{86}Sr$ ratios (0.712 to 0.729) compared to primary $^{87}Sr/^{86}Sr$ ratio of the Mbuji-Mayi Supergroup ranging between 0.705 and 0.710 (Demaiffe and Fieremans, 1981). Elevated $^{87}Sr/^{86}Sr$ ratios result from geochemical alteration of crustal materials (Derry et al., 1992), i.e. detrital clay from the riverine input, or attributed to hydrothermal circulating fluids in carbonates. The slightly low $^{87}Sr/^{86}Sr$ ratios correspond closely to non-radiogenic strontium signatures in late Neoproterozoic oceans, and suggest that Mbuji-Mayi carbonates preserved their marine compositions.

6.2.2. Attempts of correlation

According that $\delta^{13}C_{carb}$ values preserved primary marine signatures, $\delta^{13}C_{carb}$ data can be used as a stratigraphic tool for the late Mesoproterozoic - middle Neoproterozoic period. The Mbuji-Mayi Supergroup age is estimated, on base of $^{207}Pb/^{206}Pb$ and K-Ar ages between ~0.95 and ~1.16 Ga (Cahen, 1954; Holmes and Cahen, 1955; Raucq, 1957; Delhal et al., 1989; Cahen et al., 1974, 1984). The Mesoproterozoic-Neoproterozoic transition is poorly documented from carbon-isotope and radiometric ages. Bartley et al. (2001) and Frank et al. (2003) argued an increase in $\delta^{13}C_{carb}$ amplitude from middle to late Mesoproterozoic in Siberia and NE Canada. No precise composition has been defined for this age interval but marine conditions generally are between +3‰ and +5‰ $\delta^{13}C_{carb}$. Kah et al. (1999) suggested that $\delta^{13}C_{carb}$ isotopic composition of late Mesoproterozoic seawater was around +3‰. Halverson (2006) argued that sustained $\delta^{13}C_{carb} \geq 5‰$ did not start until early to middle Neoproterozoic as shown from Little Dal Group in Mackenzie Mountains (NW Canada), with low $\delta^{13}C_{carb}$ values from 0‰ to 5‰ in a ramp setting followed by high values (> 5‰) up to the onset of Bitter Springs anomaly. The Bitter Springs negative anomaly was firstly

documented in the Bitter Springs Formation in the Amadeus Basin of Central Australia (Hill et al., 2000) and correlated with the Akademikerbree Group in Svalbard (Halverson et al., 2005). This anomaly, defined by reciprocal $\delta^{13}C_{carb}$ negative shifts of > 8‰, is constrained to *ca*. 810 Ma (Halverson et al., 2005). The composite $\delta^{13}C_{carb}$ curve of Mbuji-Mayi carbonates (**Fig. 13**) shows precipitous declines in $\delta^{13}C_{carb}$ of the BIIc subgroup, followed by intervals with strong $\delta^{13}C_{carb}$ enrichments. The declines were estimated with negative shifts of 4.0‰ and 6.1‰. No glaciogenic sediments are associated with these negative $\delta^{13}C_{carb}$ values.

Moreover, strontium-isotope record through late Mesoproterozoic - early Neoproterozoic transition is presumably estimated to 0.7055 (Bartley et al., 2001) after $^{87}Sr/^{86}Sr$ isotopic limestone compilation of the Atar Group in the Taoundenni Basin (0.7056, Veizer et al., 1983), recently dated at 1.1 Ga (Rooney et al., 2010), the lower Little Dal Group (Halverson et al., 2007), and the Burovaya Formation in NW Siberia (0.7055; Gorokhov et al., 1995). $^{87}Sr/^{86}Sr$ ratio had risen from 0.7070 to 0.7063 with onset of the Bitter Springs anomaly. The Mbuji-Mayi $^{87}Sr/^{86}Sr$ composite profile for the unaltered samples (**Fig. 13**) ranges between 0.7069 and 0.7071 just before backstepping to the positive $\delta^{13}C_{carb}$ excursion in the BIIc subgroup. The base and end of the $\delta^{13}C_{carb}$ negative excursion vary from 0.7063 to 0.7074 (minor diagenetic effects) successively. Above, $^{87}Sr/^{86}Sr$ ratios increase from 0.7060 to 0.7081.

Our combined $\delta^{18}O_{carb}$, $\delta^{13}C_{carb}$, and $^{87}Sr/^{86}Sr$ data from the carbonate samples of the Mbuji-Mayi Supergroup, which preserved the primary marine signals, plotted against the Bitter Springs negative anomaly around *ca*. 810 Ma suggest that both successions are coeval. Other evidences, as appearance of new life forms, in particular the arcritarcha (Maithy, 1975) or the possible Sturtian diamictite of the Kabele and Kabenga Conglomerate in extreme south of the

SMLL Basin overlying the Mbuji-Mayi Supergroup, suggest also a pre-Sturtian age for these carbonates.

6.3. $^{40}Ar/^{39}Ar$ dating on dolerite

Based on a comparison of both experiments we retain the mean average of both highest apparent ages obtained, this is 882.2 ± 8.8 Ma, as the most reliable age estimate for the closure of the K-rich phase within this dolerite sample, likely to reflect the emplacement age of this dolerite. The lower saddle plateau age of 643.7 ± 6.7 Ma obtained during the second experiment can be invoked as referring to a Pan-African reactivation. This signature is however reflected by more retentive sites and therefore inferred to be the result of metamorphism.

7. Implication for the basin evolution

During the same time period, deposition of ~500 m and ~3000 m thick siliciclastic sediments is documented in the northern and southern parts of the SMLL Basin, respectively. According to the dominant zircon population (45.6%) within the BI group, the provenance areas of the detrital inputs were south-east and east (**Fig. 14**). This detrital zircon population represents a late Mesoproterozoic age range of between ~1.0 Ga-1.4 Ga, corresponding to the Kibaran orogenic event in Central Africa, but may also include detrital input from the KAB. The regional distribution and the sedimentological character of the BI successions suggest an intracratonic late Mesoproterozoic-early Neoproterozoic sedimentation, during which the KIB and/or KAB mountains were partially eroded with deposition of molasse in the SMLL Basin. The end of the BI group sedimentation is marked by an important change in the sedimentary

supply from a predominantly BI siliciclastic group to the deposition of the BII group carbonates. This period was constrained by the age of BIe galena mineralization at between 1040 and 1065 Ma (Cahen, 1954; Holmes and Cahen, 1955; Raucq, 1957).

The late Mesoproterozoic and early Neoproterozoic time period was marked by rifting along the southern and western margins of the Congo Craton related to break-up of the Rodinia Supercontinent, with the opening of the Adamastor Ocean (starting *ca.* 880 Ma ago; Tack et al., 2001) and subsequent passive margin-type sedimentation manifested by the Katanga Supergroup (Master and Wendorff, 2011) to the south and the West Congolian Group to the west (Tait et al., 2011). As suggested by geophysical studies (Kadima et al., 2011), the Mbuji-Mayi sedimentation started from late Mesoproterozoic to early Neoproterozoic times during a poorly defined intracratonic rifting stage that failed to develop into a real continental break-up.

Porada and Berhorst (2000) suggested that the Katangan Supergroup rifting started during the eastern opening of the proto-Mozambique ocean, which propagated westwards into the area of the Zambezi Belt, and thereafter northwestwards into the area of the Lufilian Belt. The basin widened allowing development of the Roan Group marine rift-basin (Afar/Red Sea type proto-ocean). The early rifting stage is marked by deposition of the siliciclastic Mindola Subgroup in Zambia, and the arenaceous-clayey-dolomitic 'R.A.T.' Subgroup in Katanga.

The transgression continued, firstly with deposition of Kitwe and Mines subgroups in Zambia and Katanga (**Fig. 15**), then followed by the Bancroft and Dipeta subgroups in Zambia and Katanga. The mixed siliciclastic-carbonate Dipeta Sugroup is interpreted as an infilling basin from the northern hinterland. The SMLL failed rift basin became more stable, at 1.0 Ga, with

deposition of ~1000 m thick transgressive carbonates on a possible passive margin. The low $\delta^{13}C_{carb}$ interval in the BIIc subgroup, coeval in age with the Bitter Srings anomaly at *ca*. 810 Ma, appears to be related to eustatic changes (Halverson et al., 2010) due to the possible reorganisation of ocean currents and changes in erosion and sedimentation resulting from a inertial interchange true polar wander event (Maloof et al., 2006). Similar eustatic changes including a 8 ‰ $\delta^{13}C$ positive shift during a 'long term' sea level transgression are observed in the BIIb and BIIc transition (Delpomdor et al., *in* revision). These authors highlighted relationships between the third-order cycles of sea level and $\delta^{13}C$ variations, and showed that (i) during 'long term' transgressive System Tracts (TST), circulation of ramp-top marine water masses was enhanced while effects of meteoric diagenesis on ramp-top carbonates were strongly reduced, causing an isotope shift towards higher more marine values, and a productivity increase due to increased global circulation; and (ii) during 'long term' Highstand System Tracts (HST), circulation of ramp-top marine water masses was reduced, and effects of meteoric diagenesis on ramp-top carbonates much increased, leading to a negative $\delta^{13}C$ shift.

The second rifting stage resulting from differential movements of northeastern plates (Congo and Tanzania cratons) allowed plate break-up propagating from more advanced eastern section of the Roan rift-basin leading to the opening of the Kundelungu rift aulacogen. it resulted an extensional basin trending northeasterwards along pre-existing Kibaran structures (Porada and Berhorst, 2000). The transgression is not recorded in the SMLL basin (**Fig. 15**), because no deposition is recorded. The rifting was accompanied by syn-rift basaltic volcanism with intrusions (dykes and sills) and flows (or aerial hyaloclastic basalts) of basalts during the transgression of the Mwashya Subgroup into the Kundelungu aulacogen and into the northeastern Roan platform. Similar intrusions reported in the Katanga and Bas-Congo

provinces, were dated successively at 765 ± 5 Ma, by U-Pb SHRIMP on basalts in the Mwashya Subgroup (Key et al., 2001), and 694 ± 4 Ma, by U-Pb baddeleyite TIMS analyses on doleritic sill intrusions (Straathof, 2011). An 882 ± 8.8 Ma $^{40}Ar/^{39}Ar$ age for the dolerite sill from the Lomami part of the SMLL Basin, crossing the Mbuji-Mayi Supergroup or between the BI and BII groups, suggest that the SMLL Basin was also affected by early Neoproterozoic extension within Rodinia as for Katangan series.

In response to the opening and rapid subsidence of the extensional Kundulungu aulacogen, elevated margins offered favourable conditions for inland glaciation during the Sturtian glaciation. The possible Sturtian diamictite of the Kabele and Kabenga Conglomerate (Cahen and Mortlemans, 1947) overlying the Mbuji-Mayi Supergroup in the extreme south of the SMLL Basin suggest a pre-Sturtian age for these carbonates (**Fig. 15**). Kabele and Kabenga Conglomerate with more than 50% fragments of Mbuji-Mayi carbonates, may be considered as equivalent to the Grand Conglomérat Formation in Katanga (Cahen and Mortelmans, 1947), and reflected the instability of the basin.

8. Paleoclimate in the late Mesoproterozoic - middle Neoproterozoic (1300 Ma-800 Ma)

The paleoclimate is poorly constrained during the late Mesoproterozoic - middle Neoproterozoic times (1300 Ma-800 Ma). However, the end of the Mesoproterozoic Era (*ca*. 1250 Ma-1300 Ma; e.g. in the early Upper Riphean to Middle Riphean Uchur-Maya and Turukhansk Uplift in Siberia; Bartley et al., 2001) is marked by a subsequent $\delta^{13}C$ increase related to the change in atmospheric oxygen content associated with the break-up of the Rodinia (Des Marais et al., 1992; Canfield, 1999). This positive $\delta^{13}C$ shift reflects increased

biomass and/or increased burial of isotopically light organic matter (Knoll, 1992; Hoffman, 1999).

Hayes et al. (1999) and Rothman et al. (2003) discussed values of the isotopic fractionation between the carbonate carbon and organic carbon (ε_{TOC}) through the last 800 Ma, as useful indicator for the geochemistry of the ocean-atmosphere systems. Halverson et al. (2005) demonstrated that ε_{TOC} variations are a consequence of an unusually large oceanic reservoir of organic carbon during this period (Rothman et al., 2003). ε_{TOC} values of +28‰ to +30‰ in limestones are typical for much of Neoproterozoic and Phanerozoic records, usually associated with warm periods, oxic bottom waters and relatively high CO_2 atmospheric content. ε_{TOC} values of +32‰ to +34‰ (i.e. recording a 4‰ increase from normal values) are associated with strong diagenetic effects on $\delta^{13}C_{org}$, and imply that significant inputs of sulfide oxidizing or chemoautotrophic bacteria occurred during Neoproterozoic interglacials (Hayes et al., 1999). In contrast, low ε_{TOC} values are less common and usually associated with cooler periods of Earth history - including Sturtian and Marinoan glaciations, low levels of atmospheric CO_2, and rapid phytoplanktonic growth rates and/or high volume ratios of cells to surface area (Alene et al., 2006). In our study, the Mbuji-Mayi carbonates show an average ε_{TOC} value of +28.6‰, high values between +30.4‰ and +32.9‰ are measured in the BIIc subgroup. This suggests that the Mbuji-Mayi carbonates were deposited during warm periods. Moreover, sedimentary features, such as chicken-wire structures and evaporites (gypsum, anhydrite, halite) suggest a hot and arid climate (Delpomdor et al., *in* revision). However, the BIIb and BIId subgroups are interpreted as ephemeral supratidal lacustrine ponds, seasonally flooded by marine water with precipitation of evaporitic minerals during dried season, and development of cyanobacterial mats and stratiform stromatolites during wet season, temporarily affected by meteoric influx during humid periods (Delpomdor et al., *in* revision;

Delpomdor et al., submitted). An example can be found in marine levels of the Bitter Springs Formation in Central Australia, which we believe is coeval in age with the Mbuji-Mayi carbonates, where $\delta^{13}C_{org}$ have relatively normal values of −28 to −30‰ with $\varepsilon_{TOC} \approx +28‰$. Associated evaporites in the Australian sequence suggested hot and arid environments (Hill et al., 2000). Alene et al. (2006) suggested that low ε_{TOC} must reflect differences in regional factors (temperature or biologic parameters) rather than CO_2 concentrations, which would be the same globally.

9. Conclusion

The span of geologic time that streches from the late Mesoproterozoic through the middle Neoproterozoic (1300 Ma-800 Ma) heralded extraordinary climatic and biological changes related to the tectonic changes that resulted in the assembly and the break-up of Rodinia. During late Mesoproterozoic to early Neoproterozoic times, the eastern margin of the Congo Craton is marked by the *ca*. 880-850 Ma continental break-up of Rodinia, which probably started at the newly eastern passive margin formed during the opening of the proto-Mozambique ocean. A post-rift differential subsidence, related to transgression from the southeast, controlled sedimentation, marked by deposition of the Roan Group in the Zambezi and Katanga basins, and of possible correlatives in the failed-rift of the Sankuru-Mbuji-Mayi-Lomami-Lovoy Basin of the Mbuji-Mayi Supergroup.

The Mbuji-Mayi Supergroup is divided into ~500 to ~3000 m thick of siliciclastic BI group and ~1000 m thick of carbonate BII group deposited in warm periods interlaced with temporarily dry and wet seasons. These late Mesoproterozoic - middle Neoproterozoic (1152 Ma – *ca*. 800 Ma) climatic conditions are indicative of a greenhouse world, with the

equatorial currents encircling the globe, favouring the exchange of tropical and polar waters. The age of the Mbuji-Mayi Supergroup is constrained by new LA-ICP-MS U-Pb data obtained from 355 detrital zircon grains in BI siliciclastics combined with C-O-Sr chemostratigraphical data from 246 samples of BII carbonates. New $^{40}Ar/^{39}Ar$ data constrain the minimum age of the Mbuji-Mayi Supergroup. These data show that:

(i) the minimum U-Pb age on detrital zircon grains from the BId subgroup is 1174 ± 22 Ma. This age is concordant with the maximum age of 1152 ± 15 Ma in the Kibaran Belt Supergroup established by K-Ar methods on biotite, pyroxene and amphibole from E-W trending syenodiorite dykes which outcrop in the eastern part of the Lulua complex (Delhal et al., 1989);

(ii) the main sedimentary sources of the BI group of the Sankuru-Mbuji-Mayi-Lomami-Lovoy Basin came from the Kibaran Belt and/or Karagwe-Ankole Belt supergoups, the Bangweulu block and the Kasai block. They indicate a detrital transport from the south-east and/or east;

(iii) the ~1000 m thick transgressive carbonates show negative shifts in $\delta^{13}C_{carb}$ of 4.0‰ and 6.1‰, followed by a $\delta^{13}C_{carb}$ increase in the BIIc subgroup. The Mbuji-Mayi $^{87}Sr/^{86}Sr$ composite profile ranges between 0.7069 and 0.7071 preceding backstepping to positive $\delta^{13}C_{carb}$ excursion in the BIIc subgroup. These $^{87}Sr/^{86}Sr$ values are 'coeval' with the rise of $^{87}Sr/^{86}Sr$ ratios from 0.7070 to 0.7063 during the onset of the Bitter Springs anomaly (~810 Ma);

(iv) the BII group can be correlated with the upper Mines and Dipeta subgroups between 750-880 Ma;

(v) a $^{40}Ar/^{39}Ar$ age of 882.2 ± 8.8 Ma for the dolerite sill from the Lomami part of the Sankuru-Mbuji-Mayi-Lomami-Lovoy Basin, crossing the Mbuji-Mayi Supergroup

or between the BI and BII groups, suggests that the Sankuru-Mbuji-Mayi-Lomami-Lovoy Basin was also affected by early Neoproterozoic extension of the Kundelungu aulacogen.

Acknowledgements

Financial support from the TOTAL PhD scholarship (grant ULB/TOTAL-FR00003322) is gratefully acknowledged. The Royal Museum for Central Africa (RMCA, Belgium) is thanked for providing samples from the Mbuji-Mayi Supergroup, and De Beers Exploration for the core samples of the 'Lomami' dolerite sill.

References

Alene, M., Jenkin, G.R.T., Leng, M.J., Darbyshire, D.P.F, 2006. The Tambian Group, Ethiopia: An early Cryogenian (*ca*. 800-735Ma) Neoproterozoic sequence in the Arabian-Nubian Shield. Precambrian Research 147, 79-99.

Alkmim, F.F., Marshak, S., Pedrosa-Soares, A.C., Peres, G.G., Pereira Cruz, S.C., Whittington, A., 2006. Kinematic evolution of the Araçuai-West Congo orogen in Brazil and Africa: nutcracker tectonics during the Neoproterozoic assembly of Gondwana. Precambrian Research 149, 43–64.

Alkmim F.F., Pedrosa-Soares A.C., Noce C.M., Cruz S.C.P., 2007. Sobre a evolução tectônica do Orógeno Araçuaí-Congo Ocidental. Geonomos 15, 25-43.

Allan, J.R., Matthews, R.K., 1982. Isotope signatures associated with early meteoric diagenesis. Sedimentology 29, 797-817.

Andersen, L.S., Unrug, R., 1984. Geodynamic evolution of the Bangweulu Block, northern Zambia. Precambrian Research 25, 187–212.

Armstrong, R.A., Master, S., Robb, L.J., 2005. Geochronology of the Nchanga Granite and constraints on the maximum age of the Katanga Supergroup, Zambian Copperbelt. Journal of African Earth Sciences 42, 32-40.

Asmerom, Y., Jacobsen, S., Knoll, A.H., Butterfield, N.J., Swett, K., 1991. Strontium isotope variations of Neoproterozoic seawater : implications for crustal evolution. Geochimica et Cosmochimica Acta 55, 2883-2894.

Azmy, K., Veizer, J., Misi, A., de Oliveira, T.F., Sanches, A.L., Dardenne, M.A., 2001. Dolomitization and isotope stratigraphy of the Vazante Formation, Sao Francisco Basin, Brazil. Precambrian Research 112, 303-329.

Bartley, J.K., Semikhatov, M.A., Kaufman, A.J., Knoll, A.H., Pope, M.C., Jacobsen, S.B., 2001. Global events across the Mesoproterozoic-Neoproterozoic boundary: C and Sr isotopic evidence from Siberia. Precambrian Research 111, 165-202.

Batumike, J.M., Griffin, W.L., O'Reilly, S.Y. Belousova, E.A., Pawlitschek, M., 2009. Crustal evolution in the central Congo-Kasai Craton, Luebo, D.R. Congo: Insights from zircon U-Pb ages, Hf-isotope and trace-element data. Precambrian Research 170, 107-115.

Begg, G.C., Griffin, W.L., Natapov, L.M., O'Reilly, S.Y., Grand., S.P., O'Neill, C.J., Hronsky, J.M.A., Poudjom Djomani, Y., Swain, C.J., Deen, T., Bowden, P., 2009. The lithospheric architecture of Africa: Seismic tomography, mantle petrology, and tectonic evolution. Geosphere 5 (1), 23-50.

Bertrand-Sarfati, J., 1972. Stromatolites columnaires de certaines formations carbonatées du Précambrien supérieur du basin congolais (Bushimay, Lindien, Ouest-Congolien). Annales du Musée royal de l'Afrique Centrale, Tervuren, Belgique, Série in-8 - n° 74, 45 pp.

Bond, G.C., Nickeson, P.A., Kominz, M.A., 1984. Breakup of a supercontinent between 625 and 555 Ma: new evidence and implications for continental histories. Earth and Planetary Science Letters 70, 325-345.

Boven, A., Theunissen, K, Sklyarov, E.V., Klerkx, J., Melnikov, A., Mruma, A., Punzalan, L., 1999. Timing of exhumation of a high-pressure mafic granulite terrane of the Palaeoproterozoic Ubende belt (West Tanzania). Precambrian Research 93, 119-137.

Brand, U., Veizer, J., 1980. Chemical diagenesis of a multicomponent carbonate system, 1. Trace elements. Journal of Sedimentary Petrology 50, 1219–1236.

Brasier, M., McCarron, G., Tucker, R., Leather, J., Allen, P., Shields, G., 2000. New U-Pb zircon dates for the Neoproterozoic Ghubrah glaciation and for the top of the Huqf Supergroup, Oman. Geology 28, 175-178.

Brewer, M.S., Haslam, H.W., Darbyshire, D.P.F., Davis, A.E., 1979. The petrology and geochronology of hypersthene granites in the Mchinji area, Malawi. Report of Institute Geological of Sciences 79 (1).

Buchwaldt, R., Toulkeridis, T., Todt, W., Ucakuwun, E.K., 2008. Crustal age domains in the Kibaran belt of SW-Uganda: Combined zircon geochronology and Sm-Nd isotopic investigation. Journal of African Earth Sciences 51, 4-20.

Burke, W., Denison, R., Hetherington, E, Koepnik, R., Nelson, M., Omo, J., 1982. Variations of seawater $^{87}Sr/^{86}Sr$ throughout Phanerozoic shales. Geology 10, 516-519.

Burret, C., Berry, R., 2000. Proterozoic Australia-Western United-States (AUSWUS) fit between Laurentia and Australia. Geology 28 (2), 103-106.

Cahen, L., 1954. Extension et âge d'une minéralisation Cu, Pb, Zn en Afrique centrale et australe. Bulletin de la Société belge de Géologie, Hydrologie, Paléontologie 63, 89–100.

Cahen, L., Mortelmans, G., 1947. Le système de la Bushimaie au Katanga. Bulletin de la Société belge de Géologie, Hydrologie, Paléontologie 56, 217-253.

Cahen, L., Lepersonne, J., 1967. The Precambrian of the Congo, Rwanda and Burundi. In: Rankama, K. (Ed.), The Precambrian, Interscience Publication 3, pp. 143-290.

Cahen, L., Delhal, J., Deutsch, S., 1967. Rubidium-strontium geochronology of some granitic rocks from the Kibaride Belt (Central Katanga, Républic of Congo). Annales du Musée royale de l'Afrique Centrale, Tervuren, Belgique 59, 11–65.

Cahen, L., Ledent, D., Snelling, N.J., 1974. Données géochronologiques dans le Katangien inférieur du Kasai oriental et du Shaba nord-oriental (République du Zaïre). Musée royal de l'Afrique Centrale, Tervuren, Rapport annuel du Département de Géologie et de Minéralogie, 59-70.

Cahen, L., Snelling, N.J., Delhal, J. Vail, J.R., 1984. Geochronology and Evolution of Africa. Clarendon Press, Oxford, 512 pp.

Calver, C.R., 1998. Isotope stratigraphy of the Neoproterozoic Togari Group, Tasmania. Australian Journal of Earth Sciences 45, 865-874.

Canfield, D.E., 1999. A new model for Proterozoic ocean chemistry. Nature 396, 450-453.

Dalziel, I.W.D., 1991. Pacific margins of Laurentia and East Antarctica-Australia as a conjugate rift pair: evidence and implication for an Eocambrian supercontinent. Geology 19, 598-601.

Dalziel, I.W.D., 1997. Neoproterozoic-Paleozoic geography and tectonics: Review, hypothesis and environmental speculation. Bulletin of Geological Society of America 109, 16-42.

Delhal, J., Liégeois, J.-P., 1982. Le socle granito-gneissique du Shaba occidental (Zaïre) - Pétrographie et géochronologie. Annales de la Société Géologie de Belgique 105, 295–301.

Delhal, J., Deutsch, S., Snelling, N.J., 1989. Datation du Complexe sédimentaire et volcanique de la Lulua (Protérozoïque inférieur, Kasai, Zaïre). Musée royal de l'Afrique Centrale, Tervuren (Belgique), Département de Géologie et de Minéralogie, Rapport Annuel 1987-88, 93-99.

Delhal, J., 1991. Situation géochronologique 1990 du Précambrien du sud-Kasai et de l'ouest-Shaba. Musée royal de l'Afrique Centrale, Tervuren (Belgique), Rapport Annuel 1989-1990, 119-125.

Delpomdor, F., Préat, A., 2012. Hydrocarbon reservoir potential of Neoproterozoic carbonates in the Mbuji-Mayi Supergroup (Sankuru-Bushimay area), Democratic Republic of Congo: stratigraphy, sedimentology, geochemistry, petrophysics. ULB/Total-FR00003322, 276pp. (unpublished, confidential document).

Delpomdor, F., Blanpied, C., Virgone, A., Préat, A, *in* revision. Early Neoproterozoic carbonate succession of Mbuji-Mayi Supergroup in Democratic Republic of Congo: sedimentology, chemostratigraphy and sequence stratigraphic framework. In: De Wit, M., Guillocheau, F. (Eds.), The Geology and Resource Potential of the Congo Basin: Geology and Resource Potential of the Congo Basin.

Delpomdor, F., Blanpied, C., Virgone, A., Préat, A., submitted to the Journal African Earth Sciences. Paleoenvironments in Neoproterozoic Mbuji-Mayi carbonates from the Democratic Republic of Congo – Microfacies analysis combined with C-O-Sr isotopes, major-trace elements and REE+Y distributions.

Demaiffe, D., Fieremans, M., 1981. Strontium-isotopic geochemistry of the Mbuji Mayi and Kundelungu kimberlites (Zaire, Central Africa). Chemical Geology 31, 311-323.

Derry, L.A., Kaufman, A.J., Jacobsen, S.B., 1992. Sedimentary cycling and environmental change in the Late Proterozoic: evidence from stable and radiogenic isotopes. Geochimica et Cosmochimica Acta 56, 1317-1329.

Des Marais, D.J., 1994. Tectonic control of the crustal organic carbon reservoir during the Precambrian. Chemical Geology 114, 303-314.

Des Marais, D.J., Strauss, H., Summons, R.E., Hayes, J.M., 1992. Carbon isotope evidence for the stepwise oxidation of the Proterozoic environment. Nature 359, 605-609.

De Waele, B., 2005. The Proterozoic geological history of the Irumide belt, Zambia. PhD Thesis, Curtin University of Technology, Perth, 468 pp.

De Waele, B., Fitzsimons, J.C.W., 2007. The nature and timing of Palaeoproterozoic sedimentation at the southearn margin of the Congo Craton. Precambrian Research, 159, 95-116.

Dickson, J.A.D., Coleman, M.L., 1980. Changes in carbon and oxygen isotope composition during limestone diagenesis. Sedimentology 27, 107-118.

Fairchild, I.J., Marshall, J.D., Bertrand-Sarfati, J., 1990. Stratigraphic shifts in carbon isotopes from Proterozoic stromatolitic carbonates (Mauritania): influences of primary mineralogy and diagenesis. American Journal of Science 291-A, 46-79.

Fernandez-Alonso, M., Cutten, H., De Waele, B., Tack, L., Tahon, A., Baudet, D., Barrit, S.D., 2012. The Mesoproterozoic Katagwe-Ankole Belt (former NE Kibaran belt): the result of prolonged extensional intracratonic basin development punctuated by two short-lived far-field compressional events. Precambrian Research 216-219, 63-86.

Fitzsimons, I.C.W., 2000. A review of tectonic events in the East Antarctic shield, and their implications for Gondwana and earlier supercontinents. Journal of African Earth Sciences 31, 3-23.

Frank, T.D., Kah, L.C., Lyons, T.W., 2003. Changes in organic matter production and accumulation as a mechanism for isotopic variation in the Mesoproterozoic ocean. Geological Magazine 140, 397-420.

Gérard, J., Ledent, D., 1970. Grands traits de la géologie du Rwanda. Différents types des roches granitiques et premières données sur les âges de ces roches. Annales de la Société Géologie de Belgique 93, 477–489.

Gorokhov, I.M., Semikhatov, M.A., Baskakov, A.V., Kutyavin, E.P., Mel'nikov, N.M., Sochava, A.V., Turchenko, T.L., 1995. Sr isotopic composition in Riphean, Vendian, and Lower Cambrian carbonates from Siberia. Stratigaphy and Geological Correlation 3, 1-28.

Gray, D.R., Foster, D.A., Meert, J.G., Goscombe, B.D., Armstrong, R., Trouw, R.A.J., Passchier, C.W., 2008. A Damara orogen perspective on the assembly of southwestern Gondwana. Geological Society, London, Special Publications 294 (1), 257-278.

Gross, M.G., 1964. Variations in the $^{18}O/^{16}O$ and $^{13}C/^{12}C$ ratios of diagenetically altered limestones in the Bermuda Island. Geology 72, 170–194.

Halverson, G.P., 2006. A Neoproterozoic chronology. In: Xiao, S, Kaufman, A. (Eds.), Neoproterozoic Geobiology and Paleobiology. Topics in Geobiology 27, Springer, New York, pp. 231-271.

Halverson, G.P., Dudas, F.O., Maloof, A.C., Bowring, S.A., 2007. Evolution of the $^{87}Sr/^{86}Sr$ composition of Neoproterozoic seawater. Palaeogeography, Palaeoclimatology, Palaeoecology 256, 103-129.

Halverson, G.P., Hoffman, P.F., Schrag, D.P., Maloof, A.C., Rice, A.H.N., 2005. Towards a Neoproterozoic composite carbon isotope record. Geological Society of America Bulletin 117, 1181–1207.

Halverson, G.P., Hurtgen, M.T., Porter, S.M., Collins, A.S., 2010. Neoproterozoic-Cambrian Biogeochemical Evolution. In: Gaucher, C., Sial, A.N., Frimmel, H.E., Halverson, G.P. (Eds.), Neoproterozoic-Cambrian

Tectonics, Global Change And Evolution: A Focus On South Western Gondwana. Developments in Precambrian Geology 16, pp. 351-365.

Hanson, R.E., Wilson, T.J., Wardlaw, M.S., 1988. Deformed batholiths in the Pan-African Zambezi Belt, Zambia: Age and implications for regional Proterozoic tectonics. Geology 16, 1134-1137.

Hayes, J.M., Strauss, H., Kaufman, A.J., 1999. The abundance of ^{13}C in marine organic matter and isotopic fractionation in the global biogeochemical cycle of carbon during the past 800 Ma. Chemical Geology 161, 103–126.

Hendry, J.P., 1993. Calcite cementation during bacterial manganese, iron and sulphate reduction in Jurassic shallow marine carbonates. Sedimentology 40, 87–106.

Hill, A.C., Arouri, K., Gorjan, P., Walter, M.R., 2000. Geochemistry of marine and non-marine environments of a Neoproterozoic cratonic carbonate/evaporite: The Bitter Springs Formation, Central Australia. In: Grotzinger, J.P., James, N.P. (Eds.), Carbonate Sedimentation and Diagenesis in an Evolving Precambrian World, Tulsa, Society and Economic Palaeontologists and Mineralogists, Special Publication 67, pp. 327–344.

Hoffman, P.F., 1991. Did the breakout of Laurentia turn Gondwanaland inside-out? Science 252, 1409-1412.

Hoffman, P.F., 1999. The breakup of Rodinia, birth of Gondwana, true polar wander, and the Snowball Earth. Journal of African Earth Sciences 28, 9-26.

Hoffman, P.F., Schrag, D.P., 2002. The snowball Earth hypothesis: testing the limits of global change. Terra Nova 14, 129-155.

Hoffman, P., Kaufman, A., Halverson, G., Schrag, D., 1998. A Neoproterozoic snowball Earth. Science 281, 1342-1346.

Holmes, A., Cahen, L., 1955. African geochronology. Colonial Geology and Mineral Resources 5(1), 3-38.

Jacobsen, S.B., Kaufman, A.J., 1999. The Sr, C and O isotopic evolution of Neoproterozoic seawater. Chemical Geology 161, 37-57.

Johnson, S.P., Rivers, T., De Waele, B., 2005. A review of the Mesoproterozoic to Early Paleozoic magmatic and tectonothermal history of Central Southern Africa: Implications for Rodinia and Gondwana. Journal of the Geological Society 162, 433-450.

Kabengele, M., Lubala, R.T., Cabanis, B., 1991. Caractérisation pétrologique et géochimique du magmatisme ubendien du secteur de Pepa-Lubumba, sur le plateau des Marungu (Nord-Est du Shaba, Zaire). Signification géodynamique dans l'évolution de la chaîne ubendienne. Journal of African Earth Sciences 13, 243–265.

Kadima, E., Delvaux, D., Sebagenzi, S.N., Tack, L., Kabeya, M., 2011. Structure and geological history of the Congo Basin: An integrated interpretation of gravity, magnetic and reflection seismic data. Basin Research, 23, 499-527.

Kah, L.C., 2000. Depositional $\delta^{18}O$ signatures in Proterozoic dolostones: constraints on seawater chemistry and early diagenesis. In: Grotzinger, J.P., James, N.P. (Eds.), Carbonate Sedimentation and Diagenesis in the Evolving Precambrian World. Society and Economic Paleontologists and Mineralogists, Special Publication 67, pp. 345–360.

Kah, L.C., Sherman, A.B., Narbonne, G.M., Kaufman, A.J., Knoll, A.H., James, N.P., 1999. $\delta^{13}C$ isotope stratigraphy of the Mesoproterozoic Bylot Supergroup, Northern Baffin Island: Implications for regional lithostratigraphic correlations. Canadian Journal of Earth Sciences 36, 313-332.

Kampunzu, A.B., Rumvegeri, B.T., Kapenda, D., Lubala, R.T., Caron, J.P., 1986. Les Kibarides d'Afrique centrale et orientale: une chaîne de collision. UNESCO, Geology for Economic Development Newsletter 5, 125–137.

Kapenda, D., Kampunzu, A.B., Canabis, B., Namegabe, M., Tshimanga, K., 1998. Petrology and Geochemistry of Post-Kinematic Mafic Rocks from the Palaeoproterozoic Ubendian Belt, NE Katanga (DRC). Geologische Rundschau 87, 345–362.

Karlstrom, K.E., Harlan, S.S., Williams, M.L., McClelland, J., Geissman, J.W., Ahall, K.-I., 1999. Efining Rodinia: geologic evidence for the Australia-western US connection in the Proterozoic. Geological Society of America Today 9 (10), 1-7.

Kaufman, A.J., Knoll, A.H., 1995. Neoproterozoic variations in the C-isotopic composition of seawater: stratigraphic and biogeochemical implications. Precambrian Research 73, 27-49.

Kaufman, A.J., Jacobsen, S.B., Knoll, A.H., 1993. The Vendian record of Sr and C isotopic variations in seawater: Implications for tectonics and paleoclimate. Earth and Planetary Science Letters 120, 409-430.

Kaufman, A.J., Knoll, A.H. Narbonne, G.M., 1997. Isotopes, ice ages, and terminal Proterozoic earth history. Proceedings of the National academy of Sciences of the United States of America 95, 6600-6605.

Kaufman, A.J., Jiang, G., Christie-Blick, N., Banerjee, D.M., Rai, V., 2006. Stable isotope of the terminal Krol platform in the Lesser Himalayas of northern India. Precambrian Research 147 (1-2), 156-185.

Key, R.M., Liyungu, A.K., Njamue, F.M., Somwe, V., Banda, J., Mosley, P.N., Armstrong, R.A., 2001. The western arm of the Lufilian Arc in NW Zambia and its potential for copper mineralization. Journal of African Earth Sciences 33, 503–528.

Kirschvink, J., 1992. Late Proterozoic low-latitude glaciation: the Snowball Earth. In: Schopf, J., Klein, C. (Eds.), The Proterozoic Biosphere. Cambridge University Press, pp. 51-52.

Knauth, L.P., Kennedy, M.J., 2009. The late Precambrian greening of the Earth. Nature 460, 728–731.

Knoll, A.H., 1992. Biological and geochemical preludes to Ediacaran radiation. In: Lipps, J.H., Signor, P.W. (Eds.), Origin and Early evolution of the Metazoa. Topics in Geobiology 10, Plenum, New York, pp. 53-84.

Knoll, A.H., Kaufman, A.J., Semikhatov, M.A., 1995. The carbon isotopic composition of Proterozoic carbonates: Riphean successions from Northwestern Siberia (Anabar Massif, Turukhansk uplift). American Journal of Science 295, 823-850.

Knoll, A., Hayes, J., Kaufman, A., Swett, K., Lambert, I., 1986. Secular variation in carbon isotope ratios from Upper Proterozoic successions of Svalbard and east Greenland. Nature 321, 832-837.

Kokonyangi, J., Armstrong, R.A., Kampunzu, A.B., Yoshida, M., 2001. SHRIMP U–Pb zircon geochronology of granitoids in the Kibaran type area, Mitwaba-Central Katanga (Congo). Gondwana Research 4, 661–663.

Kokonyangi, J., Armstrong, R.A., Kampunzu, A.B., Yoshida M., Okudaira, T., 2004. U–Pb zircon geochronology and petrology of granitoids from Mitwaba (Katanga, Congo): implications for the evolution of the Mesoproterozoic Kibaran belt. Precambrian Research 132, 79–106.

Kokonyangi, J., Kampunzu, A.B., Okudaira, T., Yoshida, M., Shabeer, K.P., 2005. Geochronology and petrology of Mesoproterozoic mafic rocks from Mitwaba (Central Katanga, Congo): implications for the evolution of the Kibaran belt. Geological Magazine 142, 109–130.

Kokoyangi, J.W., Kampuzu, A.B., Armstrong, R., Yoshida, M., Okudaira, T., Arima, M., Ngulube, D.A., 2006. The Mesoproterozoic Kibaride belt (Katanga, SE D.R. Congo). Journal of African Earth Sciences 42, 1-35.

Kuznetsov, A.B., Gorokhov, I.M., Semikhatov, M.A., Melnikov, N.N., Kozlov, V.I., 1997. Strontium isotopic composition from the Inzer Formation limestones, the Upper Riphean type section in southern Urals. Transactions. Russian Academy Science, Earth Science Section 353, 319-324.

Land, L.S., Epstein, S., 1970. Late Pleistocene diagenesis and dolomitization, North Jamaica. Sedimentology 14, 184-200.

Ledent, D., 1979. Données géochronologiques relatives aux granites Kibariens de type A ou G1 et B ou G2 du Shaba, du Rwanda, du Burundi et du Sud-Ouest de l'Ouganda. Musée royal de l'Afrique Centrale, Tervuren, Département de Géologie et Minéralogie, Rapport annuel 1978, 101–105.

Lenoir, J.L., Liégeois, J.-P., Theunissen, K., Klerkx, J., 1994. The Palaeoproterozoic Ubendian shear belt in Tanzania: geochronology and structure. Journal of African Earth Sciences 19, 169–184.

Li, Z.X., Bogdanova, S.V., Collins, A.S., Davidson, A., De Waele, B., Ernst, R.E., Fitsimons, I.C.W., Fuck, R.A., Gladkochub, D.P., Jacobs, J., Karlstom, K.E., Lu, S., Natapov, L.M., Pease, V., Pisarevsky, S.A., Thrane, K., Vernikovsky, V., 2008. Assembly, configuration, and break-up history of Rodinia: A synthesis. Precambrian Research 160 (1-2), 179-210.

Lonchampt, D., Heinry, C., 1972. Rapport Bureau des Recherches Géologique et Minière, Mission Shaba Nord, deuxième campagne 1971, 50 pp.

Ludwig, K.R., 2001. Users manual for Isoplot/Ex Rev. 2.49. Berkeley Geochronology Center Special Publication 1a, 1–56.

Maithy, P.K., 1975. Micro-organisms from the Bushimay system (Late Precambrian) of Kanshi, Zaire. The Paleobotanist 22, 133-149.

Maloof, A., Halverson, G., Kirschvink, J., Weiss, D.S.B., Hoffman, P., 2006. Combined paleomagnetic, isotopic and stratigraphic evidence for true polar wander from the Neoproterozoic Akademikerbreen Group, Svalbard. Geological Society of America 118, 1099-1124.

Master, S., Wendorff, M., 2011. Neoproterozoic glaciogenic diamictites of the Katanga Supergroup, Central Africa. In: Arnaud, E., Halverson, G.L., Shields-Zhou, G. (Eds.), The Geological Record of Neoproterozoic Glaciations. Geological Society Memoir, London 36, pp. 173-184.

McKirdy, D.M., Burgess, J.M., Lemon, N.M., Yu, X., Cooper, A.M., Gostin, V.A., Jenkins, R.J.F., Both, R.A., 2001. A chemostratigraphic overview of the late Cryogenian interglacial sequence in the Adelaide Fold-Thrust Belt, South Australia. Precambrian Research 106, 149-186.

McMenamin, M.A.S., McMenamin, D.L.S, 1990. The emergence of Animals: The Cambrian Breakthrough. Columbia University Press, New York, 217 pp.

Meert, J.G., 2003. A synopsis of events related to the assembly of eastern Gondwana. Tectonophysics 362, 1-40.

Melezhik, V., Gorokhov, I, Kuznetsov, A., Fallick, A., 2001. Chemostratigraphy of Neoproterozoic carbonates: implications for 'blind dating'. Terra Nova 13, 1-11.

Minoura, K., 1992. Dolomitization of Permian reef carbonates in a Jurassic subduction complex, central Japan. Sedimentary Geology 80, 41-52.

Montanez, I., Banner, J., Osleger, D., Borg, L., Bosserman, P., 1996. Integrated Sr isotope variations and sea-level history of Middle and Upper Cambrian platform carbonates: implications for the evolution of Cambrian seawater $^{87}Sr/^{86}Sr$. Geology 24, 917-920.

Moores, E.M., 1991. Southwest U.S.-East Antarctic (SWEAT) connection: a hypothesis. Geology 19, 425-428.

Mortelmans, G., 1951. Stratigraphie et tectonique des Monts de Kibara dans la région Mitwaba-Kina. Bulletin de la Société belge de Géologie 59, 359–382.

Narbonne, G.M., Kaufman, A.J., Knoll, A.H., 1994. Integrated chemostratigraphy and biostratigraphy of the Windermere Supergroup, northwestern Canada: Implications for Neoproterozoic correlations and the early evolution of animals. Geological Society of American Bulletin 106, 1281–1292.

Pedrosa-Soares, A.C., Noce, C.M., Wiedemann, C.M., Pinto, C.P., 2001. The Araçuaí-West Congo orogen in Brazil: An overview of a confined orogen formed during Gondwanland assembly. Precambrian Research 110, 307-323.

Pedrosa-Soares, A.C., Noce, C.M., Alkmim, F.F., Silva, L.C., Babinski, M., Cordani, U., Castañeda, C., 2007. Orógeno Araçuaí: síntese do conhecimento 30 anos após Almeida 1977. Geonomos 15, 1-16.

Pedrosa-Soares, A.C., Alkmin, F.F., 2011. How many rifting events preceded the development of the Araçuai-West Congo orogen? Geonomos 19 (2), 244-251.

Pierson, B.J., 1981. The control of cathodoluminescence in dolomite by iron and manganese. Sedimentology 28, 601-610.

Pinna, P., Cocherie, A., Thieblemont, D., Feybesse, J.-L., Lagny, Ph., 1996. Evolution géodynamique du Craton Est-Africain et déterminisme gîtologique. Geodynamic evolution and metallogenic controls in the East-African Craton (Tanzania, Kenya, Uganda). Bureau des Recherches Géologiques et Minières, Chroniques des Recherches Minières 525, 33-43.

Piper, J.D.A., 1976. Palaeomagnetic evidence for a Proterozoic supercontinent. Philosophical Transactions of the Royal Society, London A280, 469-490.

Piper, J.D.A., 2000. The Neoproterozoic supercontinent: Rodinia or Palaeopangea? Earth and Planetary Science Letters 176, 131-146.

Pisarevsky, S.A., Wingate, M.T.D., Powell, C.M., Johson, S., Evans, D.A.D., 2003. Models of Rodinia assembly and fragmentation. Geological Society of London, Special Publications 206 (1), 35-55.

Podkovyrov, V.N., Semikhatov, M.A., Kuznetsov, A.B., Vinogradov, D.P., Kozlov, V.I., Kislova, I.V., 1998. Carbonate carbon isotopic composition in the Upper Riphean Stratotype, the Karatau Group, Southern Urals. Stratigraphy and Geological Correlation 6, 319-335.

Polinard, E., 1929. Les gisements plombo-cuprifères de la Lubi et de la Lukala. Leur genèse et leurs rapports avec la stratigraphie de la région. Annales de la Société Géologique de Belgique, Publication Relative au Congo Belge 48, 41-123.

Porada, H., Berhorst, V., 2000. Towards a new understanding of the Neoproterozoic-Early Paleozoic Lufilian and northern Zambezi Belts in Zambia and DRC. Journal of African Earth Sciences 30 , 727-771.

Raucq, P., 1957. Contribution à la reconnaissance du Système de la Bushimay. Annales du Musée royal du Congo Belge (Tervuren), Série 8, vol.18, 427 pp.

Raucq, P., 1958. Carte géologique provisoire du degré carré S7/23 - Inédit. Archives du Département de Géologie et de Minéralogie, Musée royal de l'Afrique Centrale, Tervuren (Belgique).

Raucq, P., 1970. Nouvelles acquisitions sur le système de la Bushimay (République Démocratique du Congo). Annales du Musée royal de l'Afrique Centale, Tervuren, Belgique, Série in-8°- n° 69.

Ring, U., Kröner, A., Toulkerides, T., 1997. Palaeoproterozoic granulite facies metamorphism and granitoid intrusions in the Ubendian- Usagaran Orogen of northern Malawi, east-central Africa. Precambrian Research 85, 27–51.

Rooney, A.D., Selby, D., Houzait, J.-P., Renne, P.R., 2010. Re-Os geochronology of a Mesoproterozoic sedimentary succession, Taoudeni basin, Mauritania: Implications for basin-wide correlations and Re-Os organic-rich sediments systematic. Earth and Planetary Science Letters 289, 486-496.

Rosenbaum, J., Sheppard, S.M.F., 1986. An isotopic study of siderites, dolomites and ankerites at high temperatures. Geochimica et Cosmochimica Acta 50, 1147-1150.

Rothman, D.H., Hayes, J.M., Summons, R.E., 2003. Dynamics of the Neoproterozoic carbon cycle. Proceedings of the National Academy of Sciences of the United States of America 100, 8124–8129.

Schandelmeier, H., 1980. Regionale Gliederung des Prekambriums und Aspeckte der Krustenentwicklung um Mambwe/Nordost - Zambia. Giessener Geologische Schriftten 23. Lenz-Verlag, Giessen, 111 pp.

Schandelmeier, H., 1983. The geochronology of post-Ubendian granitoids and dolerites from the Mambwe area. Northern Province, Zambia. Report of Institute of Geological Sciences 83, 40–46.

Sears, J.W., Price, R.A., 2000. New look at the Siberian connection: no SWEAT. Geology 28, 423-426.

Semikhatov, M.A., Gorokhov, I.M., Kuznetsov, A.B., Mel'Nikov, N.N., Podkovyrov, V.N., Kislova, I.V., 1998. The strontium isotopic composition in early Late Riphean seawater: Limestones of the Lakhanda Group, the Uchur-Maya region, Siberia. Trans. (Dokl.) Russian Academy Sciences, Earth Sciences Section 360, 488-492.

Shields, G., 1999. Working towards a new stratigraphic calibration scheme for the Neoproterozoic-Cambrian. Eclogae Geologicae Helvitae 92, 221-233.

Sircombe, K.N., 2004. AGEDISPLAY: an EXCEL workbook to evaluate and display univariate geochronological data using binned frequency histograms and probability density distributions. Computers and Geosciences 30, 21–31.

Stacey, J.S., Kramers, J.D., 1975. Approximation of terrestrial lead isotope evolution by a two-stage model. Earth and Planetary Science Letters 26, 207–221.

Steiger, R.H., Jäger, E., 1977, Subcommission on geochronology: Convention on use of decay constants in geo- and cosmochronology: Earth and Planetary Science Letters 126, 359–362.

Straathof, G., 2011. Neoproterozoic Low Latitude Glaciations : An African Perspective. PhD thesis, University of Edinburgh, 285 pp.

Strauss, H., 1997. The isotopic composition of sedimentary sulfur through time. Palaeogeography, Palaeoclimatology, Palaeoecology 132, 97-118.

Tack, L., Wingate, M.T., Liégeois, J.P., Fernandez-Alonso, M., Deblond, A., 2001. Early Neoproterozoic magmatism (1000-910 Ma) of the Zadinian and Mayumbian Groups (Bas-Congo): onset of Rodinia rifting at the western edge of the Congo craton. Precambrian Research 110, 277-306.

Tack, L., Wingate, M.T.D., De Waele, B., Meert, J., Belousova, E., Griffin, B., Tahon, A., Fernandez-Alonso, M., 2010. The 1375 Ma 'Kibaran event' in Central Africa: Prominent emplacement of bimodal magmatism under extensional regime. Precambrian Research 180, 63-84.

Tait, J., Delpomdor, F., Préat, A., Tack., L., Straathof, G., Kanda Nkula, V., 2011. Neoproterozoic sequences of the West Congo and Lindi/Ubangi Supergroups in the Congo Craton, Central Africa. In: Arnaud, E., Halverson, G.L., Shields-Zhou, G. (Eds.), The Geological Record of Neoproterozoic Glaciations. Geological Society Memoir, London 36, pp. 185-194.

Tewari, V.C., Sial, A.N., 2007. Neoproterozoic-Early Cambrian isotopic variation and chemostyratigraphy of the Lesser Himalaya, India, Eastern Gondwana. Chemical Geology 237, 64-88.

Unrug, R., 1983. The Lufilian arc: a microplate in the Pan-African collision zone of the Congo and the Kalahari cratons. Precambrian Research 21, 181-196.

Van de Steen, J., 1953. Schéma géologique du degré carré de Mitwaba au 2.000.000^{e}. Direction Géologique du Département des Mines, République du Zaïre, 67 pp.

Van de Steen, J., 1959. Le système de Kibara. Bulletin Géologique du Congo-Belge Rwanda-Urundi 1, 8–22.

Veizer, J., Compston, W., Clauer, N., Schidlowski, M., 1983. $^{87}Sr/^{86}Sr$ in Late Proterozoic carbonates: evidence for a 'mantle' event at 900 Ma ago. Geochimica et Cosmochimica Acta 47, 295-302.

Villeneuve, M., Chorowicz, J., 2004. Les sillons plissés du Burundien superieur dans la chaîne kibarienne d'Afrique centrale. Comptes Rendus de Géosciences 336, 807–814.

Wachter, E.A., Hayes, J.M., 1985. Exchange of oxygen isotopes in carbon dioxide phosphoric acid systems. Chemical Geology 52, 365-374.

Walraven, F., Rumvegeri, B.T., 1993. Implications of whole-rock Pb–Pb and zircon evaporation dates for the early metamorphic history of the Kasai Craton Southern Zaire. Journal of African Earth Sciences 16, 395–404.

Weil, A.B., Van der Voo, R., Mac Niocaill, C., Meert, J.G., 1998. The Proterozoic supercontinent Rodinia: paleomagnetically derived reconstructions for 1100 to 800 Ma. Earth and Planetary Science Letters 154 (1-4), 13-24.

Wingate, M.T.D., Pisarevsky, S.A., Evans, D.A.D., 2002. Rodinia connections between Australia and Laurentia: no SWEAT, no AUSWUS? Terra Nova 14 (2), 121-128.

Table captions

Table 1: Simplified stratigraphy of the Mbuji-Mayi Supergroup in the north Sankuru-Mbuji-Mayi-Lomami-Lovoy Basin, Kasai-Oriental Province, Democratic Republic of Congo (after Raucq, 1970).

Table 2: LA-ICP-MS analytical data for spot analyses of detrital zircon grains from the siliciclastic Mbuji-Mayi BI group of the Democratic Republic of Congo. For location see Figure 1.

Table 3: C, O and Sr isotope analyses and geochemistry of the carbonates from the Mbuji-Mayi BII group of the Democratic Republic of Congo.

Table 4: $^{40}Ar/^{39}Ar$ analytical results of the matrix aliquots separated from the 'Lomami' dolerite.

Figure captions

Figure 1: Geographic distribution of the Eastern Gondwana at *ca*. 490 Ma (modified after Meert, 2003).

Figure 2: Simplified geological map of the Sankuru-Mbuji-Mayi-Lomami-Lovoy Basin (Democratic Republic of Congo) with location of (i) studied drillholes (S70 Tshinyama, B13 Kanshi, Bena Kalenda, Bena Tshovu, Kaf.15) stored at the Royal Museum for Central Africa (RMCA); (ii) studied drillhole of de Beers stored at the Société Minière de Bakwanga (MIBA); and (iii) samples retrieved from outcrops (226, 243, 628, Forminière) kept at the Royal Museum for Central Africa (RMCA).

Figure 3: Litholog of the drillholes and outcrops studied in the Sankuru-Mbuji-Mayi-Lomami-Lovoy Basin with sample positions. Sampling for LA-ICP-MS U-Pb dating is refered with the serial number of the Royal Museum for Central Africa (RMCA), and horizontal bars display the sampling for chemostratigraphy. Lithological units from the BIb to BIIe subgroups of the Mbuji-Mayi Supergroup are described in the text.

Figure 4: U-Pb ages of detrital zircon grains separated from BIc-d_1 and BIc-d_4 stratigraphic units in the S70 Tshinyama drillhole. (A) U-Pb concordia diagram and (B) combined frequency and probability density distribution plots of detrital zircons grains in the range of 1000 to 3000 Ma.

Figure 5: U-Pb ages of detrital zircon grains separated from two samples in the BId_2 stratigraphic unit the Kaf. 15 drillhole. (A) U-Pb concordia diagram and (B) combined frequency and probability density distribution plots of detrital zircons grains in the range of 1000 to 3000 Ma .

Figure 6: Composite chemostratigraphic-isotope profiles and stratigraphic column of the Mbuji-Mayi Supergroup from drillholes and outcrops. Note the presence of negative $\delta^{13}C_{carb}$ anomaly in the lower parts of the BIIb and BIIc subgroups. $^{87}Sr/^{86}Sr$ isotope values show that BIe samples are altered. $\delta^{13}C_{carb}$ values are also indicative of chemical alteration.

Figure 7: $^{40}Ar/^{39}Ar$ incremental release spectrum of mafic mineral mixture from a low-grade metamorphic dolerite in the Lomami area of the Sankuru-Mbuji-Mayi-Lomami-Lovoy Basin (stippled line shows the Ca/K ratio).

Figure 8: Tectono-magmatic and orogenic events combined with binned frequency plots of all U-Pb ages of analyzed zircon grains showing a degree of concordance in the range of 90 to 110%. Hatched area shows multiple sedimentation cycle related to the reworking of Palaeoproterozoic Ubendian-Ruzisian belts and Bangweulu block.

Figure 9: All Mbuji-Mayi limestone/dolostone data patterns expected from mixing seawater and meteoric waters ('lithification domain') and effect of diagenetic alteration (after Knauth and Kennedy, 2009). Notice that $\delta^{18}O_{carb}$ primary marine signals of Mbuji-Mayi carbonate samples are not preserved, but $\delta^{13}C_{carb}$ conserved the primary marine signal.

Figure 10: (A) Sr/Ca *vs.* Mn elemental concentrations. All Mbuji-Mayi carbonates have low Sr/Ca ratios, except some BIIb and BIIc samples. High Sr/Ca ratios in the BIIb subgroup are near the present-day seawater Sr/Ca ratio (0.0086). Elevated Sr/Ca ratios in the BIIc subgroup are attributed to clay-rich contents in dolostones. Increase of Mn concentration records alteration from non-marine fluids (meteoric, mixed-water or evaporitic brines). (B) Mn *vs.* Fe elemental concentrations in the Mbuji-Mayi carbonate Supergroup. Arrows indicate direction of alteration during interaction with non-marine fluids. (C) Mn *vs.* $\delta^{18}O_{carb.}$ in the Mbuji-Mayi carbonate Supergroup. Arrow A (left arrow) indicates interaction with meteoric or mixed-waters. Arrow B (right arrow) indicates interaction with evaporitic brines (modified after Kah, 2000).

Figure 11: Mn/Sr *vs*. Rb/Sr ratios in the Mbuji-Mayi carbonate Supergroup. Non-diagenetic carbonate rocks (in grey square) have Mn/Sr < 3.0 and Rb/Sr < 0.01 (dolostones) and Mn/Sr < 1.5 and Rb/Sr < 0.01 (limestones).

Figure 12: Sr elemental concentration *vs.* $^{87}Sr/^{86}Sr$ ratio in the Mbuji-Mayi carbonate Supergroup. Primary marine $^{87}Sr/^{86}Sr$ signatures range between 0.706 and 0.707 (see text).

Figure 13: Global $\delta^{13}C_{carb}$ and $^{87}Sr/^{86}Sr$ correlations of the Mbuji-Mayi Supergroup. Data of Central Australia, $^{87}Sr/^{86}Sr$ ratios from Fanning (1986) reproduced *in* Hill et al. (2000), Calver (1998) and McKirdy et al. (2001). Data of NW Canada, $^{87}Sr/^{86}Sr$ ratios from Narbonne et al. (1994), Kaufman et al. (1997) and Halverson et al. (2007). Svalbard: $^{87}Sr/^{86}Sr$ ratios from Halverson et al. (2005, 2007). Central Australia, NW Canada and Svalbard: $\delta^{13}C_{carb}$ from Halverson et al. (2007).

Figure 14: Early Neoproterozoic palaeogeographic reconstruction of the Zambezi-Katanga rifting basins and relationship with the Sankuru-Mbuji-Mayi-Lomami-Lovoy failed-rift basin. (1) reworked ~1.9-2.0 Ga sediments from the Ubendian-Ruzisian Belt, ~1.7-2.1 Ga sediments from the Bangweulu Block, and (2) >1.9 Ga fluvial, aeolian and lacustrine sediments from the Mporokoso Group at ~1.0-1.4 Ga Kibaran Belt. (3) southeastern provenances of detrital zircon grains for the Mbuji-Mayi BI group from the Kibara Belt (KIB). (4) West to east transports from ~2.4-2.8 Ga metamorphic and magmatic Kasai block to the Mbuji-Mayi BI group. (5) possible northeastern provenances of detrital zircon grains for the Mbuji-Mayi BI from ~1.0-1.4 Ga Karagwe-Ankole Belt (KAB). Continous arrow: transport of sediments; dashed arrow: transport of reworked sediments.

Figure 15: Regional basin evolution and stratigraphic comparison between the Zambezi, Katanga and Sankuru-Mbuji-Mayi-Lomami-Lovoy basins. The three emplacement ages for intrusive rocks in the Zambezi Basin (first column) were obtained by U-Pb upper intercept zircon age Kafue rhyolites: 879 ± 19 Ma (Hanson et al., 1994); SHRIMP - Nchanga Granite: 877 ± 11 Ma (Armstrong et al., 2005) – U-Pb upper intercept zircon age - Lusaka Granite: 865 ± 65/48 Ma. The beginning of Roan sedimentation yielded 880 Ma by U/Pb SHRIMP dating on detrital zircons (Armstrong et al., 2005). The intrusions in the Mwashya Subgroup is dated at 765 ± 5 Ma by U-Pb SHRIMP dating on detrital zircons (Key et al., 2001). In the Sankuru-Mbuji-Mayi-Lomami-Lovoy Basin, the minimum age of basement yielded 1152 ± 15 Ma by K-Ar methods on biotite, pyroxene and amphibole from a syenodiorite (Delhal et al., 1989). This age is confirmed by LA-ICP-MS U-Pb data from 355 detrital zircon grains in BI siliciclastics with a minimum age of 1174 ± 22 Ma (in this paper). Two hypotheses on base of ancient and recent data are proposed: (i) first hypothesis – the age of the siliciclastic BI group is younger than 1040 and 1065 Ma, as suggested by $^{207}Pb/^{206}Pb$ dating on galena

(Cahen, 1954; Holmes and Cahen, 1955; Raucq, 1957), (ii) second hypothesis – the BI group was deposited before 880 Ma ($^{40}Ar/^{39}Ar$ data on basalts, in this paper). The carbonate BII group is constrained at 760-820 Ma by C and Sr isotopes on 288 samples (in this paper).

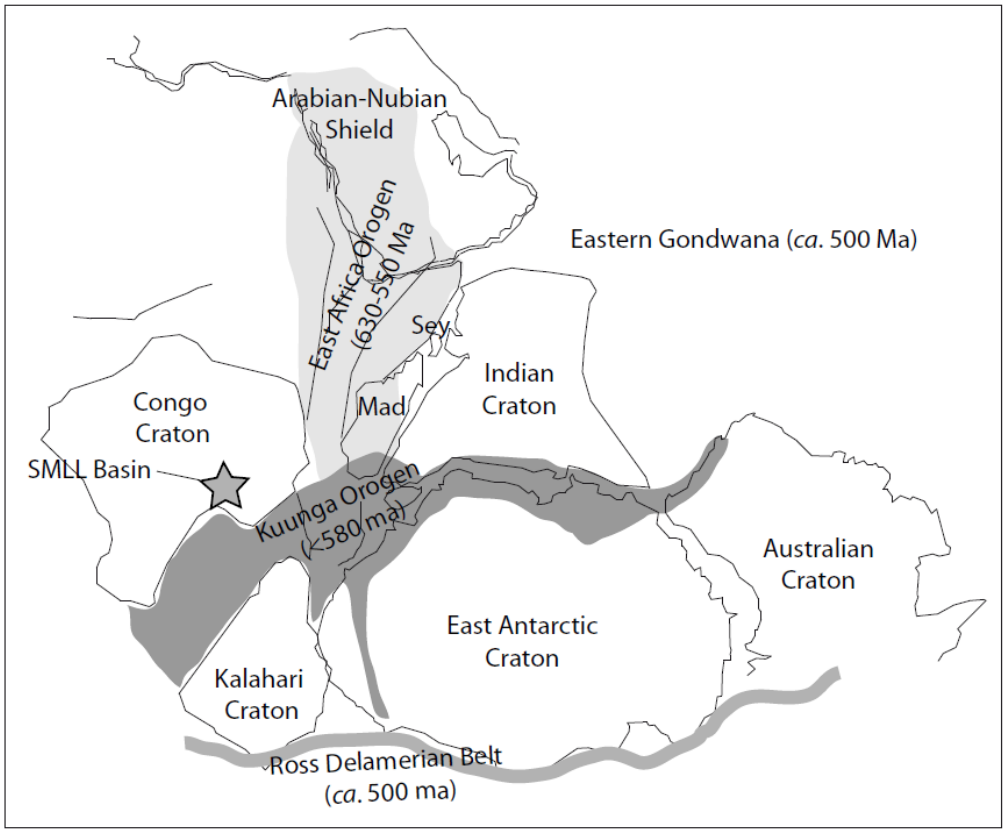

Fig. 1

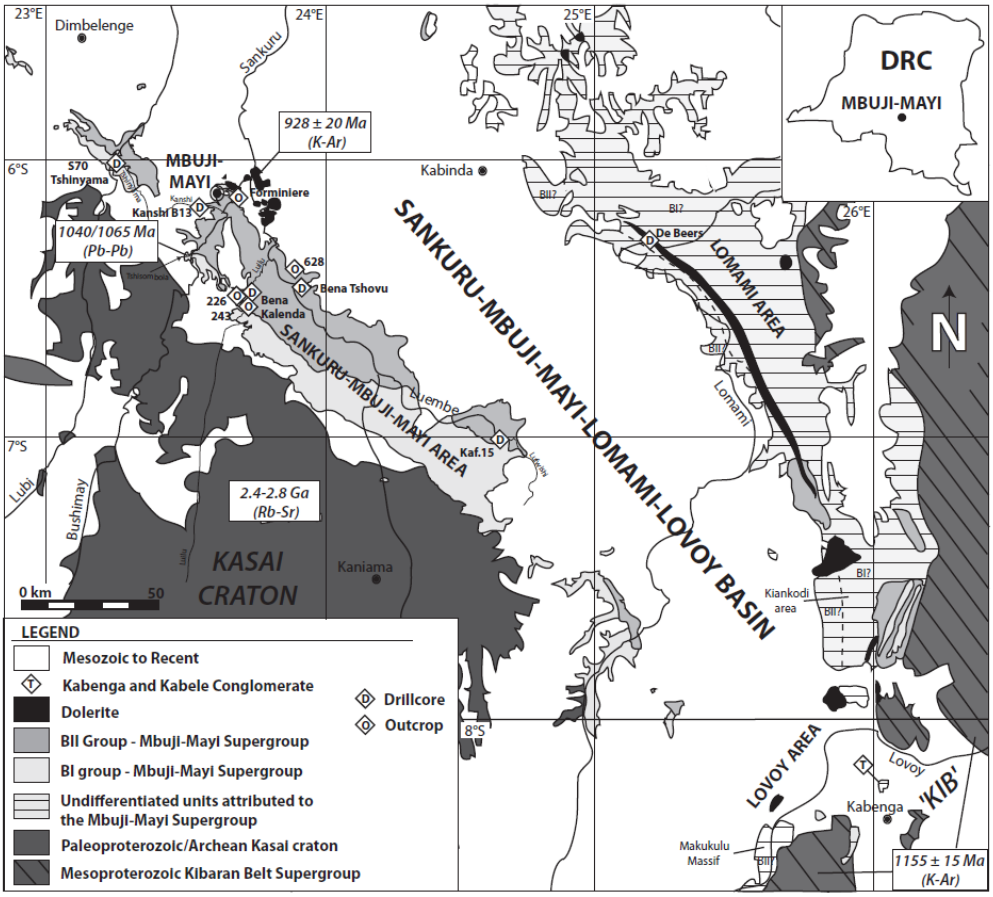

Fig. 2

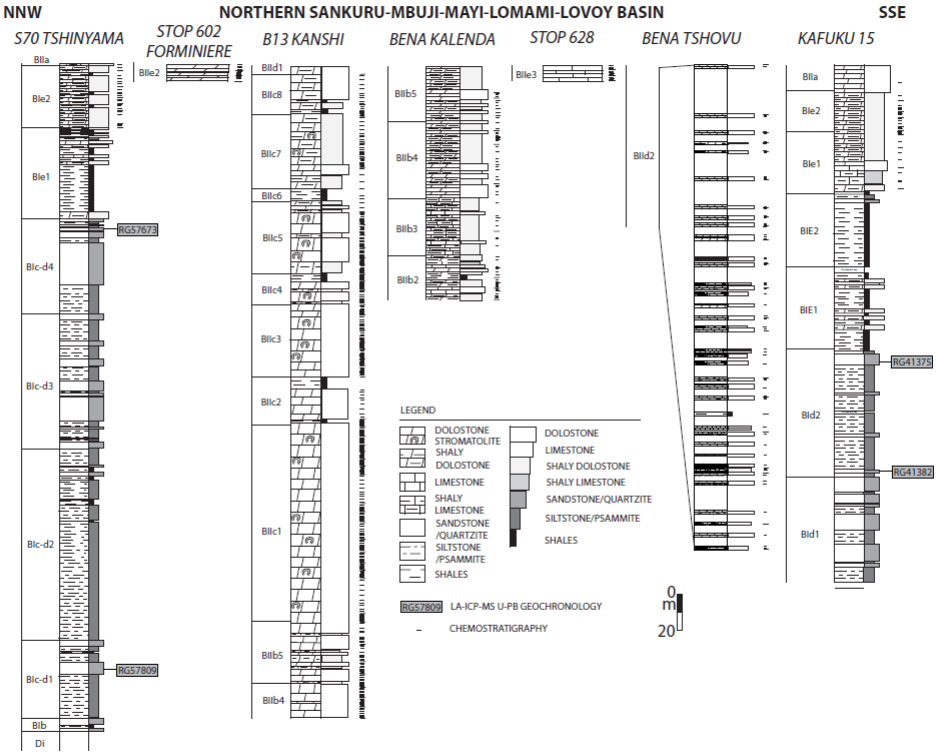

Fig. 3

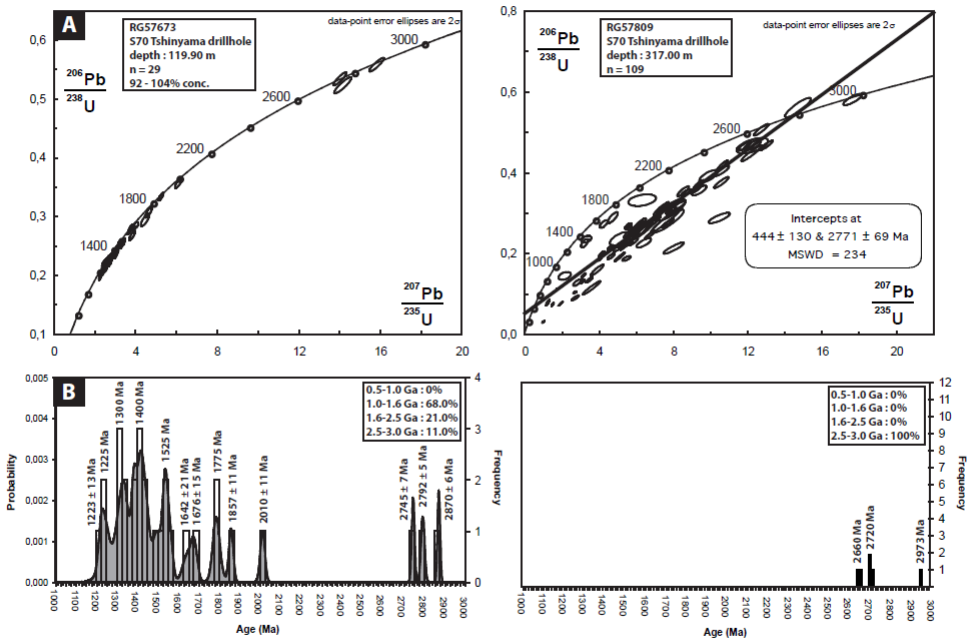

Fig. 4

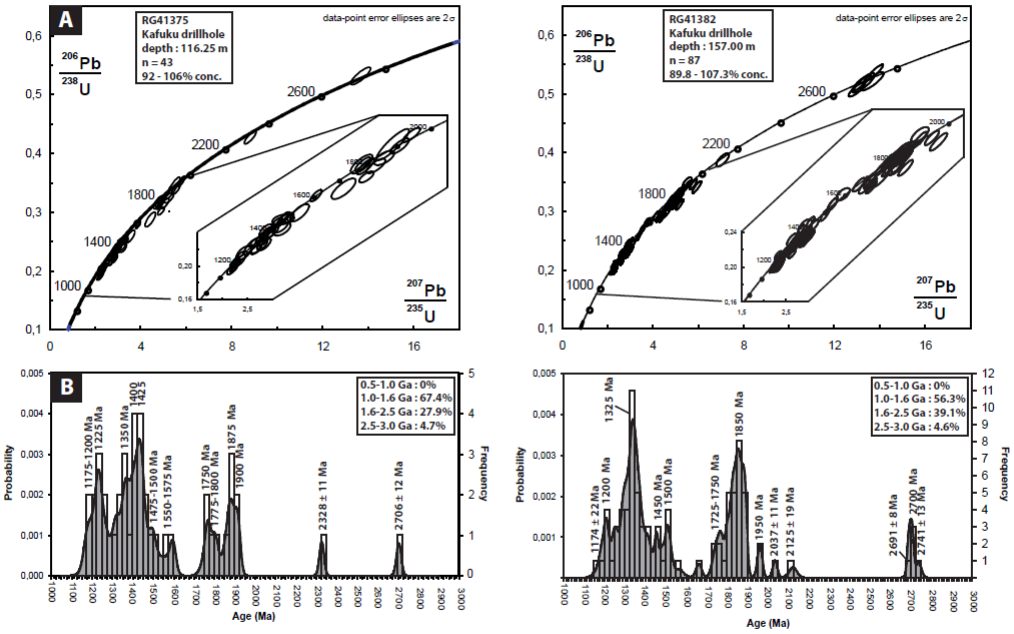

Fig. 5

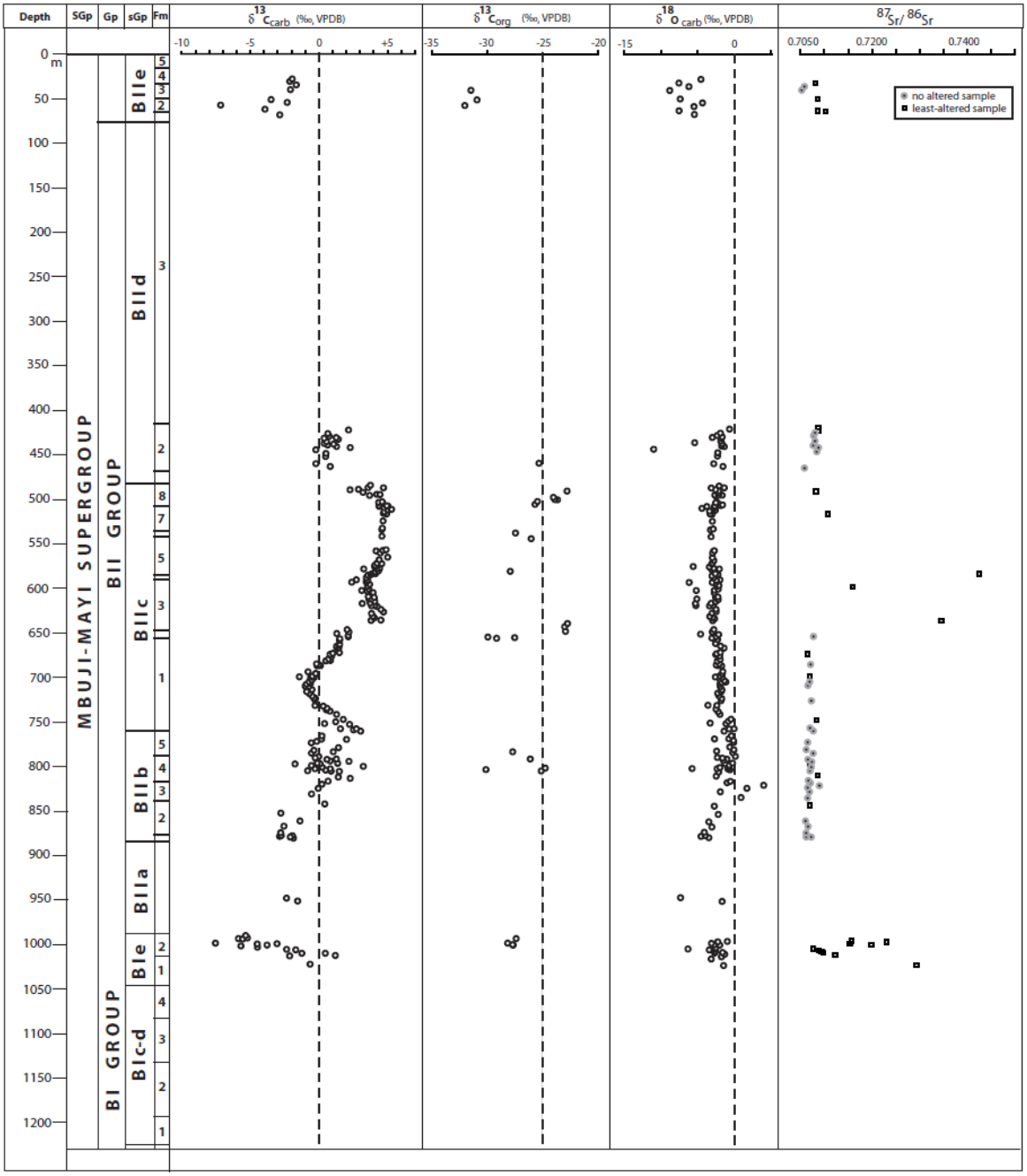

Fig. 6

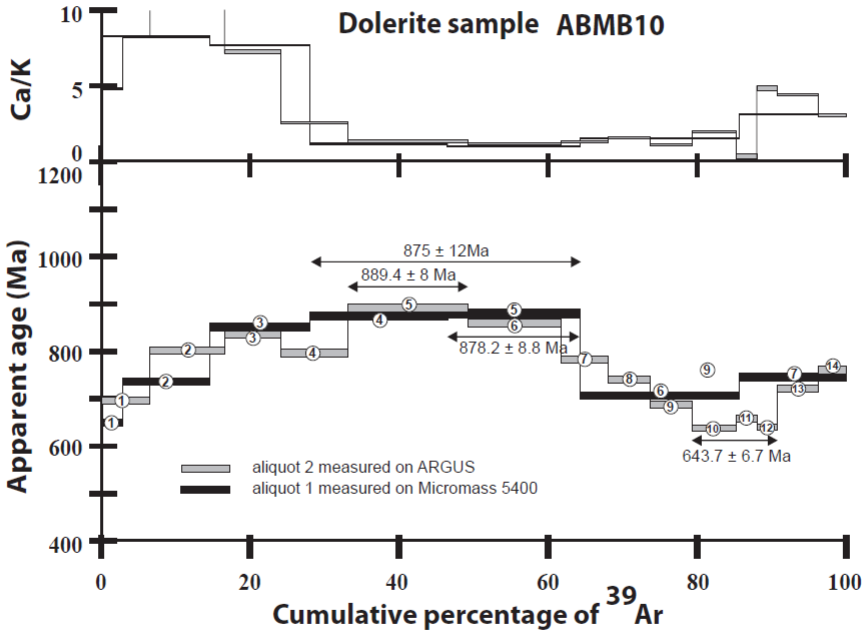

Fig. 7

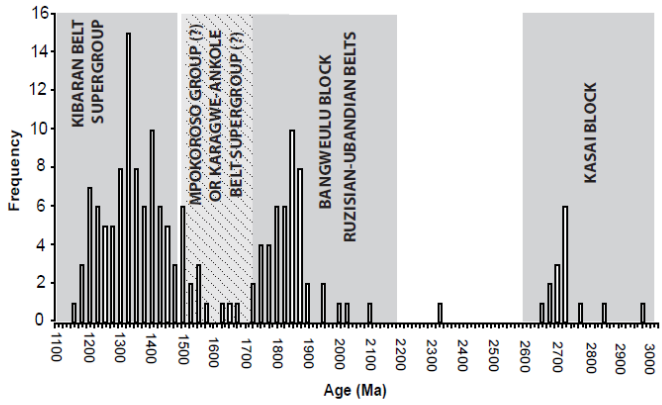

Fig. 8

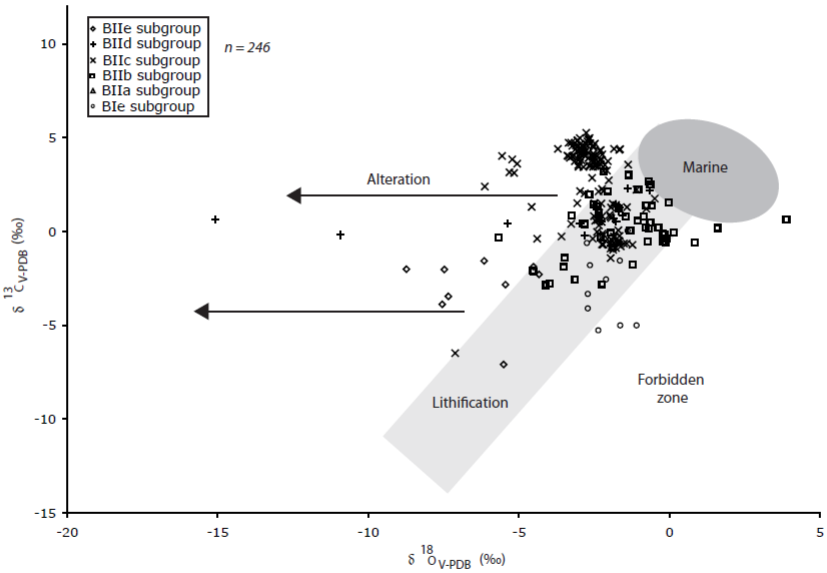

Fig. 9

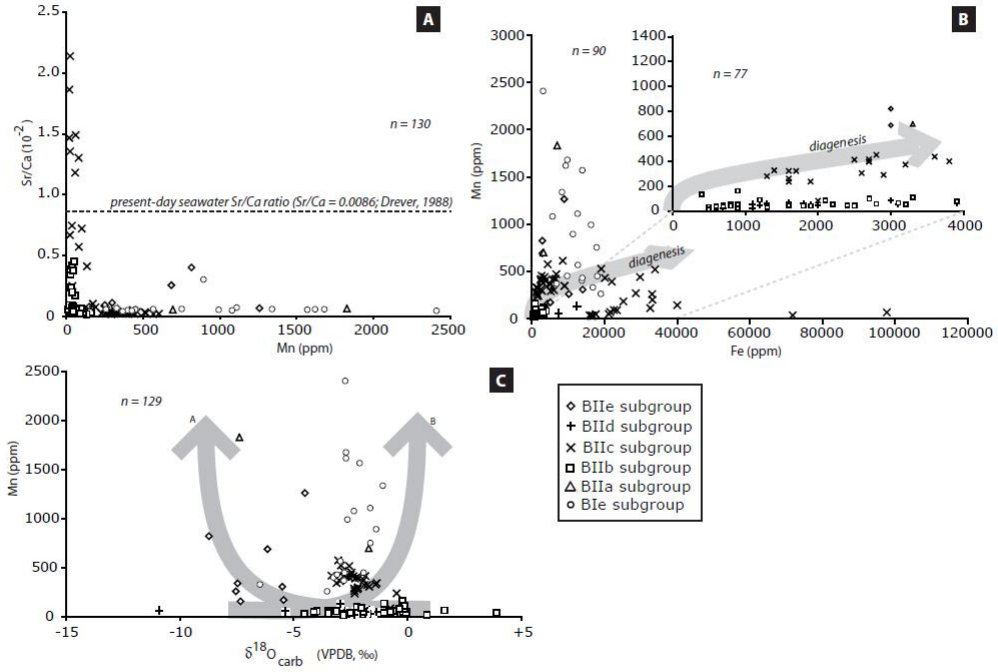

Fig. 10

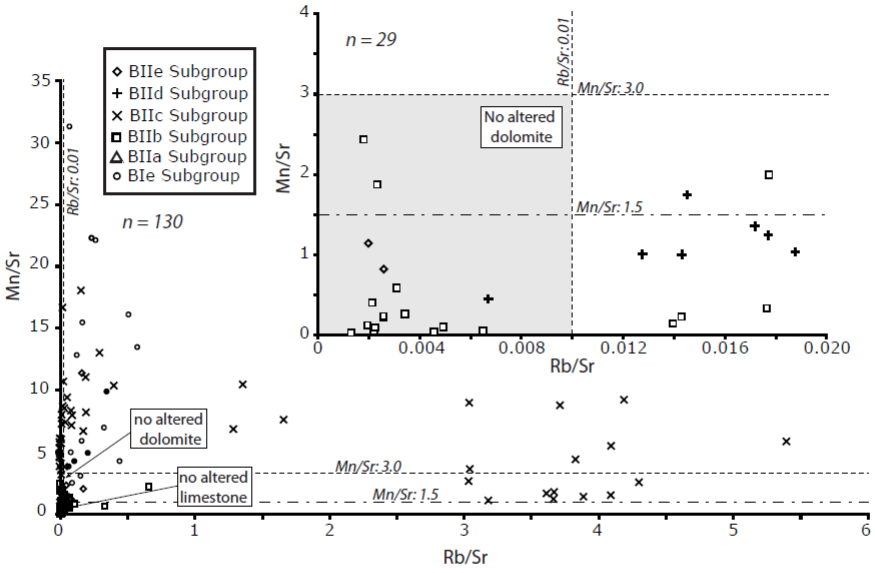

Fig. 11

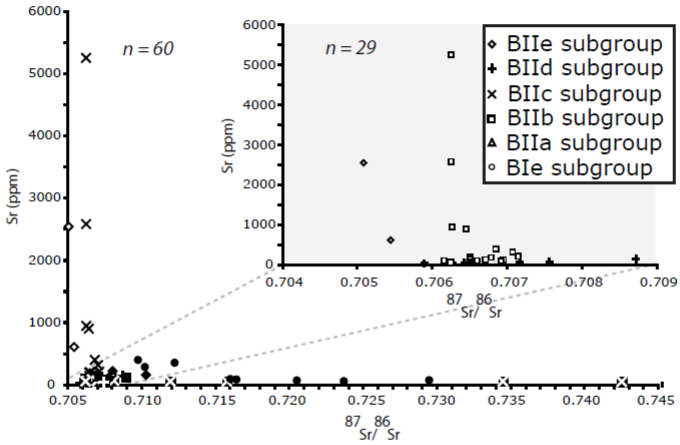

Fig. 12

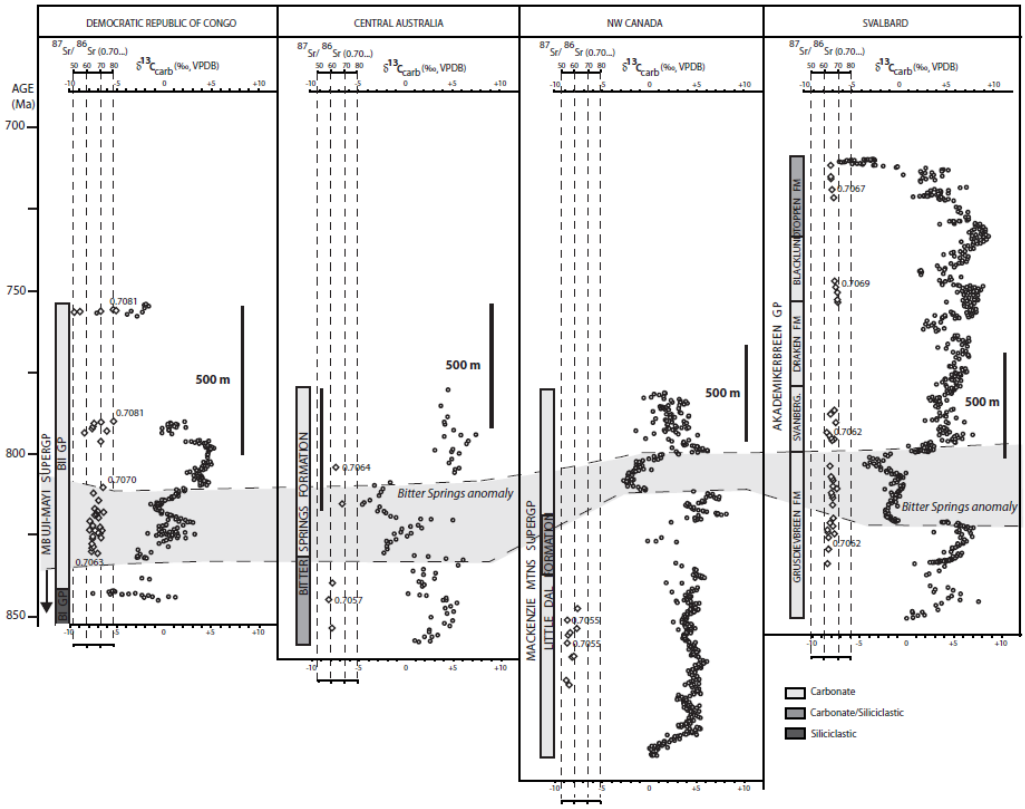

Fig. 13

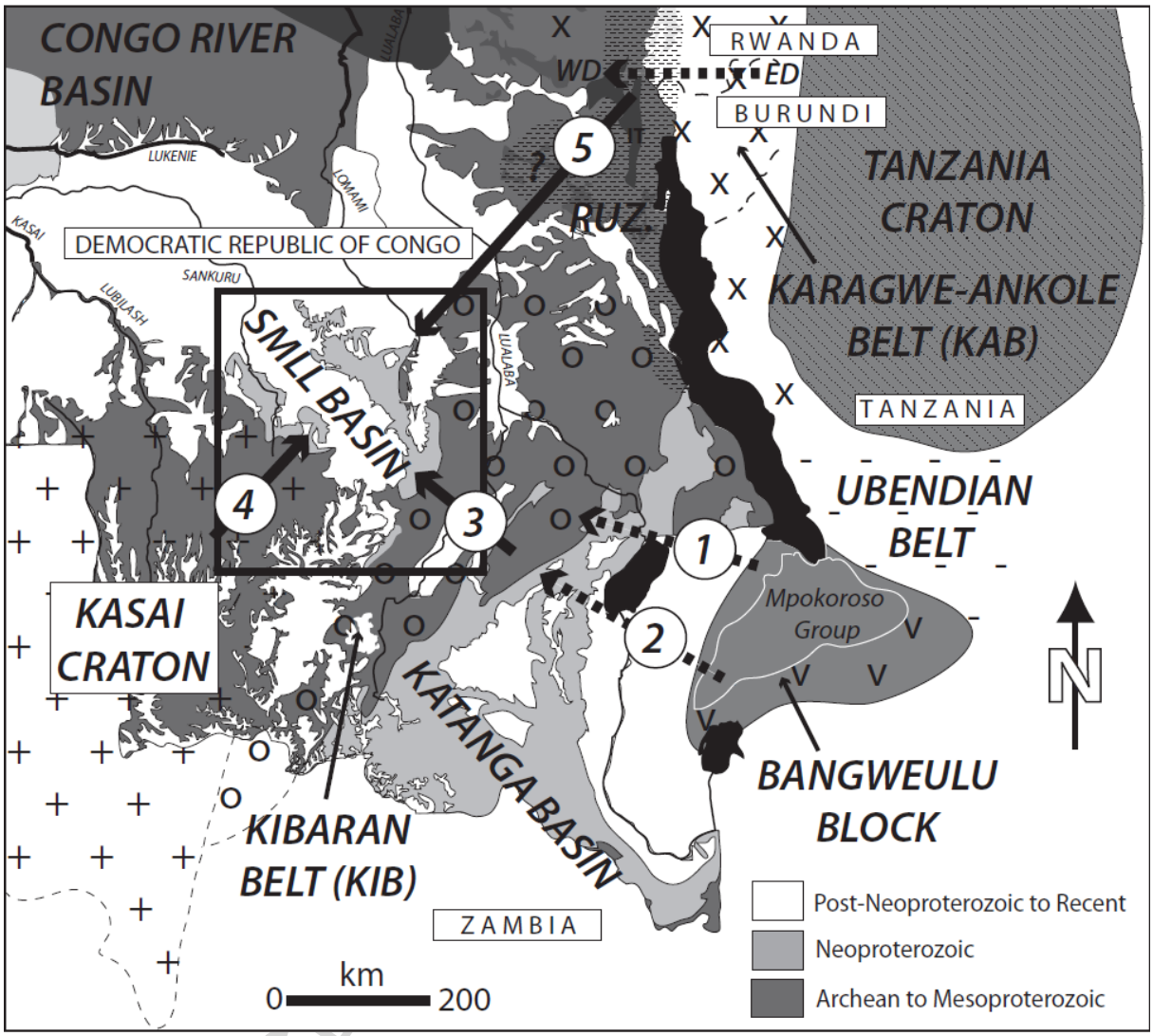

Fig. 14

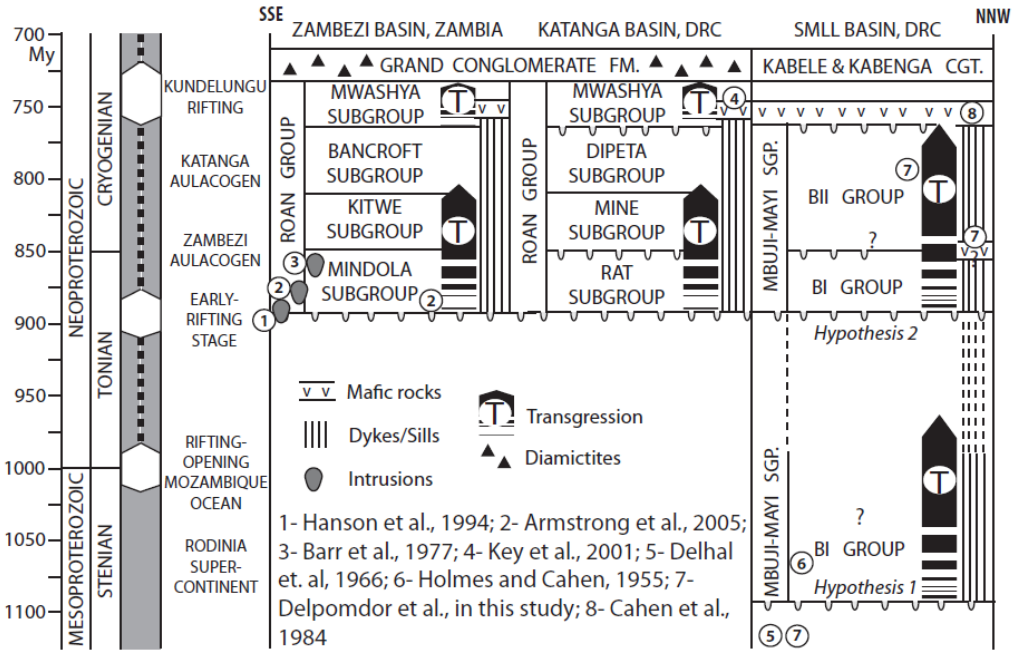

Fig. 15

Table 1

Mbuji-Mayi Supergroup, DRC

Group	Subgroup	Formation	Lithostratigraphy
	948 ± 20 Ma (Cahen et al., 1974, 1984)		
BII	BIIe	*BIIe$_5$*	grey limestones with stromatolites (17.5 m)
		BIIe$_4$	brecciated grey limestones, stromatolites (24 m)
		BIIe$_3$	pink limestones (11 m)
		BIIe$_2$	grey limestones, grey to pink dolostones (15 m)
		BIIe$_1$	pink to grey shaly to calcareous dolostones (13.5 m)
	BIId	*BIId$_3$*	grey cherty dolostones with cherts, pink shaly dolostones (343 m)
		BIId$_2$	grey dolostones, shaly dolostones and dolomitic limestones (42 m)
		BIId$_1$	shales with cherts (15 m)
	BIIc	*BIIc$_8$*	dark shales, green to purple shaly dolostones (24 m)
		BIIc$_7$	grey dolostones with stromatolites (5 m)
		BIIc$_6$	dark shales, grey shaly dolostones (27 m)
		BIIc$_5$	grey dolostones with stromatolites (25 m)
		BIIc$_4$	dark shales, grey shaly dolostones (12.5 m)
		BIIc$_3$	grey dolostones with stromatolites (88 m)
		BIIc$_2$	dark shales, grey shaly dolostones (21 m)
		BIIc$_1$	grey dolostones with stromatolites (89 m)
	BIIb	*BIIb$_5$*	dark cherty dolostone, shaly dolostones (25 m)
		BIIb$_4$	shaly calcareous dolostones (23 m)
		BIIb$_3$	polygenetic conglomerates (19 m)
		BIIb$_2$	shaly dolostones and calcareous dolostones, often brecciated (39 m)
		BIIb$_1$	grey cherty dolostones (9 m)
	BIIa		grey dolostones with stromatolites (105 m)
	BIe	*BIe$_2$*	grey-pink feldspathic psammites (1 m), grey shaly dolostones (26.5 m)
		BIe$_1$	grey to pink dolostones with galena (25.5 m)
	1040-1065 Ma (Cahen, 1954; Holmes and Cahen, 1955; Raucq, 1957)		
BI	(BIE)	*BIE$_2$*	locally visible in the Kafuku area - red shales, shaly psammites, grey calcareous dolostones (28 m)
		BIE$_1$	locally visible in the Kafuku area - pink to brown shales, grey dolostones (31.5 m)
	BId	*BId$_2$*	quartzites (308 m)
		BId$_1$	red sandy psammites, sometimes dolomitic
	BIc	*BIc$_2$*	red shales and shaly psammites (180 m)
		BIc$_1$	conglomerates
	BIb		basal conglomerate, alternations of sandstones and conglomerates (17 m)
	BIa		only visible in south SBLL basin - shales and quartzites (500 to 1500 m)
	1155 ± 15 Ma (Delhal et al., 1966)		
	1310 ± 25 Ma (Cahen et al., 1984)		

Table 2

drillcore	core number	depth (m)	grain number	^{207}Pb (cps)	U^{a} (ppm)	Pb^{a} (ppm)	$\underline{Th}^{c}$ U	$\underline{^{206}Pb}$ ^{204}Pb	$\underline{^{206}Pb}^{e}$ ^{238}U	2 s %	$\underline{^{207}Pb}^{e}$ ^{235}U	2 s %	$\underline{^{207}Pb}^{e}$ ^{206}Pb	2 s %	rho	$\underline{^{206}Pb}$ ^{238}U	2 s (Ma)	$\underline{^{207}Pb}$ ^{235}U	2 s (Ma)	$\underline{^{207}Pb}$ ^{206}Pb	2 s (Ma)	conc %
S70 Tshinyama	RG57673	119.90	a32	23953	423	51	0.68	766	0.11406	4.1	1.42353	4.6	0.09051	2.1	0.89	696	27	899	28	1436	40	48
S70 Tshinyama	RG57673	119.90	a8	14318	255	36	1.41	3367	0.11849	2.2	1.39874	3.5	0.08561	2.7	0.64	722	15	888	21	1329	52	54
S70 Tshinyama	RG57673	119.90	a2	26903	286	43	1.14	840	0.13856	4.0	1.97445	7.0	0.10335	5.7	0.58	837	31	1107	48	1685	105	50
S70 Tshinyama	RG57673	119.90	a58	44457	228	42	0.73	620	0.16506	2.9	2.64540	3.4	0.11624	1.7	0.86	985	27	1313	25	1899	31	52
S70 Tshinyama	RG57673	119.90	a53	46542	315	60	0.66	593	0.17075	4.9	2.13208	5.2	0.09056	1.6	0.95	1016	47	1159	37	1437	30	71
S70 Tshinyama	RG57673	119.90	a37	10363	170	33	0.93	9440	0.17146	2.3	2.06178	3.0	0.08721	1.8	0.78	1020	22	1136	21	1365	36	75
S70 Tshinyama	RG57673	119.90	a55	16881	120	24	0.95	20699	0.17973	1.7	2.02620	2.6	0.08176	1.9	0.65	1066	16	1124	18	1240	38	86
S70 Tshinyama	RG57673	119.90	a20	5459	63	11	0.51	3409	0.18308	2.4	2.33225	3.8	0.09239	2.9	0.64	1084	24	1222	27	1475	55	73
S70 Tshinyama	RG57673	119.90	a19	30810	337	64	0.35	1336	0.18687	3.0	2.42637	3.9	0.09417	2.4	0.79	1104	31	1250	28	1512	45	73
S70 Tshinyama	RG57673	119.90	a43	289	4	1	6.34	336	0.19033	13.5	2.35843	40.4	0.08987	38.1	0.34	1123	141	1230	339	1423	727	79
S70 Tshinyama	RG57673	119.90	a23	22042	284	58	0.65	1910	0.19096	2.7	2.36566	3.5	0.08985	2.3	0.76	1127	28	1232	25	1422	43	79
S70 Tshinyama	RG57673	119.90	a17	24713	294	63	0.59	28985	0.19118	2.2	2.25749	2.7	0.08564	1.6	0.80	1128	23	1199	19	1330	31	85
S70 Tshinyama	RG57673	119.90	a9	87588	710	150	0.69	3670	0.19138	10.2	3.10369	10.3	0.11762	1.3	0.99	1129	107	1434	83	1920	24	59
S70 Tshinyama	RG57673	119.90	a41	10479	96	19	0.31	738	0.19424	3.4	2.28357	5.9	0.08527	4.7	0.59	1144	36	1207	42	1322	92	87
S70 Tshinyama	RG57673	119.90	a52	27101	179	39	0.79	1299	0.19825	2.0	2.70024	3.5	0.09878	2.9	0.58	1166	22	1329	27	1601	54	73
S70 Tshinyama	RG57673	119.90	a18	68796	712	149	0.36	1822	0.20027	3.0	2.62098	4.1	0.09492	2.8	0.73	1177	33	1307	31	1526	53	77
S70 Tshinyama	RG57673	119.90	a10	23236	275	61	0.59	6210	0.20028	2.3	2.41896	2.9	0.08760	1.8	0.78	1177	24	1248	21	1374	35	86
S70 Tshinyama	RG57673	119.90	a39	20739	240	51	0.49	12550	0.20122	2.4	2.27637	3.0	0.08205	1.7	0.82	1182	26	1205	21	1247	34	95
S70 Tshinyama	RG57673	119.90	a3	21192	249	59	0.43	25024	0.21378	2.5	2.51181	3.8	0.08521	2.8	0.68	1249	29	1275	28	1320	53	95
S70 Tshinyama	RG57673	119.90	a16	11170	124	32	0.74	13221	0.21534	2.0	2.51776	3.0	0.08480	2.2	0.68	1257	23	1277	22	1311	42	96
S70 Tshinyama	RG57673	119.90	a8	43340	469	106	0.49	48424	0.21806	2.0	2.70286	2.5	0.08990	1.6	0.77	1272	23	1329	19	1423	31	89
S70 Tshinyama	RG57673	119.90	a21	24078	307	73	0.41	29802	0.21867	2.4	2.44448	2.8	0.08108	1.3	0.87	1275	28	1256	20	1223	26	104

drillcore	core number	depth (m)	grain number	^{207}Pb (cps)	U[a] (ppm)	Pb[a] (ppm)	Th[c]/U	^{206}Pb/^{204}Pb	^{206}Pb[e]/^{238}U	2 s %	^{207}Pb[e]/^{235}U	2 s %	^{207}Pb[e]/^{206}Pb	2 s %	rho	^{206}Pb/^{238}U	2 s (Ma)	^{207}Pb/^{235}U	2 s (Ma)	^{207}Pb/^{206}Pb	2 s (Ma)	conc %
S70 Tshinyama	RG57673	119.90	a5	18502	164	37	0.25	20196	0.21961	1.9	2.78805	5.6	0.09208	5.2	0.34	1280	22	1352	43	1469	99	87
S70 Tshinyama	RG57673	119.90	a1	24184	351	88	0.52	10280	0.22237	3.3	2.51291	5.1	0.08196	3.9	0.64	1294	39	1276	38	1245	76	104
S70 Tshinyama	RG57673	119.90	a45	15284	121	28	0.36	17163	0.22431	2.2	2.75547	2.8	0.08909	1.7	0.79	1305	26	1344	21	1406	32	93
S70 Tshinyama	RG57673	119.90	a47	10180	62	18	1.40	9943	0.22544	2.8	3.20094	5.2	0.10298	4.4	0.53	1311	33	1457	41	1679	82	78
S70 Tshinyama	RG57673	119.90	a12	33323	345	82	0.84	6770	0.22722	1.8	2.75525	2.1	0.08794	1.2	0.83	1320	21	1344	16	1381	23	96
S70 Tshinyama	RG57673	119.90	a4	3254	28	8	0.68	3840	0.23025	2.8	2.70014	5.0	0.08505	4.2	0.56	1336	34	1328	38	1317	81	101
S70 Tshinyama	RG57673	119.90	a33	63308	778	183	0.25	34378	0.23050	2.0	2.73113	2.6	0.08593	1.7	0.77	1337	24	1337	19	1337	32	100
S70 Tshinyama	RG57673	119.90	a54	9391	50	12	0.51	7966	0.23169	2.8	2.76115	3.8	0.08643	2.6	0.74	1343	34	1345	29	1348	49	100
S70 Tshinyama	RG57673	119.90	a7	23810	214	54	0.63	5418	0.23938	2.8	3.06694	3.3	0.09292	1.7	0.85	1383	35	1424	26	1486	33	93
S70 Tshinyama	RG57673	119.90	a44	30566	225	56	0.31	33686	0.23933	2.4	3.00426	3.0	0.09104	1.7	0.82	1383	30	1409	23	1447	32	96
S70 Tshinyama	RG57673	119.90	a34	11306	122	30	0.23	12571	0.24142	2.1	2.93633	2.6	0.08821	1.6	0.79	1394	26	1391	20	1387	31	101
S70 Tshinyama	RG57673	119.90	a26	16701	171	42	0.17	18601	0.24236	3.9	2.98980	4.2	0.08947	1.6	0.92	1399	49	1405	33	1414	31	99
S70 Tshinyama	RG57673	119.90	a51	2093	13	3	0.43	2574	0.24415	3.0	2.75082	6.8	0.08171	6.1	0.44	1408	38	1342	52	1239	120	114
S70 Tshinyama	RG57673	119.90	a27	20320	188	50	0.30	22727	0.24932	1.9	3.08380	2.4	0.08971	1.4	0.81	1435	25	1429	19	1419	27	101
S70 Tshinyama	RG57673	119.90	a6	31735	239	62	0.24	33273	0.25469	1.9	3.34962	2.2	0.09538	1.2	0.85	1463	25	1493	17	1536	22	95
S70 Tshinyama	RG57673	119.90	a59	33065	139	41	0.56	36597	0.25745	2.2	3.21609	2.7	0.09060	1.6	0.80	1477	29	1461	21	1438	31	103
S70 Tshinyama	RG57673	119.90	a5	18251	164	44	0.22	19211	0.25785	1.5	3.38987	2.2	0.09535	1.6	0.70	1479	20	1502	17	1535	29	96
S70 Tshinyama	RG57673	119.90	a4	17969	166	44	0.23	19155	0.25966	1.9	3.37274	2.8	0.09421	2.1	0.67	1488	25	1498	22	1512	39	98
S70 Tshinyama	RG57673	119.90	a29	26194	214	65	1.42	9714	0.27005	2.1	3.82991	2.7	0.10286	1.6	0.79	1541	29	1599	22	1676	30	92
S70 Tshinyama	RG57673	119.90	a50	45718	192	60	0.71	1959	0.27284	4.1	4.02647	4.8	0.10703	2.6	0.84	1555	57	1640	40	1749	48	89
S70 Tshinyama	RG57673	119.90	a6	55171	500	143	0.44	4520	0.28072	2.3	3.73824	2.7	0.09658	1.4	0.85	1595	32	1580	22	1559	27	102
S70 Tshinyama	RG57673	119.90	a46	1E+05	583	181	0.63	29170	0.28338	3.5	4.53573	3.7	0.11609	1.4	0.93	1608	49	1738	32	1897	25	85
S70	RG57673	119.90	a3	17011	105	33	0.49	16737	0.28717	1.6	3.99694	2.8	0.10094	2.3	0.57	1627	23	1634	23	1642	43	99

drillcore	core number	depth (m)	grain number	^{207}Pb (cps)	U[a] (ppm)	Pb[a] (ppm)	Th[c] U	^{206}Pb ^{204}Pb	^{206}Pb[e] ^{238}U	2 s %	^{207}Pb[e] ^{235}U	2 s %	^{207}Pb[e] ^{206}Pb	2 s %	rho	^{206}Pb ^{238}U	2 s (Ma)	^{207}Pb ^{235}U	2 s (Ma)	^{207}Pb ^{206}Pb	2 s (Ma)	conc %
Tshinyama S70	RG57673	119.90	a35	43456	298	100	0.47	39769	0.29658	3.0	4.47073	3.7	0.10933	2.2	0.80	1674	44	1726	31	1788	41	94
Tshinyama S70	RG57673	119.90	a2	63697	372	127	0.96	19971	0.30586	1.5	5.20157	2.2	0.12334	1.7	0.66	1720	22	1853	19	2005	30	86
Tshinyama S70	RG57673	119.90	a7	98615	586	202	0.93	19574	0.30770	3.4	5.20442	3.6	0.12267	1.1	0.95	1729	52	1853	31	1995	19	87
Tshinyama S70	RG57673	119.90	a14	16166	101	37	1.01	8048	0.30892	2.3	4.64139	2.8	0.10897	1.6	0.82	1735	36	1757	24	1782	29	97
Tshinyama S70	RG57673	119.90	a49	35484	121	47	0.46	31352	0.33594	1.6	5.25827	2.0	0.11352	1.2	0.81	1867	26	1862	17	1857	21	101
Tshinyama S70	RG57673	119.90	a25	17204	82	34	0.57	13959	0.35854	1.8	6.11473	2.2	0.12369	1.3	0.82	1975	31	1992	19	2010	22	98
Tshinyama S70	RG57673	119.90	a13	2E+05	461	255	0.28	55111	0.52338	2.1	14.13676	2.4	0.19590	1.1	0.90	2713	47	2759	23	2792	17	97
Tshinyama S70	RG57673	119.90	a57	98590	100	59	0.21	51942	0.53433	1.7	14.02333	1.9	0.19034	0.8	0.91	2760	39	2751	18	2745	13	101
Tshinyama S70	RG57673	119.90	a12	58487	105	79	0.78	28569	0.55841	1.7	15.82124	1.9	0.20549	0.8	0.91	2860	39	2866	18	2870	12	100
Tshinyama S70	RG57809	317.00	a1	3142	15	4	0.15	568	0.28036	2.6	4.21054	3.9	0.10892	2.8	0.68	1593	37	1676	32	1781	52	89
Tshinyama S70	RG57809	317.00	a2	2E+05	483	146	0.79	4569	0.24979	2.6	5.78399	3.0	0.16794	1.5	0.87	1437	34	1944	27	2537	26	57
Tshinyama S70	RG57809	317.00	a3	1E+05	271	115	1.14	727	0.32009	4.2	8.14036	4.7	0.18445	2.1	0.89	1790	66	2247	44	2693	35	66
Tshinyama S70	RG57809	317.00	a4	2E+05	758	215	0.42	3200	0.27444	2.0	5.55152	2.8	0.14671	1.9	0.72	1563	28	1909	25	2308	33	68
Tshinyama S70	RG57809	317.00	a7	2E+05	517	237	0.36	5501	0.31595	3.9	7.28746	4.4	0.16729	1.9	0.90	1770	61	2147	40	2531	31	70
Tshinyama S70	RG57809	317.00	a8	2E+05	824	220	0.32	2876	0.25067	1.6	5.53607	1.9	0.16018	1.0	0.86	1442	21	1906	16	2458	16	59
Tshinyama S70	RG57809	317.00	a9	2E+05	749	216	0.30	2226	0.27612	1.7	5.49399	1.9	0.14431	0.8	0.90	1572	24	1900	16	2280	14	69
Tshinyama S70	RG57809	317.00	a10	2E+05	804	244	0.33	2238	0.27926	2.1	6.27940	2.8	0.16308	1.9	0.74	1588	30	2016	25	2488	32	64
Tshinyama S70	RG57809	317.00	a11	7060	3	4	1.02	29	0.52987	14.3	39.52137	15.5	0.54096	5.9	0.92	2741	328	3759	166	4357	87	63
Tshinyama S70	RG57809	317.00	a12	27235	130	35	0.36	2284	0.19299	4.0	3.71702	24.4	0.13968	24.1	0.16	1138	42	1575	217	2223	417	51
Tshinyama S70	RG57809	317.00	a13	5601	26	5	1.12	3260	0.15613	36.6	4.32139	52.5	0.20074	37.7	0.70	935	327	1697	565	2832	615	33
Tshinyama S70	RG57809	317.00	a14	17986	39	23	0.76	159	0.39716	3.0	9.86477	4.1	0.18014	2.8	0.73	2156	55	2422	39	2654	47	81

S70																					
Tshinyama	RG57809	317.00	a15	2E+05	871	185	0.16	3207	0.19453	1.8	4.00653	2.0	0.14937	0.9	0.91	1146	19	1636	17	2339	15	49
S70																					
Tshinyama	RG57809	317.00	a16	2E+05	584	171	0.23	733	0.23462	2.0	5.59856	2.6	0.17307	1.6	0.79	1359	25	1916	22	2588	26	53
S70																					
Tshinyama	RG57809	317.00	a17	2E+05	394	91	0.86	3706	0.20014	4.5	5.07556	4.7	0.18393	1.1	0.97	1176	49	1832	40	2689	18	44
S70																					
Tshinyama	RG57809	317.00	a18	91711	245	87	0.67	14315	0.31458	6.9	7.80175	8.6	0.17987	5.3	0.79	1763	107	2208	81	2652	87	66
S70																					
Tshinyama	RG57809	317.00	a19	2E+05	1036	262	0.11	2389	0.22911	2.4	5.41820	2.7	0.17151	1.3	0.88	1330	28	1888	23	2572	22	52
S70																					
Tshinyama	RG57809	317.00	a20	2E+05	259	176	0.41	26189	0.58415	1.9	17.63310	2.3	0.21893	1.3	0.82	2966	45	2970	22	2973	21	100
S70																					
Tshinyama	RG57809	317.00	a21	1E+05	356	122	0.93	6636	0.28274	4.8	6.87293	4.9	0.17630	1.1	0.97	1605	69	2095	45	2618	19	61
S70																					
Tshinyama	RG57809	317.00	a22	3929	6	5	0.85	78	0.49248	5.3	18.30309	12.6	0.26955	11.4	0.42	2581	113	3006	129	3303	179	78
S70																					
Tshinyama	RG57809	317.00	a23	3589	6	4	0.99	77	0.42934	11.0	16.68349	14.0	0.28183	8.7	0.78	2303	216	2917	144	3373	136	68
S70																					
Tshinyama	RG57809	317.00	a24	2E+05	741	182	0.52	539	0.20897	1.8	4.16973	2.4	0.14472	1.6	0.75	1223	20	1668	20	2284	27	54
S70																					
Tshinyama	RG57809	317.00	a25	2E+05	469	170	0.71	3802	0.30004	2.5	7.10222	2.8	0.17168	1.1	0.92	1692	38	2124	25	2574	18	66
S70																					
Tshinyama	RG57809	317.00	a26	40690	85	40	0.90	88	0.22171	5.1	7.97374	5.6	0.26083	2.5	0.90	1291	60	2228	52	3252	39	40
S70																					
Tshinyama	RG57809	317.00	a27	1583	1	1	1.60	19	0.22172	5.1	12.72177	90.9	0.41613	90.7	0.06	1291	60	2659	1876	3968	1359	33
S70																					
Tshinyama	RG57809	317.00	a28	2E+05	576	214	0.70	4182	0.31462	2.3	7.26823	2.5	0.16755	0.8	0.94	1763	36	2145	22	2533	14	70
S70																					
Tshinyama	RG57809	317.00	a29	87309	173	79	0.72	2812	0.38157	2.8	10.55088	3.1	0.20055	1.2	0.92	2084	51	2484	29	2831	20	74
S70																					
Tshinyama	RG57809	317.00	a30	7699	5	6	3.41	41	0.25821	14.4	17.44065	15.1	0.48988	4.3	0.96	1481	194	2959	156	4211	64	35
S70																					
Tshinyama	RG57809	317.00	a31	7580	23	7	1.82	3880	0.28720	8.1	7.68878	9.0	0.19416	4.0	0.90	1628	117	2195	84	2778	66	59
S70																					
Tshinyama	RG57809	317.00	a32	2E+05	430	203	0.57	9291	0.42457	2.1	10.62851	2.2	0.18156	0.8	0.94	2281	40	2491	21	2667	13	86
S70																					
Tshinyama	RG57809	317.00	a33	2E+05	1232	151	0.08	556	0.10049	4.9	2.71515	5.4	0.19596	2.3	0.91	617	29	1333	41	2793	37	22
S70																					
Tshinyama	RG57809	317.00	a34	2E+05	762	233	0.52	3630	0.25698	3.7	5.63973	4.7	0.15917	2.8	0.80	1474	49	1922	41	2447	47	60
S70																					
Tshinyama	RG57809	317.00	a35	1E+05	607	188	0.35	1890	0.26278	2.9	5.99170	3.1	0.16537	0.8	0.96	1504	40	1975	27	2511	14	60
S70																					
Tshinyama	RG57809	317.00	a36	2E+05	733	223	0.34	1E+05	0.26460	6.4	6.32146	7.0	0.17327	2.8	0.91	1513	87	2021	63	2589	47	58
S70																					
Tshinyama	RG57809	317.00	a37	48797	208	27	1.00	52	0.04070	21.6	0.89494	22.9	0.15948	7.7	0.94	257	55	649	116	2450	130	10
S70																					
Tshinyama	RG57809	317.00	a38	1E+05	430	176	0.82	5205	0.36051	2.8	8.49936	3.2	0.17099	1.5	0.88	1985	48	2286	29	2567	26	77

drillcore	core number	depth (m)	grain number	^{207}Pb (cps)	U[a] (ppm)	Pb[a] (ppm)	Th[c] U	^{206}Pb ^{204}Pb	^{206}Pb[e] ^{238}U	2 s %	^{207}Pb[e] ^{235}U	2 s %	^{207}Pb[e] ^{206}Pb	2 s %	rho	^{206}Pb ^{238}U	2 s (Ma)	^{207}Pb ^{235}U	2 s (Ma)	^{207}Pb ^{206}Pb	2 s (Ma)	conc %
S70 Tshinyama	RG57809	317.00	a39	1E+05	997	106	0.08	801	0.08508	4.2	1.47626	4.4	0.12584	1.4	0.95	526	21	921	27	2041	25	26
S70 Tshinyama	RG57809	317.00	a40	96418	265	137	1.13	6094	0.47287	2.1	12.24050	3.0	0.18774	2.1	0.71	2496	44	2623	28	2722	34	92
S70 Tshinyama	RG57809	317.00	a41	33944	188	32	0.45	265	0.12454	10.8	3.55744	11.2	0.20718	3.0	0.96	757	78	1540	93	2884	49	26
S70 Tshinyama	RG57809	317.00	a42	16655	54	14	1.21	474	0.19643	2.6	5.44362	3.6	0.20099	2.6	0.71	1156	27	1892	32	2834	42	41
S70 Tshinyama	RG57809	317.00	a43	2E+05	521	97	0.56	2935	0.15513	3.0	3.13885	3.3	0.14675	1.3	0.92	930	26	1442	26	2308	22	40
S70 Tshinyama	RG57809	317.00	a44	1E+05	147	82	0.50	59507	0.47242	2.0	12.97020	2.2	0.19912	0.9	0.91	2494	42	2677	21	2819	15	88
S70 Tshinyama	RG57809	317.00	a45	1E+05	307	89	0.65	3592	0.26814	4.7	6.42566	5.0	0.17380	1.6	0.95	1531	65	2036	45	2595	27	59
S70 Tshinyama	RG57809	317.00	a46	1E+05	122	64	0.22	35760	0.47156	3.3	12.21527	5.6	0.18787	4.6	0.58	2490	68	2621	54	2724	75	91
S70 Tshinyama	RG57809	317.00	a48	1E+05	169	92	0.56	18936	0.47135	1.8	11.81720	2.2	0.18183	1.3	0.81	2489	37	2590	21	2670	21	93
S70 Tshinyama	RG57809	317.00	a49	1E+05	841	116	0.12	609	0.11867	2.5	1.68561	2.6	0.10302	0.7	0.97	723	17	1003	17	1679	12	43
S70 Tshinyama	RG57809	317.00	a50	45162	66	31	0.80	7011	0.38329	14.0	9.51286	15.2	0.18000	6.0	0.92	2092	254	2389	150	2653	100	79
S70 Tshinyama	RG57809	317.00	a51	2E+05	227	89	0.65	10589	0.36666	2.7	9.21895	3.0	0.18236	1.4	0.89	2014	47	2360	28	2674	22	75
S70 Tshinyama	RG57809	317.00	a52	2E+05	237	94	0.45	4225	0.35721	1.9	8.64192	2.5	0.17546	1.5	0.79	1969	33	2301	23	2610	25	75
S70 Tshinyama	RG57809	317.00	a53	2E+05	368	106	0.45	505	0.23163	2.5	5.27218	2.8	0.16508	1.1	0.91	1343	30	1864	24	2508	19	54
S70 Tshinyama	RG57809	317.00	a54	2E+05	244	119	0.68	13407	0.41049	2.6	10.57013	3.0	0.18676	1.6	0.85	2217	49	2486	29	2714	26	82
S70 Tshinyama	RG57809	317.00	a55	2E+05	286	81	0.51	1255	0.22399	2.6	5.30892	2.7	0.17190	0.8	0.96	1303	31	1870	23	2576	13	51
S70 Tshinyama	RG57809	317.00	a56	1120	2	1	0.49	993	0.26338	8.4	4.25920	14.0	0.11728	11.1	0.60	1507	114	1686	122	1915	199	79
S70 Tshinyama	RG57809	317.00	a57	2E+05	350	98	0.14	3498	0.23834	2.9	5.83563	3.4	0.17758	1.7	0.86	1378	36	1952	30	2630	29	52
S70 Tshinyama	RG57809	317.00	a58	1E+05	157	45	0.66	6031	0.25425	3.2	6.70697	3.5	0.19132	1.3	0.93	1460	42	2074	31	2754	21	53
S70 Tshinyama	RG57809	317.00	a59	2E+05	274	74	0.66	1801	0.22856	2.1	5.03077	2.5	0.15964	1.3	0.85	1327	25	1825	21	2452	22	54
S70 Tshinyama	RG57809	317.00	a60	9796	1	5	4.87	17	1.91571	1.5	234.64670	33.4	0.88835	33.4	0.05	6898	65	5546	411	5070	472	136
S70 Tshinyama	RG57809	317.00	a1	2E+05	928	211	0.13	3351	0.20166	2.9	4.62267	3.5	0.16625	2.0	0.82	1184	31	1753	30	2520	34	47
S70 Tshinyama	RG57809	317.00	a3	2E+05	797	250	0.35	671	0.26682	1.8	5.78599	2.2	0.15728	1.2	0.83	1525	25	1944	19	2427	21	63

drillcore	core number	depth (m)	grain number	^{207}Pb (cps)	U[a] (ppm)	Pb[a] (ppm)	Th[c] U	^{206}Pb/^{204}Pb	^{206}Pb[e]/^{238}U	2 s %	^{207}Pb[e]/^{235}U	2 s %	^{207}Pb[e]/^{206}Pb	2 s %	rho	^{206}Pb/^{238}U	2 s (Ma)	^{207}Pb/^{235}U	2 s (Ma)	^{207}Pb/^{206}Pb	2 s (Ma)	conc %
Tshinyama S70	RG57809	317.00	a4	1273	11	0	1.70	891	0.01891	227.6	0.40324	228.8	0.15467	24.0	0.99	121	278	344	1088	2398	408	5
Tshinyama S70	RG57809	317.00	a5	1E+05	418	143	0.87	3148	0.28650	2.4	6.68662	2.6	0.16927	1.0	0.92	1624	34	2071	23	2550	17	64
Tshinyama S70	RG57809	317.00	a6	45244	210	68	0.54	17085	0.29622	3.7	4.71135	4.6	0.11535	2.7	0.80	1673	54	1769	39	1885	49	89
Tshinyama S70	RG57809	317.00	a7	2E+05	347	164	1.11	154	0.29536	3.6	10.44430	4.4	0.25646	2.6	0.81	1668	53	2475	42	3225	41	52
Tshinyama S70	RG57809	317.00	a8	72210	1356	136	0.16	572	0.08925	6.1	1.21374	7.0	0.09864	3.3	0.88	551	33	807	40	1599	61	34
Tshinyama S70	RG57809	317.00	a9	13684	141	26	0.62	2392	0.16621	10.5	2.34985	15.2	0.10254	11.0	0.69	991	98	1228	114	1671	203	59
Tshinyama S70	RG57809	317.00	a10	946	4	1	0.05	500	0.23017	5.6	4.26611	12.3	0.13443	10.9	0.46	1335	68	1687	106	2157	190	62
Tshinyama S70	RG57809	317.00	a11	2E+05	1597	263	0.09	1711	0.13724	4.7	2.80135	6.2	0.14804	4.0	0.76	829	37	1356	48	2323	69	36
Tshinyama S70	RG57809	317.00	a13	905	4	1	0.27	333	0.26894	3.4	4.38826	12.0	0.11834	11.5	0.28	1535	46	1710	105	1931	207	80
Tshinyama S70	RG57809	317.00	a14	795	3	1	0.26	588	0.33824	3.4	6.28233	9.8	0.13471	9.1	0.35	1878	56	2016	89	2160	159	87
Tshinyama S70	RG57809	317.00	a15	1E+05	293	128	0.91	14701	0.37777	2.2	9.36239	2.4	0.17974	1.1	0.88	2066	38	2374	23	2651	19	78
Tshinyama S70	RG57809	317.00	a16	1E+05	249	133	0.68	5324	0.45230	3.4	12.17514	3.6	0.19523	1.2	0.94	2405	69	2618	34	2787	19	86
Tshinyama S70	RG57809	317.00	a17	1E+05	250	89	0.83	3052	0.28304	3.2	7.66136	3.4	0.19632	1.2	0.94	1607	45	2192	31	2796	20	57
Tshinyama S70	RG57809	317.00	a18	2E+05	1344	75	0.24	1398	0.04176	5.5	0.99157	5.9	0.17220	2.2	0.93	264	14	700	31	2579	37	10
Tshinyama S70	RG57809	317.00	a19	1858	2	2	2.93	112	0.52503	14.8	18.94655	17.8	0.26172	9.8	0.83	2720	337	3039	188	3257	155	84
Tshinyama S70	RG57809	317.00	a20	2E+05	743	262	0.39	2996	0.32624	2.1	7.53765	2.2	0.16757	0.9	0.92	1820	33	2177	20	2534	14	72
Tshinyama S70	RG57809	317.00	a22	2E+05	1116	138	0.11	492	0.08623	4.9	1.90768	4.9	0.16045	0.9	0.98	533	25	1084	33	2460	15	22
Tshinyama S70	RG57809	317.00	a23	2612	8	2	0.59	65	0.12523	11.8	6.73126	32.0	0.38985	29.7	0.37	761	85	2077	331	3870	448	20
Tshinyama S70	RG57809	317.00	a24	56937	330	68	0.75	3500	0.16850	6.3	3.87121	6.9	0.16663	2.7	0.92	1004	59	1608	57	2524	46	40
Tshinyama S70	RG57809	317.00	a27	1916	11	3	0.03	1949	0.24338	2.7	3.31441	6.8	0.09877	6.3	0.40	1404	34	1484	55	1601	117	88
Tshinyama S70	RG57809	317.00	a28	1E+05	391	139	0.35	128	0.24455	5.4	5.12405	8.9	0.15197	7.0	0.61	1410	69	1840	78	2368	119	60
Tshinyama S70	RG57809	317.00	a29	51130	242	53	1.50	2784	0.14418	3.7	3.43188	4.2	0.17263	2.0	0.88	868	30	1512	34	2583	33	34

S70																					
Tshinyama	RG57809	317.00	a30	1E+05	501	158	0.75	7165	0.26605	2.2	6.52132	2.3	0.17778	0.7	0.95	1521	30	2049	21	2632	12	58
S70																					
Tshinyama	RG57809	317.00	a31	2E+05	706	243	0.49	4363	0.32149	2.3	7.70725	2.8	0.17387	1.6	0.81	1797	36	2197	26	2595	27	69
S70																					
Tshinyama	RG57809	317.00	a32	94984	327	126	0.86	5909	0.29064	8.7	7.57802	9.0	0.18910	2.4	0.96	1645	127	2182	84	2734	39	60
S70																					
Tshinyama	RG57809	317.00	a33	904	1	3	1.68	832	1.03180	1.6	16.96420	36.4	0.11924	36.3	0.04	4570	54	2933	427	1945	649	235
S70																					
Tshinyama	RG57809	317.00	a34	4647	5	5	0.81	47	0.51217	7.1	25.55738	8.9	0.36191	5.4	0.80	2666	158	3330	91	3758	82	71
S70																					
Tshinyama	RG57809	317.00	a35	2E+05	831	266	0.56	3306	0.28276	3.3	6.20369	3.9	0.15912	2.0	0.85	1605	47	2005	34	2446	34	66
S70																					
Tshinyama	RG57809	317.00	a36	2E+05	1712	217	0.06	5562	0.11390	2.0	2.67480	2.4	0.17031	1.2	0.85	695	13	1322	18	2561	21	27
S70																					
Tshinyama	RG57809	317.00	a37	1E+05	589	165	0.83	3638	0.22568	4.3	5.06906	5.0	0.16291	2.6	0.85	1312	51	1831	44	2486	44	53
S70																					
Tshinyama	RG57809	317.00	a38	2E+05	551	230	0.85	7193	0.36190	2.6	9.35741	3.4	0.18753	2.2	0.75	1991	44	2374	32	2721	37	73
S70																					
Tshinyama	RG57809	317.00	a39	1E+05	382	140	1.05	985	0.32596	3.2	8.22313	3.9	0.18297	2.2	0.83	1819	51	2256	36	2680	36	68
S70																					
Tshinyama	RG57809	317.00	a40	2E+05	1225	200	0.10	2024	0.13995	3.1	3.06881	3.5	0.15904	1.6	0.89	844	25	1425	27	2445	27	35
S70																					
Tshinyama	RG57809	317.00	a41	1E+05	210	138	0.86	16865	0.51047	2.2	12.70849	2.5	0.18056	1.0	0.91	2659	49	2658	23	2658	17	100
S70																					
Tshinyama	RG57809	317.00	a42	11539	128	12	0.74	1829	0.07255	18.6	1.91520	32.5	0.19145	26.6	0.57	452	81	1086	244	2755	438	16
S70																					
Tshinyama	RG57809	317.00	a43	18631	216	35	0.37	729	0.15340	5.1	2.11204	12.7	0.09986	11.6	0.40	920	44	1153	91	1621	216	57
S70																					
Tshinyama	RG57809	317.00	a44	2E+05	527	149	0.25	4486	0.27386	3.8	5.99022	4.1	0.15864	1.5	0.92	1560	52	1974	36	2441	26	64
S70																					
Tshinyama	RG57809	317.00	a46	2E+05	635	165	0.38	1642	0.22338	2.4	4.61360	2.8	0.14979	1.4	0.87	1300	28	1752	23	2344	23	55
S70																					
Tshinyama	RG57809	317.00	a47	1E+05	126	84	0.34	63777	0.56458	3.4	14.68070	3.8	0.18859	1.8	0.88	2886	79	2795	37	2730	30	106
S70																					
Tshinyama	RG57809	317.00	a48	1E+05	251	66	0.61	3283	0.23432	3.9	6.37752	5.2	0.19739	3.4	0.75	1357	48	2029	47	2805	56	48
S70																					
Tshinyama	RG57809	317.00	a49	1E+05	521	112	0.49	5375	0.20718	2.4	4.08343	2.6	0.14295	0.9	0.94	1214	27	1651	21	2263	15	54
S70																					
Tshinyama	RG57809	317.00	a51	3203	6	2	0.75	1690	0.24406	12.7	6.82216	20.3	0.20273	15.9	0.63	1408	163	2089	198	2848	258	49
S70																					
Tshinyama	RG57809	317.00	a52	2E+05	227	82	0.45	5306	0.31390	2.5	7.83245	2.9	0.18097	1.5	0.85	1760	38	2212	26	2662	25	66
S70																					
Tshinyama	RG57809	317.00	a53	599	1	1	0.43	237	0.34541	14.0	7.14489	21.6	0.15002	16.4	0.65	1913	236	2130	213	2346	280	82
S70																					
Tshinyama	RG57809	317.00	a55	16100	2	5	0.47	27	0.75707	5.0	65.28503	6.5	0.62542	4.2	0.77	3634	141	4258	67	4568	61	80
S70																					
Tshinyama	RG57809	317.00	a56	15887	3	6	1.84	28	0.83438	3.5	68.25181	5.7	0.59327	4.5	0.61	3911	104	4303	59	4492	66	87

drillcore	core number	depth (m)	grain number	^{207}Pb (cps)	U[a] (ppm)	Pb[a] (ppm)	Th[c] / U	^{206}Pb / ^{204}Pb	^{206}Pb[e] / ^{238}U	2 s %	^{207}Pb[e] / ^{235}U	2 s %	^{207}Pb[e] / ^{206}Pb	2 s %	rho	^{206}Pb / ^{238}U	2 s (Ma)	^{207}Pb / ^{235}U	2 s (Ma)	^{207}Pb / ^{206}Pb	2 s (Ma)	conc %
S70 Tshinyama	RG57809	317.00	a57	2E+05	287	90	0.65	6240	0.27953	2.2	6.52151	2.4	0.16921	1.0	0.92	1589	31	2049	21	2550	16	62
S70 Tshinyama	RG57809	317.00	a58	5647	14	3	0.01	1119	0.23325	3.5	3.18308	5.1	0.09897	3.8	0.67	1352	42	1453	40	1605	71	84
Kaf.15	RG41375	116.25	a55	50039	355	32	0.57	82	0.04960	3.0	1.68002	3.5	0.24567	1.8	0.86	312	9	1001	22	3157	28	10
Kaf.15	RG41375	116.25	a30	99609	1323	150	0.33	131	0.08412	2.4	2.25634	3.3	0.19453	2.3	0.71	521	12	1199	24	2781	38	19
Kaf.15	RG41375	116.25	b3	95427	1245	139	0.28	143	0.08549	4.0	2.09442	5.3	0.17768	3.6	0.75	529	20	1147	37	2631	59	20
Kaf.15	RG41375	116.25	a57	61696	299	38	0.37	350	0.09914	4.4	1.22213	5.5	0.08940	3.3	0.81	609	26	811	31	1413	62	43
Kaf.15	RG41375	116.25	a60	6486	25	4	0.37	148	0.10200	25.9	2.24868	27.5	0.15990	9.1	0.94	626	157	1196	214	2455	154	26
Kaf.15	RG41375	116.25	a14	27068	339	44	0.38	250	0.11465	2.0	2.21505	3.7	0.14013	3.0	0.55	700	13	1186	26	2229	53	31
Kaf.15	RG41375	116.25	a35	38792	388	73	0.54	180	0.13823	4.2	3.10669	5.3	0.16300	3.2	0.79	835	33	1434	41	2487	54	34
Kaf.15	RG41375	116.25	a29	21850	240	39	0.47	830	0.13893	6.9	1.67478	7.4	0.08743	2.5	0.94	839	55	999	48	1370	47	61
Kaf.15	RG41375	116.25	a44	15234	122	20	0.33	765	0.14496	3.6	2.04988	3.9	0.10256	1.6	0.91	873	29	1132	27	1671	30	52
Kaf.15	RG41375	116.25	a45	9095	65	11	1.01	356	0.14504	2.7	2.43465	4.2	0.12175	3.2	0.65	873	22	1253	31	1982	56	44
Kaf.15	RG41375	116.25	a47	45573	284	50	0.42	518	0.15513	2.3	1.89034	3.0	0.08838	2.0	0.74	930	20	1078	20	1391	39	67
Kaf.15	RG41375	116.25	a11	20855	228	44	0.75	1137	0.15841	2.4	2.03235	3.0	0.09305	1.7	0.82	948	21	1126	20	1489	32	64
Kaf.15	RG41375	116.25	b20	15921	139	27	0.42	767	0.16641	2.7	2.43568	3.2	0.10616	1.6	0.86	992	25	1253	23	1734	30	57
Kaf.15	RG41375	116.25	a2	44965	333	65	0.35	866	0.17320	3.3	2.00278	3.5	0.08386	1.2	0.94	1030	31	1116	24	1289	24	80
Kaf.15	RG41375	116.25	a42	19169	150	33	0.61	2783	0.18470	2.4	2.22443	3.1	0.08735	2.0	0.77	1093	24	1189	22	1368	38	80
Kaf.15	RG41375	116.25	b2	14310	135	32	0.78	1361	0.18860	2.0	2.26828	2.6	0.08723	1.7	0.77	1114	20	1202	18	1365	32	82
Kaf.15	RG41375	116.25	b7	27852	259	59	0.50	812	0.18997	2.2	2.19722	3.1	0.08389	2.2	0.71	1121	22	1180	22	1290	42	87
Kaf.15	RG41375	116.25	b5	6912	63	15	0.95	1132	0.19102	3.1	2.52998	4.3	0.09606	2.9	0.73	1127	32	1281	32	1549	55	73
Kaf.15	RG41375	116.25	a53	41337	163	38	0.65	410	0.19409	2.4	3.63256	3.0	0.13574	1.8	0.81	1143	25	1557	24	2174	31	53
Kaf.15	RG41375	116.25	a7	24297	262	59	0.62	2113	0.19610	2.1	2.17244	3.1	0.08035	2.3	0.67	1154	22	1172	22	1205	45	96
Kaf.15	RG41375	116.25	a40	1107	9	2	-0.07	1236	0.19664	5.0	2.43937	10.6	0.08997	9.4	0.47	1157	53	1254	80	1425	179	81
Kaf.15	RG41375	116.25	a28	5893	57	13	0.46	1848	0.19909	2.8	2.46904	8.5	0.08995	8.0	0.33	1170	30	1263	63	1424	154	82
Kaf.15	RG41375	116.25	a52	34136	172	40	0.43	1392	0.19908	2.3	2.23301	2.9	0.08135	1.8	0.78	1170	24	1191	21	1230	36	95
Kaf.15	RG41375	116.25	b4	21584	206	47	0.48	1375	0.20070	2.0	2.25555	2.4	0.08151	1.3	0.83	1179	21	1199	17	1234	26	96
Kaf.15	RG41375	116.25	b8	31591	309	72	0.47	561	0.20186	3.0	2.39589	3.6	0.08608	2.0	0.84	1185	33	1241	26	1340	39	88
Kaf.15	RG41375	116.25	a43	20306	168	37	0.44	1227	0.20405	2.1	2.25235	3.8	0.08006	3.2	0.54	1197	23	1198	27	1198	63	100
Kaf.15	RG41375	116.25	a23	12762	132	29	0.31	16156	0.20684	2.3	2.25749	2.9	0.07916	1.7	0.81	1212	26	1199	20	1176	33	103
Kaf.15	RG41375	116.25	a16	9378	88	20	0.39	9047	0.20817	2.6	2.36146	3.5	0.08227	2.3	0.76	1219	29	1231	25	1252	44	97

Kaf.15	RG41375	116.25	b22	6979	55	12	0.64	6951	0.21106	3.1	2.94014	4.1	0.10103	2.6	0.77	1234	35	1392	31	1643	48	75
drillcore	core	depth	grain	^{207}Pb	U[a]	Pb[a]	Th[c]	^{206}Pb	^{206}Pb[e]	2 s	^{207}Pb[e]	2 s	^{207}Pb[e]	2 s	rho	^{206}Pb	2 s	^{207}Pb	2 s	^{207}Pb	2 s	
	number	(m)	number	(cps)	(ppm)	(ppm)	U	^{204}Pb	^{238}U	%	^{235}U	%	^{206}Pb	%		^{238}U	(Ma)	^{235}U	(Ma)	^{206}Pb	(Ma)	conc %
Kaf.15	RG41375	116.25	a9	19935	178	41	0.45	1707	0.21330	2.2	2.38668	3.7	0.08115	3.0	0.59	1246	25	1239	27	1225	59	102
Kaf.15	RG41375	116.25	a33	4395	45	9	0.01	5443	0.21690	3.0	2.42445	5.0	0.08107	4.0	0.61	1265	35	1250	36	1223	78	103
Kaf.15	RG41375	116.25	a46	13243	82	20	0.44	7880	0.22046	2.0	2.65844	3.1	0.08746	2.4	0.64	1284	23	1317	23	1371	46	94
Kaf.15	RG41375	116.25	b11	16445	144	36	0.68	1923	0.22141	1.8	2.67547	3.0	0.08764	2.4	0.61	1289	21	1322	22	1375	46	94
Kaf.15	RG41375	116.25	b18	11505	73	21	0.74	5403	0.22133	2.2	2.84788	3.7	0.09332	2.9	0.61	1289	26	1368	28	1494	55	86
Kaf.15	RG41375	116.25	a31	26607	273	63	0.31	1461	0.22337	3.3	2.54648	3.9	0.08268	2.2	0.83	1300	38	1285	29	1262	44	103
Kaf.15	RG41375	116.25	a32	12664	133	33	0.42	2566	0.22634	2.2	2.79772	3.1	0.08965	2.2	0.71	1315	26	1355	23	1418	41	93
Kaf.15	RG41375	116.25	a36	20051	200	52	0.55	2870	0.22677	2.5	2.85055	3.3	0.09117	2.1	0.76	1318	30	1369	25	1450	40	91
Kaf.15	RG41375	116.25	b1	14496	116	27	0.21	17333	0.22885	2.2	2.65640	3.3	0.08419	2.5	0.66	1328	26	1316	25	1297	49	102
Kaf.15	RG41375	116.25	a26	11589	104	28	0.52	4355	0.23095	2.1	2.80607	3.2	0.08812	2.4	0.65	1339	25	1357	24	1385	47	97
Kaf.15	RG41375	116.25	a38	21819	187	47	0.33	25687	0.23452	2.1	2.75140	2.6	0.08509	1.5	0.82	1358	26	1342	20	1318	29	103
Kaf.15	RG41375	116.25	a24	48900	282	87	0.81	980	0.23580	3.3	3.65828	3.9	0.11252	2.0	0.86	1365	41	1562	31	1841	36	74
Kaf.15	RG41375	116.25	a22	21772	176	49	0.51	9967	0.23958	2.0	2.95356	2.7	0.08941	1.8	0.75	1384	26	1396	21	1413	34	98
Kaf.15	RG41375	116.25	a48	16232	78	20	0.25	18625	0.23949	2.4	2.88043	2.8	0.08723	1.4	0.86	1384	30	1377	21	1366	27	101
Kaf.15	RG41375	116.25	b15	16660	128	35	0.45	19412	0.24022	2.2	2.85711	2.8	0.08626	1.8	0.77	1388	27	1371	21	1344	35	103
Kaf.15	RG41375	116.25	a20	12595	92	23	0.26	14138	0.24271	2.6	2.99146	3.6	0.08939	2.5	0.72	1401	32	1405	27	1413	47	99
Kaf.15	RG41375	116.25	a34	12691	102	27	0.30	1704	0.24317	2.6	2.86987	4.0	0.08560	3.1	0.64	1403	33	1374	31	1329	60	106
Kaf.15	RG41375	116.25	a51	6163	26	7	0.22	1756	0.24518	2.6	3.19252	4.3	0.09444	3.5	0.60	1414	33	1455	34	1517	65	93
Kaf.15	RG41375	116.25	a25	18485	149	43	0.53	22313	0.24815	2.2	2.83760	2.7	0.08294	1.5	0.82	1429	28	1366	20	1268	29	113
Kaf.15	RG41375	116.25	a6	14341	108	27	0.26	11333	0.24861	2.6	3.15901	4.1	0.09216	3.2	0.62	1431	33	1447	32	1471	62	97
Kaf.15	RG41375	116.25	b6	23642	195	54	0.35	4777	0.25209	2.1	3.08795	2.9	0.08884	2.1	0.71	1449	27	1430	23	1401	40	103
Kaf.15	RG41375	116.25	b13	31416	284	73	0.15	1432	0.25627	2.8	3.20121	3.2	0.09060	1.7	0.86	1471	37	1457	25	1438	31	102
Kaf.15	RG41375	116.25	a21	2032	14	4	0.56	2245	0.25648	2.0	3.21135	5.6	0.09081	5.2	0.36	1472	26	1460	44	1443	99	102
Kaf.15	RG41375	116.25	b12	21561	156	42	0.27	23950	0.25664	1.8	3.20586	2.3	0.09060	1.5	0.75	1473	23	1459	18	1438	29	102
Kaf.15	RG41375	116.25	a8	27448	172	49	0.37	29432	0.25761	1.8	3.31962	2.5	0.09346	1.7	0.73	1478	24	1486	20	1497	33	99
Kaf.15	RG41375	116.25	a41	20769	129	34	0.19	16057	0.25909	2.0	3.24389	2.7	0.09080	1.8	0.73	1485	26	1468	21	1443	35	103
Kaf.15	RG41375	116.25	a4	15506	91	28	0.53	4051	0.26435	3.2	3.53874	4.3	0.09709	2.9	0.74	1512	43	1536	35	1569	54	96
Kaf.15	RG41375	116.25	a49	1143	6	2	0.14	1409	0.27448	4.6	3.08557	6.3	0.08153	4.4	0.73	1564	64	1429	50	1234	86	127
Kaf.15	RG41375	116.25	a58	21019	48	16	0.65	1218	0.27771	2.4	4.61931	2.9	0.12064	1.5	0.84	1580	34	1753	24	1966	28	80
Kaf.15	RG41375	116.25	b16	39835	228	65	0.13	40659	0.28450	2.0	3.86887	2.5	0.09863	1.5	0.80	1614	29	1607	20	1598	28	101
Kaf.15	RG41375	116.25	a10	38366	143	52	0.64	606	0.28904	2.7	4.50284	4.1	0.11299	3.1	0.65	1637	39	1731	35	1848	57	89
Kaf.15	RG41375	116.25	a37	44823	223	74	0.31	852	0.28920	2.6	5.16787	3.2	0.12960	1.9	0.82	1638	38	1847	28	2093	33	78

drillcore	core	depth	grain	^{207}Pb	U[a]	Pb[a]	Th[c]	^{206}Pb	^{206}Pb[e]	2 s	^{207}Pb[e]	2 s	^{207}Pb[e]	2 s	rho	^{206}Pb	2 s	^{207}Pb	2 s	^{207}Pb	2 s	
	number	(m)	number	(cps)	(ppm)	(ppm)	U	^{204}Pb	^{238}U	%	^{235}U	%	^{206}Pb	%		^{238}U	(Ma)	^{235}U	(Ma)	^{206}Pb	(Ma)	conc %
Kaf.15	RG41375	116.25	a12	24162	116	40	0.71	1748	0.29264	3.4	4.41924	4.4	0.10952	2.8	0.77	1655	50	1716	38	1792	52	92
Kaf.15	RG41375	116.25	b17	24448	101	39	0.64	10046	0.30663	1.8	4.87243	2.4	0.11525	1.6	0.73	1724	27	1798	20	1884	30	92
Kaf.15	RG41375	116.25	a54	44795	120	43	0.53	1158	0.30883	2.4	5.71652	3.7	0.13425	2.8	0.65	1735	37	1934	33	2154	49	81
Kaf.15	RG41375	116.25	a13	40021	208	73	0.41	2053	0.31909	2.5	4.85764	3.0	0.11041	1.6	0.84	1785	39	1795	25	1806	29	99
Kaf.15	RG41375	116.25	a59	21695	45	17	0.51	18911	0.31964	2.2	5.06225	3.0	0.11486	2.0	0.74	1788	35	1830	25	1878	36	95
Kaf.15	RG41375	116.25	a50	25255	70	28	0.62	23390	0.32164	2.1	4.79855	2.6	0.10820	1.4	0.83	1798	34	1785	22	1769	26	102
Kaf.15	RG41375	116.25	b10	14946	70	30	0.84	13969	0.32177	2.8	4.77632	3.8	0.10766	2.5	0.75	1798	45	1781	32	1760	45	102
Kaf.15	RG41375	116.25	a18	11529	48	19	0.47	9180	0.32904	2.1	5.22670	3.2	0.11521	2.4	0.67	1834	34	1857	27	1883	42	97
Kaf.15	RG41375	116.25	b14	14667	64	28	0.88	10582	0.34318	2.1	5.53492	2.7	0.11697	1.7	0.78	1902	35	1906	24	1911	31	100
Kaf.15	RG41375	116.25	a39	37864	168	73	0.68	6093	0.34492	4.4	5.39701	4.9	0.11348	2.3	0.89	1910	73	1884	43	1856	41	103
Kaf.15	RG41375	116.25	a27	66332	329	133	0.50	7825	0.35654	1.9	5.77225	2.4	0.11742	1.4	0.81	1966	33	1942	21	1917	25	103
Kaf.15	RG41375	116.25	b19	1E+05	234	103	0.30	2663	0.39506	2.1	11.08192	2.6	0.20345	1.5	0.82	2146	39	2530	24	2854	24	75
Kaf.15	RG41375	116.25	b9	23598	88	43	0.62	847	0.40637	1.8	6.82820	2.9	0.12186	2.2	0.62	2198	33	2089	26	1984	40	111
Kaf.15	RG41375	116.25	b21	53941	132	65	0.38	36578	0.43014	2.1	8.80167	2.4	0.14841	1.3	0.84	2306	40	2318	23	2328	22	99
Kaf.15	RG41375	116.25	a19	48123	73	46	0.39	25931	0.53328	2.3	13.66668	2.7	0.18587	1.4	0.85	2755	51	2727	26	2706	23	102
Kaf.15	RG41382	157.00	a21	1076	10	1	1.11	1039	0.09108	9.4	1.31158	14.4	0.10445	10.9	0.65	562	51	851	86	1705	200	33
Kaf.15	RG41382	157.00	a2	20030	248	38	1.04	15505	0.13631	4.6	1.58978	4.7	0.08459	1.1	0.97	824	36	966	30	1306	21	63
Kaf.15	RG41382	157.00	a42	37375	328	64	0.85	11736	0.15663	2.1	1.80635	2.6	0.08364	1.4	0.84	938	19	1048	17	1284	27	73
Kaf.15	RG41382	157.00	b54	31625	171	30	0.84	7655	0.15861	2.3	1.76875	2.7	0.08088	1.3	0.87	949	21	1034	18	1218	26	78
Kaf.15	RG41382	157.00	a17	33899	400	63	0.14	12475	0.15986	3.1	1.77672	3.3	0.08061	1.0	0.95	956	28	1037	22	1212	20	79
Kaf.15	RG41382	157.00	a43	20168	156	33	0.97	2731	0.16727	2.1	1.85665	2.9	0.08050	2.0	0.72	997	19	1066	19	1209	39	82
Kaf.15	RG41382	157.00	b18	20998	180	32	0.65	13450	0.16959	2.1	1.94603	2.9	0.08322	2.0	0.71	1010	20	1097	20	1274	40	79
Kaf.15	RG41382	157.00	a23	2110	23	10	6.78	668	0.17771	4.4	2.00433	6.4	0.08180	4.6	0.69	1054	43	1117	44	1241	91	85
Kaf.15	RG41382	157.00	a15	23369	149	33	0.20	416	0.18629	4.1	2.24532	4.9	0.08742	2.6	0.84	1101	42	1195	35	1370	51	80
Kaf.15	RG41382	157.00	a11	35984	292	57	0.43	1713	0.18642	2.2	2.28014	2.5	0.08871	1.2	0.87	1102	22	1206	18	1398	24	79
Kaf.15	RG41382	157.00	a20	41479	305	70	0.57	1388	0.19027	2.5	2.32107	3.2	0.08847	1.9	0.79	1123	26	1219	23	1393	37	81
Kaf.15	RG41382	157.00	a45	17406	95	22	0.39	777	0.19900	2.1	3.02699	3.1	0.11032	2.3	0.68	1170	23	1414	24	1805	42	65
Kaf.15	RG41382	157.00	b31	24018	210	50	0.84	12515	0.20058	2.2	2.26795	2.6	0.08201	1.4	0.84	1178	24	1202	18	1246	27	95
Kaf.15	RG41382	157.00	a57	52711	259	53	0.22	13414	0.20078	2.6	2.20555	2.9	0.07967	1.4	0.88	1179	28	1183	21	1189	27	99
Kaf.15	RG41382	157.00	a31	17320	173	36	0.40	11236	0.20100	2.4	2.23622	2.9	0.08069	1.7	0.82	1181	26	1192	21	1214	33	97
Kaf.15	RG41382	157.00	b7	30288	249	53	0.29	11060	0.20135	2.2	2.23586	2.4	0.08053	0.9	0.92	1183	24	1192	17	1210	18	98
drillcore	core	depth	grain	^{207}Pb	U[a]	Pb[a]	Th[c]	^{206}Pb	^{206}Pb[e]	2 s	^{207}Pb[e]	2 s	^{207}Pb[e]	2 s	rho	^{206}Pb	2 s	^{207}Pb	2 s	^{207}Pb	2 s	

	number	(m)	number	(cps)	(ppm)	(ppm)	U	^{204}Pb	^{238}U	%	^{235}U	%	^{206}Pb	%		^{238}U	(Ma)	^{235}U	(Ma)	^{206}Pb	(Ma)	conc %
Kaf.15	RG41382	157.00	a50	43449	243	59	0.55	10446	0.20203	2.6	2.34597	3.2	0.08422	1.9	0.81	1186	28	1226	23	1298	37	91
Kaf.15	RG41382	157.00	a34	10470	109	27	0.82	12659	0.20322	2.4	2.31371	3.0	0.08257	1.7	0.81	1193	26	1216	21	1259	34	95
Kaf.15	RG41382	157.00	b56	5564	22	5	1.01	6171	0.20364	2.4	2.53005	3.5	0.09011	2.6	0.67	1195	26	1281	26	1428	50	84
Kaf.15	RG41382	157.00	b55	25127	96	21	0.68	28527	0.20525	1.8	2.49397	2.5	0.08813	1.6	0.75	1203	20	1270	18	1385	31	87
Kaf.15	RG41382	157.00	b9	54276	420	81	0.01	64399	0.20593	2.3	2.39167	2.6	0.08423	1.3	0.87	1207	25	1240	19	1298	25	93
Kaf.15	RG41382	157.00	b49	9597	48	11	0.35	11896	0.20815	2.2	2.31280	3.1	0.08059	2.2	0.71	1219	24	1216	22	1211	43	101
Kaf.15	RG41382	157.00	b21	20211	180	41	0.32	25158	0.21069	2.3	2.33520	2.8	0.08039	1.7	0.80	1232	26	1223	20	1206	33	102
Kaf.15	RG41382	157.00	a35	18924	209	51	0.59	21002	0.21102	2.7	2.39985	3.1	0.08248	1.5	0.88	1234	31	1243	22	1257	29	98
Kaf.15	RG41382	157.00	b6	30321	295	62	0.13	6634	0.21401	2.0	2.33283	3.0	0.07906	2.2	0.67	1250	23	1222	22	1174	44	107
Kaf.15	RG41382	157.00	b23	66414	434	104	0.59	14871	0.21547	2.4	2.95208	2.6	0.09937	0.9	0.94	1258	27	1395	20	1612	17	78
Kaf.15	RG41382	157.00	b15	21652	160	39	0.72	4962	0.21642	2.0	2.63228	2.6	0.08821	1.7	0.76	1263	23	1310	19	1387	32	91
Kaf.15	RG41382	157.00	b50	60703	259	60	0.32	25328	0.21781	2.1	2.58946	2.4	0.08623	1.1	0.88	1270	24	1298	18	1343	22	95
Kaf.15	RG41382	157.00	b5	7136	54	12	0.22	3473	0.21914	2.0	2.51803	3.1	0.08334	2.4	0.64	1277	23	1277	23	1277	46	100
Kaf.15	RG41382	157.00	b41	46465	304	71	0.29	46268	0.22002	2.1	2.54241	2.3	0.08381	1.0	0.91	1282	25	1284	17	1288	19	100
Kaf.15	RG41382	157.00	a37	36619	301	73	0.35	41897	0.22465	2.5	2.70339	2.8	0.08728	1.2	0.90	1306	30	1329	21	1367	24	96
Kaf.15	RG41382	157.00	a22	12904	104	28	0.55	14999	0.22568	2.4	2.68068	2.9	0.08615	1.6	0.82	1312	28	1323	21	1342	32	98
Kaf.15	RG41382	157.00	a30	43293	390	106	0.61	11952	0.22638	2.1	2.68286	2.5	0.08595	1.4	0.84	1316	25	1324	19	1337	27	98
Kaf.15	RG41382	157.00	a19	19268	142	37	0.48	21940	0.22789	2.5	2.75984	3.0	0.08783	1.8	0.81	1323	30	1345	23	1379	34	96
Kaf.15	RG41382	157.00	a25	28890	364	88	0.66	4334	0.22784	4.1	2.69524	4.4	0.08580	1.6	0.93	1323	50	1327	33	1334	31	99
Kaf.15	RG41382	157.00	b40	30240	198	50	0.40	13513	0.22806	2.1	2.69440	2.4	0.08569	1.1	0.89	1324	25	1327	18	1331	21	99
Kaf.15	RG41382	157.00	b43	11105	64	18	0.82	13123	0.22792	2.3	2.66047	3.0	0.08466	1.9	0.77	1324	28	1318	23	1308	37	101
Kaf.15	RG41382	157.00	b42	46076	251	64	0.63	10914	0.22879	2.0	2.88444	2.2	0.09144	0.9	0.91	1328	24	1378	16	1456	17	91
Kaf.15	RG41382	157.00	a36	7185	67	17	0.33	8346	0.22916	2.1	2.71794	3.2	0.08602	2.4	0.67	1330	25	1333	24	1339	46	99
Kaf.15	RG41382	157.00	b26	14742	115	28	0.24	9799	0.22910	2.1	2.69471	2.5	0.08531	1.4	0.83	1330	25	1327	19	1323	27	101
Kaf.15	RG41382	157.00	b32	3350	32	8	0.47	4257	0.22975	2.5	2.51792	5.0	0.07949	4.3	0.51	1333	31	1277	37	1184	85	113
Kaf.15	RG41382	157.00	b47	58227	278	67	0.28	67531	0.22979	2.0	2.73142	2.4	0.08621	1.4	0.82	1333	24	1337	18	1343	26	99
Kaf.15	RG41382	157.00	b38	27762	211	51	0.30	32815	0.22997	2.2	2.68238	2.5	0.08460	1.3	0.86	1334	26	1324	19	1306	25	102
Kaf.15	RG41382	157.00	a54	41110	167	40	0.42	12053	0.23081	2.3	2.95070	2.5	0.09272	1.0	0.92	1339	28	1395	19	1482	18	90
Kaf.15	RG41382	157.00	a44	6251	39	11	0.74	7249	0.23152	1.9	2.75030	3.0	0.08616	2.3	0.65	1342	24	1342	23	1342	44	100
Kaf.15	RG41382	157.00	a56	7116	30	9	0.78	8628	0.23188	2.4	2.63663	3.4	0.08247	2.3	0.72	1344	29	1311	25	1257	46	107
Kaf.15	RG41382	157.00	b25	25297	191	48	0.35	29177	0.23188	2.0	2.77337	2.5	0.08674	1.4	0.82	1344	24	1348	18	1355	27	99
Kaf.15	RG41382	157.00	b57	8413	27	7	0.31	9775	0.23235	2.3	2.75634	3.6	0.08604	2.8	0.64	1347	28	1344	27	1339	54	101
drillcore	core number	depth (m)	grain number	^{207}Pb (cps)	U[a] (ppm)	Pb[a] (ppm)	Th[c] U	^{206}Pb ^{204}Pb	^{206}Pb[e] ^{238}U	2 s %	^{207}Pb[e] ^{235}U	2 s %	^{207}Pb[e] ^{206}Pb	2 s %	rho	^{206}Pb ^{238}U	2 s (Ma)	^{207}Pb ^{235}U	2 s (Ma)	^{207}Pb ^{206}Pb	2 s (Ma)	conc

																						%
Kaf.15	RG41382	157.00	a29	18419	159	38	0.22	15217	0.23277	2.3	2.75297	3.2	0.08578	2.2	0.72	1349	28	1343	24	1333	42	101
Kaf.15	RG41382	157.00	b35	37412	290	69	0.20	43107	0.23309	2.2	2.79462	2.8	0.08696	1.7	0.79	1351	27	1354	21	1360	34	99
Kaf.15	RG41382	157.00	b8	16034	110	29	0.44	18435	0.23473	2.0	2.80999	2.7	0.08682	1.8	0.74	1359	24	1358	20	1357	34	100
Kaf.15	RG41382	157.00	a12	73394	461	145	0.66	28332	0.23487	4.2	3.71190	4.3	0.11462	1.2	0.96	1360	51	1574	35	1874	22	73
Kaf.15	RG41382	157.00	b1	15715	104	27	0.36	18127	0.23540	2.1	2.81488	2.8	0.08673	1.7	0.78	1363	26	1360	21	1354	33	101
Kaf.15	RG41382	157.00	a58	1381	6	2	0.45	1843	0.23555	4.3	2.44393	7.7	0.07525	6.4	0.56	1364	53	1256	57	1075	128	127
Kaf.15	RG41382	157.00	a60	99354	365	86	0.19	16168	0.23673	2.1	3.05880	2.4	0.09371	1.1	0.89	1370	26	1422	18	1502	20	91
Kaf.15	RG41382	157.00	a7	19384	124	31	0.21	21153	0.23697	2.4	2.99289	2.9	0.09160	1.7	0.81	1371	29	1406	22	1459	32	94
Kaf.15	RG41382	157.00	b36	15812	122	33	0.48	12588	0.23835	2.3	2.94562	2.8	0.08963	1.6	0.82	1378	29	1394	22	1418	31	97
Kaf.15	RG41382	157.00	a51	26181	109	28	0.24	29315	0.24036	2.7	2.95674	3.1	0.08922	1.6	0.85	1389	34	1397	24	1409	31	99
Kaf.15	RG41382	157.00	a16	15098	106	26	0.17	16875	0.24233	2.1	2.98743	2.7	0.08941	1.6	0.80	1399	27	1404	21	1413	31	99
Kaf.15	RG41382	157.00	a28	25430	213	52	0.17	30043	0.24285	2.0	2.83279	2.4	0.08460	1.3	0.84	1402	26	1364	18	1306	26	107
Kaf.15	RG41382	157.00	b48	3048	13	3	0.18	3544	0.24714	2.7	2.93079	4.2	0.08601	3.3	0.63	1424	34	1390	32	1338	63	106
Kaf.15	RG41382	157.00	b37	11760	79	21	0.34	12909	0.24851	2.0	3.12595	2.7	0.09123	1.8	0.75	1431	26	1439	21	1451	35	99
Kaf.15	RG41382	157.00	b20	87293	417	117	0.37	12945	0.25075	2.6	3.77972	2.9	0.10932	1.2	0.91	1442	34	1588	23	1788	22	81
Kaf.15	RG41382	157.00	b4	22713	145	41	0.65	25883	0.25181	2.0	3.04875	2.4	0.08781	1.4	0.82	1448	26	1420	19	1378	26	105
Kaf.15	RG41382	157.00	a47	56086	242	66	0.22	59543	0.26075	2.2	3.38191	2.6	0.09407	1.3	0.87	1494	30	1500	20	1509	24	99
Kaf.15	RG41382	157.00	b22	56115	233	75	0.68	451	0.26610	2.5	4.15439	3.0	0.11323	1.6	0.84	1521	34	1665	25	1852	29	82
Kaf.15	RG41382	157.00	a32	29388	208	61	0.35	19396	0.27206	2.2	3.54546	2.7	0.09452	1.5	0.83	1551	31	1537	21	1518	28	102
Kaf.15	RG41382	157.00	a41	16086	90	27	0.32	17001	0.27285	2.1	3.55569	2.5	0.09452	1.5	0.81	1555	28	1540	20	1518	28	102
Kaf.15	RG41382	157.00	b16	68692	341	103	0.71	3064	0.27470	2.0	4.32210	2.3	0.11411	1.1	0.88	1565	28	1698	19	1866	20	84
Kaf.15	RG41382	157.00	a4	25097	118	39	1.30	5979	0.27579	2.0	4.11102	2.4	0.10811	1.3	0.84	1570	28	1656	20	1768	24	89
Kaf.15	RG41382	157.00	a8	38229	284	84	0.81	5650	0.28357	2.0	3.78680	3.2	0.09685	2.5	0.64	1609	29	1590	26	1564	46	103
Kaf.15	RG41382	157.00	b33	68401	354	120	0.57	4903	0.29170	2.0	4.42760	2.2	0.11009	1.0	0.90	1650	29	1718	19	1801	17	92
Kaf.15	RG41382	157.00	a18	26784	132	54	0.98	3301	0.29225	2.2	4.28028	2.7	0.10622	1.6	0.80	1653	32	1690	23	1736	30	95
Kaf.15	RG41382	157.00	b3	1E+05	438	137	0.28	4256	0.29422	2.2	4.66352	2.6	0.11496	1.5	0.82	1663	32	1761	22	1879	27	88
Kaf.15	RG41382	157.00	a26	13193	70	22	0.52	3621	0.29452	2.1	4.14689	2.6	0.10212	1.5	0.82	1664	32	1664	22	1663	28	100
Kaf.15	RG41382	157.00	a13	38019	171	60	0.47	34957	0.29512	2.1	4.41640	2.5	0.10853	1.4	0.83	1667	31	1715	21	1775	26	94
Kaf.15	RG41382	157.00	a52	18546	51	18	0.74	17340	0.29798	2.3	4.39167	2.6	0.10689	1.3	0.87	1681	34	1711	22	1747	24	96
Kaf.15	RG41382	157.00	b24	3884	38	12	0.32	4200	0.30205	31.2	6.45456	114.8	0.15498	110.4	0.27	1701	485	2040	5141	2402	1877	71
Kaf.15	RG41382	157.00	a59	17621	38	14	0.69	15950	0.30469	3.6	4.64594	4.3	0.11059	2.2	0.85	1715	55	1758	36	1809	41	95
Kaf.15	RG41382	157.00	b29	32226	135	48	0.42	15488	0.31232	2.2	4.81152	2.4	0.11173	1.0	0.91	1752	34	1787	21	1828	18	96
drillcore	core	depth	grain	^{207}Pb	U[a]	Pb[a]	Th[c]	^{206}Pb	^{206}Pb[e]	2 s	^{207}Pb[e]	2 s	^{207}Pb[e]	2 s	rho	^{206}Pb	2 s	^{207}Pb	2 s	^{207}Pb	2 s	
	number	(m)	number	(cps)	(ppm)	(ppm)	U	^{204}Pb	^{238}U	%	^{235}U	%	^{206}Pb	%		^{238}U	(Ma)	^{235}U	(Ma)	^{206}Pb	(Ma)	conc %

Kaf.15	RG41382	157.00	b45	50892	151	48	0.15	47174	0.31243	1.9	4.64147	2.3	0.10775	1.3	0.84	1753	30	1757	20	1762	23	99
Kaf.15	RG41382	157.00	a53	37223	89	34	0.68	8534	0.31289	1.9	4.94462	2.4	0.11462	1.4	0.81	1755	29	1810	20	1874	25	94
Kaf.15	RG41382	157.00	a24	32098	134	49	0.39	26059	0.31360	2.3	5.19096	2.6	0.12005	1.2	0.89	1758	36	1851	22	1957	21	90
Kaf.15	RG41382	157.00	b34	19881	93	34	1.07	17340	0.31370	2.1	4.97089	2.9	0.11493	1.9	0.74	1759	33	1814	25	1879	35	94
Kaf.15	RG41382	157.00	b10	35724	142	52	0.44	10363	0.31565	2.0	4.86566	2.5	0.11180	1.4	0.83	1768	31	1796	21	1829	25	97
Kaf.15	RG41382	157.00	a10	42404	181	69	0.66	36847	0.31755	2.4	5.04180	2.8	0.11515	1.4	0.86	1778	37	1826	24	1882	26	94
Kaf.15	RG41382	157.00	b11	24616	100	36	0.36	22669	0.32080	2.1	4.80093	2.5	0.10854	1.3	0.85	1794	34	1785	22	1775	25	101
Kaf.15	RG41382	157.00	a9	47194	186	66	0.59	32660	0.32185	2.0	5.00846	2.4	0.11286	1.2	0.85	1799	32	1821	20	1846	22	97
Kaf.15	RG41382	157.00	a39	59437	265	97	0.46	20010	0.32436	2.8	4.95520	3.5	0.11080	2.1	0.80	1811	45	1812	30	1813	38	100
Kaf.15	RG41382	157.00	a49	35214	91	39	0.74	30901	0.32433	2.0	5.08772	2.5	0.11377	1.4	0.83	1811	32	1834	21	1860	24	97
Kaf.15	RG41382	157.00	a46	42148	126	46	0.40	37113	0.32449	2.4	5.07658	2.8	0.11347	1.3	0.88	1812	39	1832	24	1856	24	98
Kaf.15	RG41382	157.00	b53	14035	28	11	0.58	12602	0.32512	2.3	4.99717	3.0	0.11148	2.0	0.76	1815	37	1819	26	1824	36	100
Kaf.15	RG41382	157.00	b30	58246	233	90	0.55	42081	0.32643	2.1	5.20642	2.3	0.11568	0.9	0.91	1821	33	1854	20	1890	17	96
Kaf.15	RG41382	157.00	a27	13317	60	24	0.63	7247	0.32822	2.1	5.13104	2.7	0.11338	1.6	0.78	1830	33	1841	23	1854	30	99
Kaf.15	RG41382	157.00	b2	58200	230	90	0.57	10503	0.32832	3.3	5.03090	3.7	0.11114	1.7	0.89	1830	53	1825	32	1818	32	101
Kaf.15	RG41382	157.00	b28	23950	95	42	0.92	20805	0.32827	2.0	5.21280	2.4	0.11517	1.3	0.84	1830	32	1855	20	1883	23	97
Kaf.15	RG41382	157.00	b17	22534	86	34	0.54	19784	0.32840	2.1	5.12387	2.4	0.11316	1.3	0.85	1831	33	1840	21	1851	23	99
Kaf.15	RG41382	157.00	a6	26849	100	42	0.76	23423	0.32903	2.0	5.19705	2.5	0.11456	1.4	0.81	1834	32	1852	21	1873	26	98
Kaf.15	RG41382	157.00	a14	18215	73	29	0.57	16117	0.33048	2.0	5.14611	2.6	0.11294	1.6	0.79	1841	33	1844	22	1847	28	100
Kaf.15	RG41382	157.00	b39	26711	97	35	0.32	23860	0.33351	2.2	5.15087	2.7	0.11201	1.6	0.80	1855	35	1845	23	1832	29	101
Kaf.15	RG41382	157.00	a5	22012	82	33	0.54	19325	0.33457	2.4	5.25356	2.9	0.11388	1.6	0.84	1861	39	1861	25	1862	28	100
Kaf.15	RG41382	157.00	b13	95026	297	116	0.46	9498	0.34309	2.4	5.93906	2.7	0.12555	1.2	0.89	1902	39	1967	24	2037	22	93
Kaf.15	RG41382	157.00	b44	36153	99	44	0.88	31281	0.34543	2.1	5.50599	2.4	0.11560	1.1	0.89	1913	35	1902	21	1889	20	101
Kaf.15	RG41382	157.00	b14	58880	194	78	0.42	48778	0.34777	1.9	5.78758	2.3	0.12070	1.2	0.86	1924	32	1945	20	1967	21	98
Kaf.15	RG41382	157.00	a1	11325	38	16	0.47	9910	0.35107	2.1	5.51527	2.9	0.11394	2.1	0.70	1940	35	1903	26	1863	38	104
Kaf.15	RG41382	157.00	a48	14263	29	14	0.62	10809	0.38904	2.4	7.07959	3.2	0.13198	2.1	0.74	2118	43	2121	29	2125	37	100
Kaf.15	RG41382	157.00	b12	41664	61	38	0.43	7631	0.50822	1.9	12.98593	2.3	0.18532	1.2	0.84	2649	42	2679	22	2701	21	98
Kaf.15	RG41382	157.00	a40	23046	35	27	1.47	12421	0.51918	2.6	13.27804	3.1	0.18549	1.7	0.83	2696	58	2700	30	2703	29	100
Kaf.15	RG41382	157.00	b19	34225	48	34	0.86	7414	0.52019	2.1	13.20877	2.3	0.18416	0.9	0.92	2700	47	2695	22	2691	15	100
Kaf.15	RG41382	157.00	a55	47145	39	28	0.77	24805	0.52190	2.5	13.66005	3.0	0.18983	1.6	0.85	2707	56	2726	28	2741	26	99
Kaf.15	RG41382	157.00	b46	47887	49	30	0.54	12974	0.53592	2.2	13.75041	2.3	0.18609	0.9	0.92	2766	49	2733	22	2708	15	102

[a] within-run background-corrected mean ^{207}Pb signal in counts per second

[b] U and Pb content and Th/U ratio were calculated relative to GJ-1 and are accurate to approximately 10%.

[c] corrected for background, mass bias, laser induced U-Pb fractionation and common Pb (if detectable, see analytical method) using Stacey & Kramers (1975) model Pb composition. $^{207}Pb/^{235}U$ calculated using $^{207}Pb/^{206}Pb/(^{238}U/^{206}Pb \times 1/137.88)$. Errors are propagated by quadratic addition of within-run errors (2SE) and the reproducibility of GJ-1 (2SD).

[d] Rho is the error correlation defined as $err^{206}Pb/^{238}U/err^{207}Pb/^{235}U$.

Table 3

Sample	Subgroup	Drillcore	Depth (m)	Lithology	$\partial^{13}C_{carb}$ (‰, VPDB)	$\partial^{18}O_{carb}$ (‰, VPDB)	$\partial^{13}C_{org}$ (‰, VPDB)	ε_{TOC}	Mn (ppm)	Sr (ppm)	Fe (%)	Ca/Sr	Mn/Sr	Rb/Sr	$^{87}Sr/^{86}Sr$
ULB61	BIIe	Handspecimen	-	∂Ls	-2.87	-5.43	-	-	166	151	0.52	6.5E-04	1.10	0.0874	0.7103
ULB65	BIIe	Handspecimen	-	∂Ls	-3.92	-7.53	-	-	255	216	1.03	9.0E-04	1.18	0.0787	0.7081
ULB68	BIIe	Handspecimen	-	∂Ls	-7.13	-5.49	-32	25.7	302	152	1.41	1.1E-03	1.99	0.1750	-
ULB611	BIIe	Handspecimen	-	∂Ls	-2.32	-4.31	-	-	-	-	-	-	-	-	-
ULB614	BIIe	Handspecimen	-	∂Ls	-3.50	-7.32	-30.9	28.3	153	161	0.44	7.6E-04	0.95	0.0435	0.7080
ULB72	BIIe	Handspecimen	-	∂Ls	-2.05	-8.71	-31.4	26.7	819	2536	0.3	-4.0E-03	0.82	0.0026	0.7051
ULB77	BIIe	Handspecimen	-	∂Ls	-1.60	-6.14	-	-	687	602	0.3	2.5E-03	1.14	0.0020	0.7055
ULB79	BIIe	Handspecimen	-	∂Ls	-2.07	-7.45	-	-	336	147	0.51	6.2E-04	2.29	0.0483	0.7070
ULB712	BIIe	Handspecimen	-	∂Ls	-1.91	-4.49	-	-	1260	111	0.9	6.3E-04	11.35	0.1640	-
ULB53	BIId	Bena Tshovu	80	dol	0.80	-1.53	-25.2	26.7	22	21.3	0.07	2.6E-04	1.03	0.0188	0.7059
ULB56	BIId	Bena Tshovu	77.2	dol	-0.24	-2.78	-	-	53	86.1	0.75	7.1E-04	0.62	0.3287	-
ULB521	BIId	Bena Tshovu	69.8	dol	0.50	-2.29	-	-	56	68.8	0.39	4.4E-04	0.81	0.1061	-
ULB524	BIId	Bena Tshovu	67.2	dol	0.50	-2.22	-	-	55	54.8	0.11	3.4E-04	1.00	0.0128	0.7076
ULB532	BIId	Bena Tshovu	63.5	dol	-0.23	-10.89	-	-	60	134	0.18	5.2E-04	0.45	0.0067	0.7087
ULB533	BIId	Bena Tshovu	63.15	dol	-	-	-	-	-	33.4	-	-	-	-	-
ULB536	BIId	Bena Tshovu	61.15	dol	2.28	-1.36	-	-	49	39.5	0.19	3.0E-04	1.24	0.0177	0.7063
ULB539	BIId	Bena Tshovu	60.2	dol	1.27	-1.66	-	-	67	41.9	0.16	2.8E-04	1.60	0.0310	-
ULB542	BIId	Bena Tshovu	58.7	dol	0.61	-15.07	-	-	-	-	-	-	-	-	-
ULB543	BIId	Bena Tshovu	58.1	dol	1.07	-1.66	-	-	60	34.4	0.13	2.2E-04	1.74	0.0145	0.7066
ULB547	BIId	Bena Tshovu	57.4	dol	0.40	-5.36	-	-	51	97.8	0.31	6.0E-	0.52	0.0624	-

ULB550	BIId	Bena Tshovu	55.6	dol	0.51	-1.75	-	-	43	73.1	0.2	4.3E-04	0.59	0.0342	-
ULB555	BIId	Bena Tshovu	53.3	dol	1.37	-1.76	-	-	55	40.7	0.13	2.6E-04	1.35	0.0172	0.7065
ULB560	BIId	Bena Tshovu	52.25	dol	0.37	-2.95	-	-	127	57.7	1.25	5.1E-04	2.20	0.6568	-
ULB564	BIId	Bena Tshovu	51.7	dol	1.25	-1.64	-	-	29	23.1	0.09	3.7E-04	1.26	0.0260	-
ULB573	BIId	Bena Tshovu	50.5	dol	0.73	-2.31	-	-	18	33.4	0.11	2.5E-04	0.54	0.0210	-
ULB577	BIId	Bena Tshovu	48.15	dol	0.64	-1.84	-	-	42	41.9	0.12	2.7E-04	1.00	0.0143	0.7072
ULB578	BIId	Bena Tshovu	48	∂sul	-	-	-	-	18	40.6	0.05	7.7E-04	0.44	0.0300	0.7075
ULB588	BIId	Bena Tshovu	44.3	dol	2.14	-0.62	-	-	81	63.1	0.3	5.0E-04	1.28	0.0697	0.7081
ULB41	BIIb	Kanshi	435.8	dol	0.84	-3.23	-	-	-	-	-	-	-	-	-
Sample	Subgroup	Drillcore	Depth (m)	Lithology	$\partial^{13}C_{carb}$ (‰, VPDB)	$\partial^{18}O_{carb}$ (‰, VPDB)	$\partial^{13}C_{org}$ (‰, VPDB)	e_{TOC}	Mn (ppm)	Sr (ppm)	Fe (%)	Ca/Sr	Mn/Sr	Rb/Sr	$^{87}Sr/^{86}Sr$
ULB40	BIIb	Kanshi	435.4	dol	-0.86	-1.89	-	-	-	-	-	-	-	-	-
ULB43	BIIb	Kanshi	434.8	dol	0.45	-0.63	-30.2	31.6	31	117	0.06	6.4E-04	0.26	0.0034	0.7070
ULB45	BIIb	Kanshi	433.5	dol	0.79	-0.86	-	-	38	93.7	0.06	2.5E-04	0.41	0.0021	0.7062
ULB46	BIIb	Kanshi	433.4	dol	-0.33	-5.67	-	-	-	-	-	-	-	-	-
ULB47	BIIb	Kanshi	431.8	dol	0.21	-0.80	-	-	45	90.4	0.07	2.7E-04	0.50	0.0321	0.7074
ULB410	BIIb	Kanshi	429.8	dol	-0.55	-0.73	-	-	53	103	0.09	2.8E-04	0.51	0.0078	-
ULB413	BIIb	Kanshi	428.1	dol	-1.77	-1.21	-	-	-	-	-	-	-	-	-
ULB414	BIIb	Kanshi	427.9	dol	0.03	-1.29	-	-	-	-	-	-	-	-	-
ULB417	BIIb	Kanshi	427.2	dol	-0.14	-0.23	-	-	161	85.9	0.09	3.4E-04	1.87	0.0023	0.7069
ULB422	BIIb	Kanshi	424.6	dol	0.79	-1.45	-	-	-	-	-	-	-	-	-
ULB425	BIIb	Kanshi	423.9	dol	0.56	-1.04	-	-	135	55.5	0.04	1.6E-04	2.43	0.0018	0.7062
ULB427	BIIb	Kanshi	422.4	dol	1.23	-1.66	-26.1	28.1	-	-	-	-	-	-	-
ULB429	BIIb	Kanshi	421.2	dol	-0.29	-2.29	-	-	-	-	-	-	-	-	-
ULB432	BIIb	Kanshi	419.8	dol	-0.06	0.16	-	-	-	-	-	-	-	-	-

Sample	Subgroup	Drillcore	Depth (m)	Lithology	$\partial^{13}C_{carb}$ (‰, VPDB)	$\partial^{18}O_{carb}$ (‰, VPDB)	$\partial^{13}C_{org}$ (‰, VPDB)	e_{TOC}	Mn (ppm)	Sr (ppm)	Fe (%)	Ca/Sr	Mn/Sr	Rb/Sr	$^{87}Sr/^{86}Sr$
ULB438	BIIb	Kanshi	415.8	dol	-0.57	-0.20	-	-	47	76	0.25	2.2E-04	0.62	0.0539	-
ULB440	BIIb	Kanshi	414.6	dol	1.01	-2.34	-27.7	29.5	-	-	-	-	-	-	-
ULB443	BIIb	Kanshi	412.8	dol	-0.39	-0.08	-	-	52	182	0.32	5.6E-04	0.29	0.0280	0.7073
ULB443	BIIb	Kanshi	412.8	dol	-0.39	-0.08	-	-	41	161	0.25	9.1E-04	0.25	0.0329	
ULB446	BIIb	Kanshi	400.8	dol	1.36	-0.58	-	-	37	83.2	0.07	2.4E-04	0.44	0.0024	0.7061
ULB446	BIIb	Kanshi	400.8	dol	1.36	-0.58	-	-	31	85.6	0.06	3.9E-04	0.36	0.0023	
ULB452	BIIb	Kanshi	404.4	dol	-0.57	-0.13	-	-	84	133	0.21	4.0E-04	0.63	0.0060	0.7066
ULB454	BIIb	Kanshi	402.6	dol	-0.19	-0.14	-	-	111	100	0.33	3.2E-04	1.11	0.0110	-
ULB456	BIIb	Kanshi	400.6	dol	1.97	-2.66	-	-	-	-	-	-	-	-	-
ULB457	BIIb	Kanshi	400.2	dol	0.14	-0.69	-	-	-	-	-	-	-	-	-
ULB459	BIIb	Kanshi	396.8	dol	0.21	-0.36	-	-	78	90.6	0.39	2.9E-04	0.86	0.0132	0.7073
ULB463	BIIb	Kanshi	391.4	dol	3.01	-1.36	-	-	-	-	-	-	-	-	-
ULB465	BIIb	Kanshi	389.8	dol	2.47	-0.63	-	-	57	97	0.08	3.0E-04	0.59	0.0031	0.7066
ULB467	BIIb	Kanshi	388.8	dol	2.66	-0.67	-	-	-	-	-	-	-	-	-
ULB468	BIIb	Kanshi	388.9	dol	1.52	-0.01	-	-	-	-	-	-	-	-	-
ULB471B	BIIc	Kanshi	383.6	dol	2.19	-1.07	-	-	-	-	-	-	-	-	-
ULB475	BIIc	Kanshi	382.9	dol	0.38	-3.24	-	-	-	-	-	-	-	-	-
ULB477	BIIc	Kanshi	381.1	dol	1.19	-0.75	-	-	81	61.8	0.2	1.9E-04	1.31	0.0518	0.7082
ULB478	BIIc	Kanshi	378.4	dol	1.73	-0.47	-	-	235	62.9	0.19	1.9E-04	3.74	0.0366	-
ULB482	BIIc	Kanshi	372.8	dol	1.24	-1.93	-	-	-	-	-	-	-	-	-
ULB484	BIIc	Kanshi	369.4	dol	0.79	-2.21	-	-	-	-	-	-	-	-	-
ULB486	BIIc	Kanshi	367.4	dol	0.60	-2.39	-	-	-	-	-	-	-	-	-
ULB486	BIIc	Kanshi	367.4	dol	0.55	-2.45	-	-	-	-	-	-	-	-	-
ULB489	BIIc	Kanshi	366.4	dol	0.58	-2.37	-	-	410	68.2	0.25	3.4E-04	6.01	0.0044	-
ULB493	BIIc	Kanshi	363.8	dol	0.29	-2.32	-	-	259	56.8	0.16	1.8E-04	4.56	0.0018	-
ULB494	BIIc	Kanshi	362.8	dol	-0.31	-3.56	-	-	-	-	-	-	-	-	-

Sample	Subgroup	Drillcore	Depth (m)	Lithology	$\partial^{13}C_{carb}$ (‰, VPDB)	$\partial^{18}O_{carb}$ (‰, VPDB)	$\partial^{13}C_{org}$ (‰, VPDB)	e_{TOC}	Mn (ppm)	Sr (ppm)	Fe (%)	Ca/Sr	Mn/Sr	Rb/Sr	$^{87}Sr/^{86}Sr$
ULB4104	BIIc	Kanshi	356.8	dol	-0.31	-1.83	-	-	-	-	-	-	-	-	-
ULB4107	BIIc	Kanshi	355.1	dol	-0.32	-1.80	-	-	-	-	-	-	-	-	-
ULB4112	BIIc	Kanshi	353.4	dol	-0.47	-1.91	-	-	371	93	0.32	2.8E-04	3.99	0.0129	0.7067
ULB4114	BIIc	Kanshi	352.4	dol	-0.53	-2.09	-	-	-	-	-	-	-	-	-
ULB4118	BIIc	Kanshi	349.4	dol	-0.73	-2.23	-	-	-	-	-	-	-	-	-
ULB4118	BIIc	Kanshi	349.4	dol	-0.73	-2.18	-	-	-	-	-	-	-	-	-
ULB4121	BIIc	Kanshi	347.2	dol	-0.90	-1.76	-	-	-	-	-	-	-	-	-
ULB4122B	BIIc	Kanshi	345.6	dol	-0.56	-1.65	-	-	-	-	-	-	-	-	-
334/2**	BIIc	Kanshi	344.6	dol	-	-	-32.6	32.6	435	77.4	0.36	3.8E-04	5.62	0.0129	-
ULB4132	BIIc	Kanshi	341.4	dol	-1.00	-1.85	-	-	-	-	-	-	-	-	-
ULB4133	BIIc	Kanshi	341.1	dol	-0.79	-1.89	-	-	320	85.1	0.16	4.4E-04	3.76	0.0012	0.7060
ULB4137	BIIc	Kanshi	338.8	dol	-0.94	-1.94	-	-	-	-	-	-	-	-	-
ULB4138	BIIc	Kanshi	337.8	dol	-0.72	-1.68	-	-	303	98.1	0.26	3.0E-04	3.09	0.0153	0.7066
ULB4139	BIIc	Kanshi	337.2	dol	-0.68	-1.40	-	-	325	72.3	0.14	2.2E-04	4.50	0.0014	-
ULB4140	BIIc	Kanshi	336.8	dol	-0.74	-1.20	-	-	-	-	-	-	-	-	-
ULB4142	BIIc	Kanshi	335.2	dol	-0.68	-1.50	-	-	-	-	-	-	-	-	-
ULB4143	BIIc	Kanshi	334.6	dol	-0.59	-1.71	-	-	-	-	-	-	-	-	-
ULB4145	BIIc	Kanshi	333.4	dol	-0.65	-1.93	-	-	-	-	-	-	-	-	-
ULB4146	BIIc	Kanshi	333.1	dol	-0.56	-1.66	-	-	-	-	-	-	-	-	-
ULB4150	BIIc	Kanshi	331.4	dol	-0.41	-2.53	-	-	-	-	-	-	-	-	-
ULB4151	BIIc	Kanshi	330.8	dol	-0.64	-1.84	-	-	413	79.8	0.27	2.8E-04	5.18	0.0050	0.7066
ULB4152	BIIc	Kanshi	330.4	dol	-1.45	-1.94	-	-	-	-	-	-	-	-	-
ULB4154	BIIc	Kanshi	329.8	dol	-0.53	-1.64	-	-	-	-	-	-	-	-	-
ULB4159	BIIc	Kanshi	326.8	dol	-0.27	-1.64	-	-	-	-	-	-	-	-	-
ULB4160	BIIc	Kanshi	325.4	dol	-0.83	-1.60	-	-	-	-	-	-	-	-	-
ULB4164	BIIc	Kanshi	318.6	dol	-0.14	-2.20	-	-	277	52.8	0.13	2.8E-04	5.25	0.0019	-
ULB4166	BIIc	Kanshi	318.2	dol	0.03	-1.68	-	-	-	-	-	-	-	-	-
ULB4167	BIIc	Kanshi	317.6	dol	-0.05	-2.39	-	-	-	-	-	-	-	-	-
ULB4169	BIIc	Kanshi	316.8	dol	-0.21	-2.17	-	-	288	84.4	0.29	2.9E-	3.41	0.0130	0.7067

Sample	Subgroup	Drillcore	Depth	Lithology	$\partial^{13}C_{carb}$	$\partial^{18}O_{carb}$	$\partial^{13}C_{org}$	e_{TOC}	Mn	Sr	Fe	Ca/Sr	Mn/Sr	Rb/Sr	$^{87}Sr/^{86}Sr$
ULB4177	BIIc	Kanshi	313.4	dol	0.48	-2.23	-	-	-	-	-	2.1E-04	-	-	-
ULB4180	BIIc	Kanshi	311.8	dol	0.77	-1.94	-	-	-	-	-	-	-	-	-
ULB4181	BIIc	Kanshi	311.2	dol	0.68	-1.91	-	-	-	-	-	-	-	-	-
ULB4191	BIIc	Kanshi	307.6	dol	0.85	-1.96	-	-	-	-	-	-	-	-	-
ULB4193	BIIc	Kanshi	306.2	dol	0.79	-2.48	-	-	-	-	-	-	-	-	-
ULB4195	BIIc	Kanshi	305.1	dol	0.97	-2.31	-	-	233	48.5	0.16	1.9E-04	4.80	0.0041	0.7062
ULB4201	BIIc	Kanshi	303.8	dol	1.45	-1.87	-	-	-	-	-	-	-	-	-
ULB4209	BIIc	Kanshi	299.1	dol	1.26	-1.39	-	-	-	-	-	-	-	-	-
ULB4212	BIIc	Kanshi	297.6	dol	1.21	-1.67	-	-	-	-	-	-	-	-	-
ULB4213B	BIIc	Kanshi	296.8	dol	1.38	-1.76	-	-	319	55.7	0.17	2.9E-04	5.73	0.0018	-
ULB4218	BIIc	Kanshi	293.4	dol	1.48	-2.47	-	-	-	-	-	-	-	-	-
ULB4224	BIIc	Kanshi	289.4	dol	1.47	-2.24	-	-	397	54.3	0.38	2.0E-04	7.31	0.0460	-
ULB4225	BIIc	Kanshi	288.1	dol	1.48	-3.04	-	-	-	-	-	-	-	-	-
ULB4232	BIIc	Kanshi	286.2	dol	2.10	-2.34	-	-	284	43.1	0.53	1.4E-04	6.59	0.1810	-
ULB4233	BIIc	Kanshi	284.8	dol	-	-	-29.2	-	-	-	-	-	-	-	0.7074
ULB4234	BIIc	Kanshi	284.4	dol	2.12	-2.17	-27.6	30.5	297	36	0.62	1.8E-04	8.25	0.0889	-
ULB4235	BIIc	Kanshi	283.2	dol	1.28	-4.56	-30	32.2	-	-	-	-	-	-	-
273/1*	BIIc	Kanshi	283.1	dol	-	-	-28.6	-	607	36.6	0.86	2.5E-03	16.58	0.0246	-
ULB4240	BIIc	Kanshi	280.8	dol	2.12	-2.95	-	-	-	-	-	1.5E-02	-	-	-
269/1**	BIIc	Kanshi	279.1	dol	-	-	-28.1	-	-	-	-	5.7E-03	-	-	-
ULB4243	BIIc	Kanshi	278.4	dol	2.01	-2.79	-	-	-	-	-	6.7E-03	-	-	-
ULB4244B	BIIc	Kanshi	277	∂shale	-	-	-22.9	-	43	17.5	2.13	4.8E-04	2.46	4.3714	-
ULB4244C1	BIIc	Kanshi	276	∂shale	-	-	-	-	23	20.5	1.64	2.1E-02	1.12	3.7268	-
ULB4244C2	BIIc	Kanshi	272	∂shale	-	-	-23	-	86	24.4	2.27	1.70	3.52	3.0943	-
ULB4244D	BIIc	Kanshi	270	∂shale	-	-	-	-	28	21.3	1.66	7.19	1.31	3.9531	-
ULB4244E	BIIc	Kanshi	269.5	∂shale	-	-	-	-	436	42	2.99	17.1	10.38	1.3833	-
ULB4244F	BIIc	Kanshi	268	∂shale	-	-	-22.8	-	29	17.1	7.19	2.1E-02	1.70	3.7310	-

			(m)		(‰, VPDB)	(‰, VPDB)	(‰, VPDB)		(ppm)	(ppm)	(%)				
ULB4246	BIIc	Kanshi	268.2	dol	3.76	-2.91	-	-	521	47.5	1.92	2.3E-04	10.97	0.2000	0.7345
ULB4249	BIIc	Kanshi	267.4	dol	4.46	-2.80	-	-	-	-	-	-	-	-	-
ULB4252	BIIc	Kanshi	265.4	dol	3.94	-2.95	-	-	-	-	-	-	-	-	-
ULB4255A	BIIc	Kanshi	263.4	dol	3.89	-3.28	-	-	-	-	-	-	-	-	-
ULB4259	BIIc	Kanshi	260.1	dol	3.78	-3.00	-	-	-	-	-	-	-	-	-
ULB4264	BIIc	Kanshi	258.2	dol	4.65	-2.45	-	-	449	42.3	0.28	1.7E-04	10.61	0.0307	-
ULB4269	BIIc	Kanshi	255.8	dol	4.45	-2.51	-	-	-	-	-	-	-	-	-
ULB4276A	BIIc	Kanshi	251.8	dol	4.17	-2.93	-	-	-	-	-	-	-	-	-
ULB4276B	BIIc	Kanshi	251.6	dol	3.98	-3.33	-	-	-	-	-	-	-	-	-
ULB4276B*	BIIc	Kanshi	251.6	dol	3.82	-5.20	-	-	-	-	-	-	-	-	-
ULB4282*	BIIc	Kanshi	249.2	dol	3.11	-5.29	-	-	-	-	-	-	-	-	-
ULB4282	BIIc	Kanshi	249.2	dol	3.71	-3.12	-	-	-	-	-	-	-	-	-
ULB4285	BIIc	Kanshi	246.8	dol	4.01	-2.50	-	-	-	-	-	-	-	-	-
ULB4287	BIIc	Kanshi	246.4	dol	3.96	-2.40	-	-	-	-	-	-	-	-	-
ULB4291	BIIc	Kanshi	244.2	dol	3.78	-2.55	-	-	-	-	-	-	-	-	-
ULB4291*	BIIc	Kanshi	244.2	dol	3.57	-5.04	-	-	-	-	-	-	-	-	-
ULB4293	BIIc	Kanshi	243.6	dol	3.78	-2.24	-	-	-	-	-	-	-	-	-
ULB4296	BIIc	Kanshi	242.6	dol	3.95	-2.54	-	-	395	46.7	0.27	1.9E-04	8.46	0.0385	-
ULB4299	BIIc	Kanshi	241.6	dol	3.56	-2.28	-	-	-	-	-	-	-	-	-
ULB4307	BIIc	Kanshi	237.2	dol	3.87	-2.67	-	-	-	-	-	-	-	-	-
ULB4310	BIIc	Kanshi	234.6	dol	3.46	-2.65	-	-	-	-	-	-	-	-	-
ULB4310	BIIc	Kanshi	234.6	dol	3.08	-5.14	-	-	-	-	-	-	-	-	-
ULB4314	BIIc	Kanshi	232.8	dol	3.54	-2.26	-	-	-	-	-	-	-	-	-
ULB4322	BIIc	Kanshi	229.4	dol	3.52	-2.13	-	-	393	49.9	0.27	2.1E-04	7.88	0.0982	0.7158
ULB4326	BIIc	Kanshi	228.4	dol	3.62	-2.40	-	-	-	-	-	-	-	-	-
ULB4327	BIIc	Kanshi	227.8	dol	3.51	-2.44	-	-	-	-	-	-	-	-	-
ULB4329	BIIc	Kanshi	226.6	dol	3.42	-2.52	-	-	-	-	-	-	-	-	-
ULB4330	BIIc	Kanshi	226.1	dol	3.45	-2.44	-	-	-	-	-	-	-	-	-
ULB4331	BIIc	Kanshi	225.6	dol	3.41	-3.00	-	-	-	-	-	-	-	-	-
ULB4331*	BIIc	Kanshi	225.6	dol	2.37	-6.11	-	-	-	-	-	-	-	-	-
ULB4336	BIIc	Kanshi	223.8	dol	3.42	-2.36	-	-	-	-	-	-	-	-	-

ULB4338	BIIc	Kanshi	222.8	dol	3.47	-2.61	-	-	-	-	-	-	-	-	-
Sample	Subgroup	Drillcore	Depth (m)	Lithology	$\partial^{13}C_{carb}$ (‰, VPDB)	$\partial^{18}O_{carb}$ (‰, VPDB)	$\partial^{13}C_{org}$ (‰, VPDB)	e_{TOC}	Mn (ppm)	Sr (ppm)	Fe (%)	Ca/Sr	Mn/Sr	Rb/Sr	$^{87}Sr/^{86}Sr$
ULB4338*	BIIc	Kanshi	222.8	dol	2.69	-2.00	-	-	-	-	-	-	-	-	-
ULB4343	BIIc	Kanshi	220.2	dol	3.40	-2.83	-	-	-	-	-	-	-	-	-
ULB4346	BIIc	Kanshi	218.2	dol	3.50	-3.01	-	-	-	-	-	-	-	-	-
ULB4348	BIIc	Kanshi	216.8	dol	3.82	-2.26	-	-	-	-	-	-	-	-	-
ULB4350	BIIc	Kanshi	216.1	dol	3.92	-2.48	-	-	-	-	-	-	-	-	-
ULB4351	BIIc	Kanshi	215.6	dol	4.07	-2.21	-	-	-	-	-	-	-	-	-
ULB4352	BIIc	Kanshi	214	dol	4.12	-2.51	-	-	-	-	-	-	-	-	-
ULB4353	BIIc	Kanshi	214.8	dol	4.06	-2.83	-	-	465	45.3	0.68	3.4E-04	10.26	0.4128	0.7426
ULB4355	BIIc	Kanshi	213.8	dol	4.14	-2.93	-	-	-	-	-	-	-	-	-
ULB4356	BIIc	Kanshi	213.2	dol	4.28	-2.86	-	-	-	-	-	-	-	-	-
ULB4357	BIIc	Kanshi	212.8	dol	4.16	-2.94	-	-	-	-	-	-	-	-	-
ULB4361	BIIc	Kanshi	211.8	dol	4.18	-2.80	-	-	-	-	-	-	-	-	-
ULB4363	BIIc	Kanshi	210.8	dol	4.34	-3.11	-	-	-	-	-	-	-	-	-
ULB4363	BIIc	Kanshi	210.8	dol	3.21	-2.05	-	-	-	-	-	-	-	-	-
ULB4367	BIIc	Kanshi	208.6	dol	-	-	-	-	-	-	-	-	-	-	-
ULB4368	BIIc	Kanshi	207.8	dol	3.98	-3.22	-27.9	-	-	-	-	-	-	-	-
ULB4368*	BIIc	Kanshi	207.8	dol	4.00	-5.54	-	-	-	-	-	-	-	-	-
ULB4364	BIIc	Kanshi	210.4	dol	4.28	-2.76	-	-	-	-	-	-	-	-	-
ULB4366	BIIc	Kanshi	209.4	dol	4.25	-3.04	-	-	571	31.8	0.45	1.5E-04	17.96	0.1635	-
ULB4367	BIIc	Kanshi	208.6	dol	4.01	-3.36	-	-	-	-	-	-	-	-	-
ULB4370	BIIc	Kanshi	206.4	dol	4.01	-3.16	-	-	-	-	-	-	-	-	-
ULB4372	BIIc	Kanshi	204.8	dol	4.50	-3.04	-	-	-	-	-	-	-	-	-
ULB4373	BIIc	Kanshi	204.4	dol	4.19	-2.89	-	-	-	-	-	-	-	-	-
ULB4376	BIIc	Kanshi	201.1	dol	4.34	-2.81	-	-	409	31.6	0.58	1.8E-04	12.94	0.3038	-
ULB4383	BIIc	Kanshi	197.8	dol	4.95	-2.95	-	-	359	44.2	0.52	2.3E-04	8.12	0.2014	-
ULB4391	BIIc	Kanshi	192.8	dol	4.43	-2.94	-	-	-	-	-	-	-	-	-
ULB4394	BIIc	Kanshi	190.4	dol	4.63	-2.76	-	-	-	-	-	-	-	-	-
ULB4394	BIIc	Kanshi	190.4	dol	4.11	-2.93	-	-	-	-	-	-	-	-	-
ULB4396	BIIc	Kanshi	189.6	dol	4.83	-3.03	-	-	-	-	-	-	-	-	-

Sample	Subgroup	Drillcore	Depth (m)	Lithology	$\partial^{13}C_{carb}$ (‰, VPDB)	$\partial^{18}O_{carb}$ (‰, VPDB)	$\partial^{13}C_{org}$ (‰, VPDB)	e_{TOC}	Mn (ppm)	Sr (ppm)	Fe (%)	Ca/Sr	Mn/Sr	Rb/Sr	$^{87}Sr/^{86}Sr$
ULB4413	BIIc	Kanshi	174.6	dol	4.55	-3.09	-	-	-	-	-	-	-	-	-
ULB4415B	BIIc	Kanshi	172	∂shale	-	-	-	-	41	26	1.77	7.4E-03	1.58	3.6731	-
ULB4415C	BIIc	Kanshi	171	∂shale	-	-	-26.1	-	29	20.3	1.6	1.4E-02	1.43	4.1576	-
ULB4415D	BIIc	Kanshi	170	∂shale	-	-	-	-	61	10.6	9.78	1.2E-02	5.75	5.4811	-
ULB4415E	BIIc	Kanshi	169	∂shale	-	-	-26.2	-	24	24.2	1.7	1.9E-02	0.99	3.2355	-
ULB4415F	BIIc	Kanshi	168	∂shale	-	-	-	-	177	20.4	2.53	1.0E-03	8.68	3.7745	-
ULB4416	BIIc	Kanshi	167.1	dol	4.54	-3.21	-	-	-	-	-	-	-	-	-
ULB4417	BIIc	Kanshi	166.1	dol	4.57	-2.87	-27.5	32.9	-	-	-	-	-	-	-
ULB4420	BIIc	Kanshi	157.6	dol	4.63	-2.94	-	-	-	-	-	-	-	-	-
ULB4423	BIIc	Kanshi	149.4	dol	4.82	-3.04	-	-	-	-	-	-	-	-	-
ULB4424	BIIc	Kanshi	148.8	dol	4.70	-3.25	-	-	-	-	-	-	-	-	-
ULB4430	BIIc	Kanshi	146.1	dol	4.70	-3.33	-	-	417	48.4	0.66	2.1E-04	8.62	0.0269	0.7120
ULB4432	BIIc	Kanshi	144.6	dol	4.94	-2.63	-	-	-	-	-	-	-	-	-
ULB4434	BIIc	Kanshi	144.2	dol	5.22	-2.74	-	-	-	-	-	-	-	-	-
ULB4436	BIIc	Kanshi	142.8	dol	4.67	-2.61	-	-	-	-	-	-	-	-	-
ULB4436*	BIIc	Kanshi	142.8	dol	-0.42	-4.37	-	-	-	-	-	-	-	-	-
ULB4438	BIIc	Kanshi	142.1	dol	4.76	-2.70	-	-	404	43.3	0.63	2.1E-04	9.33	0.0600	-
ULB4442	BIIc	Kanshi	140.8	dol	4.38	-3.69	-	-	-	-	-	-	-	-	-
ULB4443	BIIc	Kanshi	140.4	dol	4.93	-2.66	-	-	-	-	-	-	-	-	-
ULB4445	BIIc	Kanshi	140.1	dol	4.85	-2.66	-	-	-	-	-	-	-	-	-
ULB4446	BIIc	Kanshi	139.4	dol	4.37	-1.82	-	-	-	-	-	-	-	-	-
ULB4447	BIIc	Kanshi	138.8	dol	4.35	-1.62	-	-	-	-	-	-	-	-	-
ULB4447*	BIIc	Kanshi	138.8	dol	-6.51	-7.09	-	-	-	-	-	-	-	-	-
ULB4450	BIIc	Kanshi	136.8	dol	4.31	-2.26	-	-	-	-	-	-	-	-	-
ULB4451	BIIc	Kanshi	136.1	dol	4.55	-2.52	-	-	-	-	-	-	-	-	-
ULB4456B	BIIc	Kanshi	133	∂shale	-	-	-25.7	-	65	25.3	2.17	1.5E-02	2.57	3.0870	-
ULB4456C	BIIc	Kanshi	132	∂shale	-	-	-	-	84	19.5	2.35	1.3E-02	4.31	3.8923	-
ULB4456D	BIIc	Kanshi	131	∂shale	-	-	-	-	105	19.4	3.27	7.2E-	5.41	4.1598	-

Sample	Subgroup	Drillcore	Depth (m)	Lithology	$\partial^{13}C_{carb}$ (‰, VPDB)	$\partial^{18}O_{carb}$ (‰, VPDB)	$\partial^{13}C_{org}$ (‰, VPDB)	e_{TOC}	Mn (ppm)	Sr (ppm)	Fe (%)	Ca/Sr	Mn/Sr	Rb/Sr	$^{87}Sr/^{86}Sr$
ULB4456E	BIIc	Kanshi	130	∂shale	-	-	-25.5	-	138	15.1	4.01	4.1E-03	9.14	4.2583	-
ULB4456F	BIIc	Kanshi	129	∂shale	-	-	-	-	194	21.8	3.33	7.2E-04	8.90	3.0917	-
ULB4456	BIIc	Kanshi	128.8	dol	3.67	-2.47	-	-	426	53.7	2.02	2.6E-04	7.93	0.0186	-
ULB4457	BIIc	Kanshi	128.2	dol	4.18	-2.67	-	-	-	-	-	-	-	-	-
ULB4457B	BIIc	Kanshi	128.1	∂shale	-	-	-23.7	-	252	33.5	3.32	5.6E-04	7.52	1.6925	-
ULB4458	BIIc	Kanshi	128.1	dol	4.28	-2.30	-	-	386	54.6	2.21	2.7E-04	7.07	0.0934	-
ULB4459	BIIc	Kanshi	127.8	dol	4.33	-1.64	-	-	-	-	-	-	-	-	-
ULB4459B	BIIc	Kanshi	127	∂shale	-	-	-23.9	-	263	38.9	2.87	4.7E-04	6.76	1.3136	-
ULB4462	BIIc	Kanshi	125.4	dol	3.20	-2.17	-24	27.9	-	-	-	-	-	-	-
ULB4464	BIIc	Kanshi	122.8	dol	2.23	-2.22	-	-	-	-	-	-	-	-	-
ULB4465	BIIc	Kanshi	122.1	dol	2.83	-2.55	-	-	515	71.7	3.4	3.0E-04	7.18	0.0167	-
ULB4466	BIIc	Kanshi	119.8	dol	4.68	-3.11	-	-	341	57.2	0.91	2.6E-04	5.96	0.0140	0.7070
ULB4466	BIIc	Kanshi	119.8	dol	3.54	-1.35	-	-	341	57.2	0.91	2.6E-04	5.96	0.0140	0.7070
ULB4469	BIIc	Kanshi	118.1	dol	-	-	-22.8	-	-	-	-	-	-	-	-
ULB4470	BIIc	Kanshi	117.8	dol	3.71	-2.03	-	-	-	-	-	-	-	-	-
ULB38	BIIb	Bena Kalenda	102.5	dol	-1.90	-3.50	-	-	58	394	0.28	1.7E-03	0.15	0.0140	0.7069
ULB310	BIIb	Bena Kalenda	101.5	dol	-2.15	-4.51	-	-	30	2576	0.13	3.4E-03	0.03	0.0013	0.7063
ULB311	BIIb	Bena Kalenda	101	dol	-2.11	-4.52	-	-	30	> 1000	0.13	3.8E-03	0.03	0.0016	-
ULB313	BIIb	Bena Kalenda	100.5	dol	-2.90	-4.09	-	-	41	942	0.18	4.1E-03	0.04	0.0046	0.7063
ULB316	BIIb	Bena Kalenda	99.5	dol	-2.78	-3.98	-	-	54	> 1000	0.22	4.5E-03	0.05	0.0041	-
ULB319	BIIb	Bena Kalenda	97	dol	-2.83	-4.12	-	-	47	894	0.24	3.8E-03	0.05	0.0065	0.7065
ULB325	BIIb	Bena Kalenda	90.5	dol	-2.57	-3.13	-	-	54	5247	0.16	4.5E-03	0.05	0.0022	0.7063

ULB327	BIIb	Bena Kalenda	85	dol	-1.42	-3.48	-	-	34	473	0.05	2.4E-03	0.07	0.0011	-
ULB330	BIIb	Bena Kalenda	77	dol	-2.81	-2.23	-	-	99	134	0.27	6.1E-04	0.74	0.0239	0.7071
ULB334	BIIb	Bena Kalenda	68	dol	0.39	-2.81	-	-	13	134	0.05	5.6E-04	0.10	0.0022	0.7065
ULB340	BIIb	Bena Kalenda	58	dol	-0.58	0.84	-	-	21	203	0.09	9.1E-04	0.10	0.0049	0.7071
ULB344	BIIb	Bena Kalenda	52	dol	-0.09	-1.96	-	-	44	194	0.08	8.0E-04	0.23	0.0026	0.7065
ULB344	BIIb	Bena Kalenda	52	dol	-0.09	-1.96	-	-	46	194	0.08	7.9E-04	0.24	0.0026	0.7065
ULB346	BIIb	Bena Kalenda	48	dol	0.18	1.60	-	-	64	117	0.31	5.9E-04	0.55	0.0547	0.7090
ULB348	BIIb	Bena Kalenda	45	dol	0.64	3.88	-	-	40	175	0.19	6.9E-04	0.23	0.0143	0.7068
ULB348	BIIb	Bena Kalenda	45	dol	0.62	3.91	-	-	40	175	0.19	6.9E-04	0.23	0.0143	0.7068
ULB353	BIIb	Bena Kalenda	42	dol	2.24	-1.04	-	-	40	119	0.08	5.4E-04	0.34	0.0176	0.7067
ULB358	BIIb	Bena Kalenda	40.75	dol	1.37	-0.76	-	-	47	85.3	0.16	4.0E-04	0.55	0.0481	0.7074
ULB363	BIIb	Bena Kalenda	35	dol	1.44	-2.52	-	-	38	308	0.06	2.0E-03	0.12	0.0019	0.7071
ULB367	BIIb	Bena Kalenda	30	dol	3.18	-2.17	-25.1	-	-	-	-	-	-	-	-
ULB370	BIIb	Bena Kalenda	27	dol	1.34	-2.40	-24.7	-	-	-	-	-	-	-	-
ULB374	BIIb	Bena Kalenda	25	dol	2.16	-2.03	-	-	90	45.1	0.12	2.0E-04	2.00	0.0177	0.7065

Sample	Subgroup	Drillcore	Depth (m)	Lithology	$\partial^{13}C_{carb}$ (‰, VPDB)	$\partial^{18}O_{carb}$ (‰, VPDB)	$\partial^{13}C_{org}$ (‰, VPDB)	e_{TOC}	Mn (ppm)	Sr (ppm)	Fe (%)	Ca/Sr	Mn/Sr	Rb/Sr	$^{87}Sr/^{86}Sr$
RG31070	BIIa	Handspecimen	-	dol	-1.60	-1.70	-	-	697	90.3	0.33	5.2E-04	7.72	0.0986	-
RG31041	BIIa	Handspecimen	-	dol	-2.40	-7.37	-	-	1830	158	0.71	6.1E-04	11.58	0.1576	-
ULB11	BIe_2	S70 Tshinyama	24	dol	1.18	-1.39	-	-	895	357	1.13	3.0E-03	2.51	0.0930	0.7122
ULB15	BIe_2	S70 Tshinyama	22	dol	0.46	-1.65	-	-	1110	82.3	1.26	7.1E-04	13.49	0.5844	-
ULB17	BIe_3	S70 Tshinyama	21	sulf	-	-	-	-	25	288	0.04	5.0E-03	0.14	0.0100	0.7102
ULB18	BIe_3	S70 Tshinyama	19	sulf	-	-	-	-	40	402	0.13	3.3E-03	0.06	0.0000	0.7097

ULB19	BIe_2	S70 Tshinyama	18	dol	-1.67	-2.74	-	-	2410	77	0.31	4.6E-04	31.30	0.0727	-
ULB110	BIe_3	S70 Tshinyama	17	∂sulf	-	-	-	-	402	105	0.42	5.0E-03	3.83	0.0100	0.7078
ULB113	BIe_2	S70 Tshinyama	18	dol	-4.44	-2.65	-	-	993	61.6	1.63	5.3E-04	16.12	0.5179	-
ULB115	BIe_3	S70 Tshinyama	16	∂sulf	-	-	-	-	1750	111	0.09	5.3E-03	15.80	0.0100	0.7073
ULB117	BIe_2	S70 Tshinyama	14	dol	-5.69	-2.71	-	-	1620	72.7	0.93	5.7E-04	22.28	0.2407	-
ULB117	BIe_2	S70 Tshinyama	14	dol	-5.69	-2.71	-	-	1680	75.3	0.98	5.8E-04	22.31	0.2390	-
ULB121	BIe_2	S70 Tshinyama	11	dol	-7.54	-2.11	-27.8	20.8	1570	71	1.39	5.4E-04	22.11	0.2690	0.7205
ULB127	BIe_2	S70 Tshinyama	6	dol	-5.85	-2.36	-	-	1080	84.2	0.57	4.9E-04	12.83	0.1283	-
ULB128	BIe_2	S70 Tshinyama	5	dol	-5.21	-1.10	-	-	1340	86.6	0.83	5.9E-04	15.47	0.1697	0.7164
ULB130	BIe_2	S70 Tshinyama	3	dol	-	-	-27.4	-	-	-	-	-	-	-	-
ULB22	BIe_1	Kaf.15	45	dol	0.05	-1.64	-	-	752	76.2	1.78	6.0E-04	9.87	0.3504	0.7295
ULB26	BIe_1	Kaf.15	37	dol	-1.55	-3.26	-	-	401	81.8	1.38	5.0E-04	4.90	0.2078	-
ULB27	BIe_1	Kaf.15	34	dol	-0.61	-1.94	-	-	451	118	0.97	5.8E-04	3.82	0.0636	-
ULB29	BIe_1	Kaf.15	30	dol	-1.80	-2.78	-	-	450	106	1.8	5.6E-04	4.25	0.1066	-
ULB214	BIe_2	Kaf.15	25.9	dol	-3.32	-3.54	-	-	260	60.3	1.9	5.8E-04	4.31	0.4461	-
ULB217	BIe_2	Kaf.15	25	dol	-4.10	-6.49	-	-	329	105	1.68	6.6E-04	3.13	0.1505	-
ULB219	BIe_2	Kaf.15	24.5	dol	-2.55	-2.80	-	-	368	73.1	0.68	4.1E-04	5.03	0.0766	-
ULB226	BIe_2	Kaf.15	20	dol	-5.27	-2.96	-27.7	25.4	567	95.2	1.27	6.0E-04	5.96	0.1597	0.7160
ULB228	BIe_2	Kaf.15	18	dol	-5.01	-3.10	-28.1	26.3	429	61.1	1.39	4.7E-04	7.02	0.3273	0.7237
ULB229	BIe_2	Kaf.15	17.5	dol	-5.00	-2.57	-	-	-	-	-	-	-	-	-

Table 4

Sample:	ABMB10 dolerite		J=0.004790 ± 0.000060			Matrix aliquot sample weight = 102.2 mg				Mass spectrometer:		MICROMASS 5400			
Step #	T (in °C)	t (min)	$^{40}Ar(10^{-9}mlSTP)$	$^{40}Ar/^{39}Ar$	±1σ	$^{38}Ar/^{39}Ar$	±1σ	$^{37}Ar/^{39}Ar$	±1σ	$^{36}Ar/^{39}Ar$	±1σ	Ca/K	$\Sigma^{39}Ar$ (%)	Age (Ma) ±1σ	±1σ
1	500	10	57.5	97.792	0.19	0.0183	0.00199	1.3263	0.018	0.02531	0.0014	4.77	2.8	648.6	7.3
2	600	10	273.2	110.672	0.04	0.01811	0.00059	2.3047	0.004	0.01944	0.0004	8.3	14.6	734.6	7.6
3	700	10	358.2	127.527	0.09	0.01549	0.00067	2.1366	0.004	0.00703	0.0003	7.69	28	848.9	8.5
4	800	10	508.2	131.49	0.09	0.01481	0.00027	0.303	0.003	0.00545	0.0003	1.09	46.5	872.7	8.7
5	900	10	492.5	132.296	0.25	0.01492	0.0004	0.2621	0.004	0.0047	0.0003	0.94	64.3	878.2	8.8
6	1000	10	461.3	102.816	0.28	0.01516	0.00056	0.4144	0.011	0.00986	0.0007	1.49	85.7	705.5	7.6
7	1130	10	329.3	110.184	0.07	0.01811	0.00046	0.8609	0.002	0.01213	0.0004	3.1	100	744.2	7.7

Total fusion age = 795.3 ± 8.1 Ma (including J-error)

Weighted Mean average Age (800-900ºC) = 875 ± 6 Ma (including J-error)

Sample:	ABMB10 dolerite		J=0.004753 ± 0.000059			Matrix aliquot sample weight = 34.82 mg				Mass spectrometer:		ARGUS			
Step #	T (in °C)	t (min)	$^{40}Ar(10^{-9}mlSTP)$	$^{40}Ar/^{39}Ar$	±1σ	$^{38}Ar/^{39}Ar$	±1σ	$^{37}Ar/^{39}Ar$	±1σ	$^{36}Ar/^{39}Ar$	±1σ	Ca/K	$\Sigma^{39}Ar$ (%)	Age (Ma) ±1σ	±1σ
1	500	10	*	107.083	0.08	0.02303	0.00026	2.3003	0.012	0.02818	0.0003	8.28	6.5	694.3	7.2
2	575	10	*	122.241	0.07	0.02146	0.00025	3.6433	0.01	0.01633	0.0003	13.12	16.6	800	8
3	625	10	*	129.058	0.07	0.02321	0.00026	2.0243	0.014	0.0183	0.0002	7.29	24.1	834	8.3
4	675	10	*	121.663	0.07	0.02346	0.00016	0.6835	0.005	0.01735	0.0002	2.46	33.1	795.2	8
5	725	10	*	136.562	0.07	0.01807	0.00012	0.3423	0.004	0.00847	0.0001	1.23	49.2	889.4	8.7
6	800	10	*	129.841	0.05	0.01598	0.0002	0.3107	0.011	0.00539	0.0002	1.12	61.7	858.7	8.5
7	830	10	*	117.191	0.09	0.02067	0.0003	0.3607	0.016	0.01106	0.0002	1.3	68	780.7	7.9
8	860	10	*	111.417	0.07	0.02368	0.00035	0.4265	0.015	0.01679	0.0003	1.54	73.8	738.7	7.6
9	890	10	*	103.36	0.07	0.02245	0.00021	0.3017	0.013	0.02015	0.0005	1.09	79.4	686.4	7.1
10	930	10	*	97.101	0.06	0.0239	0.00039	0.5468	0.008	0.0272	0.0003	1.97	85.3	636.8	6.7
11	960	10	*	101.475	0.08	0.02637	0.00072	0.0871	0.039	0.03103	0.0007	0.31	88	656.3	6.9
12	1000	10	*	108.751	0.18	0.04334	0.00068	1.3378	0.052	0.0656	0.001	4.82	90.8	638.7	7
13	1050	10	*	116.18	0.08	0.02582	0.00027	1.2068	0.007	0.04408	0.0004	4.34	96.3	719.8	7.4
14	1100	10	*	135.507	0.07	0.03931	0.00067	0.8461	0.028	0.086	0.0007	3.05	100	759.3	7.8

*Absolute sensitivity of the Argus massspectrometer is not yet precisely calibrated.
Total fusion age = 783.7 ± 7.9 Ma (including J-error)

Weighted Mean Intermediate Plateau Age (930-1000ºC) = 643.7 ± 6.7 Ma
(including J-error)

Highlights

1. Mbuji-Mayi Supergroup deposited in an intracratonic failed-rift basin.
2. Minimum LA-ICP-MS U-Pb age for detrital BId zircons gave 1174 ± 22 Ma.
3. Provenance of detrital zircon grains is south-east and/or east.
4. C and Sr isotopic curves for BII group is coeval with the Bitter Springs anomaly.
5. $^{40}Ar/^{39}Ar$ age on 'Lomami' dolerite sill yielded 882.2 ± 8.8 Ma.